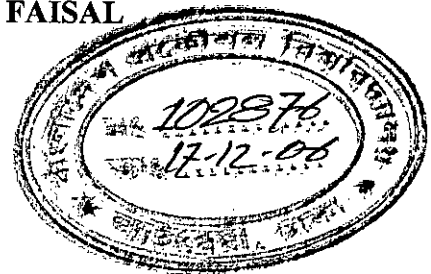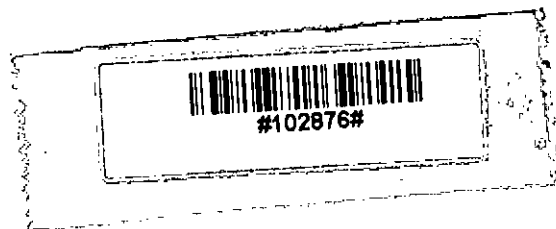# EFFECT OF PORE GEOMETRY ON FACE SEAL PERFORMANCE

A thesis submitted by

MD. TANVIR RAHMAN FAISAL

In partial fulfillment of the requirements for the degree of

MASTER OF SCIENCE IN MECHANICAL ENGINEERING

DEPARTMENT OF MECHANICAL ENGINEERING

BANGLADESH UNIVERSITY OF ENGINEERING & TECHNOLOGY

Dhaka – 1000, Bangladesh

June 2006

The thesis titled **'EFFECT OF PORE GEOMETRY ON FACE SEAL PERFORMANCE '**, submitted by Md. Tanvir Rahman Faisal, Roll No. 040310013P, Session April 2003, has been accepted as satisfactory in partial fulfillment of the requirement for the degree of **Master of Science in Mechanical Engineering** on June 25, 2006.
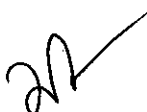
BOARD OF EXAMINERS

Dr. M. Mahabubur Razzaque
Assistant Professor
Department of Mechanical Engineering
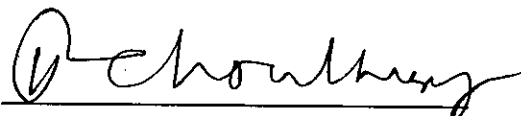BUET, Dhaka

Chairman
(Supervisor)

Dr. Mohammad Ali
Professor
Department of Mechanical Engineering
BUET, Dhaka

Member

Dr. M. Maksud Helali
Professor and Head
Department of Mechanical Engineering
BUET, Dhaka

Member
(Ex - officio)

Dr. Md. Mustafa Kamal Chowdhury
Professor
Department of Mathematics
BUET, Dhaka

Member
(External)

TABLE OF CONTENTS

Chapter 4: NUMERICAL SOLUTION

Chapter 5: RESULT AND DISCUSSION

Chapter 6: CONCLUSION AND RECOMMENDATIONS

CANDIDATE'S DECLARATION

It is hereby declared that this thesis or any part of it has not been submitted elsewhere for the award of any degree or diploma.

Md. Tanvir Rahman Faisal

ACKNOWLEDGMENT

LIST OF FIGURES

LIST OF TABLES

NOMENCLATURE

A_f	Hydraulic loading area
A_h	Sealing interface area
B_r	Balance ratio
D	Pore diameter
D_i	Inner face seal diameter
D_0	Outer face seal diameter
D_b	Balance diameter
F	Friction force
F_c	Closing Force
h	Local film thickness
h_o	Seal clearance
h_p	Pore depth
H	Dimensionless local film thickness
N	Total number of pores
N_c	number of cavitating pores
p_f	Spring pressure
p_s	Hydrostatic pressure
p	hydrodynamic pressure
Λ	Bearing number
P	Dimensionless pressure (p/Λ)
P_t	Total dimensional pressure
Q	Leakage
R	Pore radial coordinate
R_o	Pore radius
R_1	Control cell dimension
r	seal radial coordinate

S		Pore ratio (ratio of pores to ring area)
T		Friction torque
U		Average circumferential velocity
W		Opening force
x,z		Pore Cartesian coordinate
X,Z		Dimensionless coordinates (normalized by R_o)
Ψ		h_p/h_o
ξ		R_1/R_o
ω		Successive Over Relaxation Factor

ABSTRACT

Surfaces covered with micropores have recently become a topic of interest as an effective means for better lubrication and friction reduction in thrust bearings, mechanical seals, piston rings, and other machine parts. The surface structure of the sliding faces plays a vital role in their performances.

Surface pores on face seal surfaces are developed during different kinds of manufacturing operations and surface treatments and their shapes may be different. Moreover, different kinds of surface textures may be deliberately machined on the seal surface through modern techniques. It is, therefore, essential to investigate how pores/ asperities of different shapes affect the hydrodynamic behavior of face seal. In the present work, performance of mechanical face seals with pores/ asperities of square and exponential shapes is investigated.

Mathematical models are developed for different pore geometry to allow the performance prediction of liquid non-contacting face seals with regular microsurface structure in the forms of rectangular and exponential pores. Seal performance such as equilibrium face separation, friction torque and leakage across the seal are calculated and presented for a range of sealed pressure, pore size and pore ratio of the annular ring surface area. An optimum pore size is found that depend on corresponding to the maximum axial stiffness and minimum friction torque.

Chapter 1

INTRODUCTION

1.1 MECHANICAL FACE SEAL

Mechanical face seals are used to seal a fluid at places where a rotating shaft enters an enclosure. Figure 1.1 shows schematically the configuration of a mechanical face seal. The rotating seal is fixed to the shaft and rotates with it, whereas the stationary seal is mounted on the housing. The secondary seals (O-rings) prevent leakage between the rotating shaft and the rotating seal, and the housing and the stationary seal, respectively. The rotating seal is flexibly mounted in order to accommodate angular misalignment and is pressed against the stationary seal by means of the fluid pressure and a spring. The primary sealing occurs at the sealing interface of both seal faces, where the rotating face slides relative to the stationary face. For proper functioning of a mechanical face seal, a fluid film is maintained between the faces. In the configuration of Figure 1.1, the sealed fluid may also act as a lubricant. Applications of mechanical face seals are numerous. The most common example of application is in pumps for the chemical industry. Also propellor shafts in ships and

submarines, compressors for air conditioners of cars and turbo jet engines and liquid propellant rocket motors in the aerospace industry require mechanical face seals.
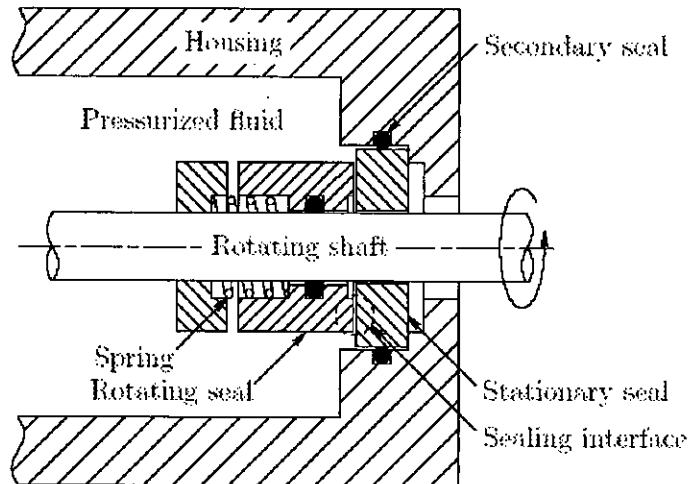
Figure 1.1: Mechanical face seal, schematically [1]

Mechanical face seals have become the first choice for sealing rotating shafts operating under conditions of high fluid pressures and high speeds, at the expense of soft-packed glands. The reason for this is lower leakage, less maintenance and longer life. A disadvantage of face seals is that when they fail, they do so completely, whereas a soft-packed gland can continue, although less efficiently.

The advent of a range of microfabrication techniques (Galvanoforming Abforming, Laser Machining) coupled with developments in microscopy (Scanning Electron Microscope and Atomic Force Microscope) has had a profound effect on the resurgence of tribological applications at microscopic level. With the help of this new technology, it is now possible to produce microstructures on bearing seal surfaces to improve the overall tribological performance including reduction in friction, wear and interfacial temperatures, improvement in reliability, and in severity conditions, lowering energy consumption and minimizing maintenance costs.

1.2 RELATED AND EARLIER RESEARCH

The problem of parallel surface lubrication has been of considerable interest to people involved in rotary shaft face seal and thrust bearing technology for many years. The basic aspect of parallel surface lubrication that distinguishes it from other areas of lubrication is that classical lubrication theory does not predict the existence of stable hydrodynamic film for steady state, isothermal incompressible flow between smooth, parallel surfaces. Hydrodynamic films between apparently parallel surfaces have been observed in practice and are often essential for the reliable performance of seals. However, experience shows that hydrodynamic films do develop in so called parallel face seals, generally because of some mechanisms which relaxes one or more of the assumptions in the classical theory.

The present effort to determine the effect of pore geometry on the performance of face seals is a consequence of numerous research works. One of the early works on thrust bearing and seals was done by Salama [2] who studied the effect of macroroughness on the performance of parallel thrust bearings. He studied the effect of a sinusoidal sliding surface on the pressure and friction in a thrust bearing. Similar studies were carried out for wavy mechanical seals by Pape [3]. He focused on the effect of waviness in radial face seals. Etsion [4] performed quite similar investigation in a later time. He studied the effects of combined coning and waviness on the separating force in mechanical face seals. The load carrying capacity in these cases is due to an asymmetric hydrodynamic pressure distribution over the wavy surfaces. The pressure increases in the converging film regions is much larger than the pressure drop in diverging film regions. This is due to the fact that diverging film region is bounded from below by cavitation whereas the converging film region has no upper limit pressure rise.

Apart from the above macrosurface structure, microsurface structure in the mechanical seals was also studied by different researchers. One of the earliest works in the field of microasperity lubrication was based on the experimental evidence found at Battelle Memorial Institute by Hamilton et al. [5]. A lapped carbon graphite

stator with 5 micro inch (RMS value) surface roughness was run against an optically flat transparent rotor. Mineral oil with a kinematic viscosity of 400 centistokes was used as an interfacial film. Narrow, long discontinuous cavitation streamers were observed. The interruptions in streamers corresponded with the surface roughness of the carbon graphite stator.

Subsequent experiments were carried out to find the effect of surface roughness on cavitation. A smooth, nickel-plated steel stator was run against a pyrex rotor. Initially it produced high torque but later, with the appearance of a broad band of cavitation near the inner radius, the torque dropped sharply. Cavitation streamers soon appeared almost over the entire interface.

The next set of experiments was conducted using a flat, but rough stator surface. Roughening was done in one case by lapping with 600-grit compound and in the other by light vapor blasting. Numerous cavitation streamers were found in both cases. An attempt to relate the topography of lapped carbon graphite to seal performance was infeasible because of the difficulty in mathematically representing the surface that is composed of many irregular microscopic pits and asperities of varying sizes and shapes. Hence, regular patterns were generated on a flat metallic stator surface to facilitate modeling. With photoetching cylindrical micropore heights up to 100 micro inches and flatness on the grooves to within +/- 8 micro inches were achieved. The photoetched copper ring was soft soldered to a steel substrate and run against smooth pyrex and steel rotors in different experiments. Three different patterns, one varying in asperity diameter and the other in asperity height, were used in this study. Load carrying capacity was found to vary linearly with speed in all of these cases. However, the magnitudes were different. Further experiments conducted on an identical pattern but with varying heights showed an inverse relationship between load capacity and asperity height.

The characterization of microasperity lubrication by the combined effect of asperity dimensions and the association of cavities with each asperity, as pointed out earlier, have thus formed a basis for theoretical models.

At first, a simple one-dimensional model was used to show the association of cavities and asperities. Two-dimensional analytical models, with approximations in boundary conditions, were later used to study the combined effects of asperity geometry and cavitation. The experimental critical speeds, below which no cavitation occurs and hence load support is zero, agreed with the theoretical data, within a given experimental error. However, the model could not reproduce the pattern of cavity representation. In addition, the experimental values of load support were higher, 14.2 psi (0.1 N/mm^2) instead of 7.2 psi (0.05 N/mm^2). The reason for this difference was partially attributed to the assumption of the type of cavities used in theoretical analysis, in which streamers of cavitation were not accounted for. In conclusion, the authors have claimed that their theory is in qualitative agreement with experiments.

In an attempt to explain the difference in load support values, the authors assumed small tilts on asperity tops in a subsequent paper[6]. The tilt was 0.86 microinches (34.4 micrometers) in a diameter of 0.3048 mm. The theoretical model was simplified by approximating the solution as a summation of infinite series and then by truncating the resulting series. The justification of these assumptions was based on the use of small inclination for the tilt. A good correlation between the experimental and theoretical results, both for film thickness and for friction coefficient, was observed. The standard deviation of the experimental data for film thickness, from the fitted curve was 50 micrometers. Since Talysurf measurements could not detect the small tilts, the authors were unable to demonstrate their claim on the tilt theory. Instead, indirect evidence was shown by increased load support values based on increased tilts.

In a third paper in 1969 [7], authors Anno et al., compared the load support and leakage performances of positive and negative asperities using the previously mentioned small tilt theory of asperity tops. They compared positive square asperities with negative circular asperities, both distributed in a square array. Different arrays (patterns) for microasperities were also used in this study such as, positive circular asperities in a hexagonal array.

Figure 1.2 shows the arrays considered in their study. For all the cases, the protruding area, other than the asperity area, was taken as the effective area while comparing positive and negative asperities. The authors have found similar load support with all of the above shapes. However, experimental leakage rates for negative asperities were very less when compared to positive ones.
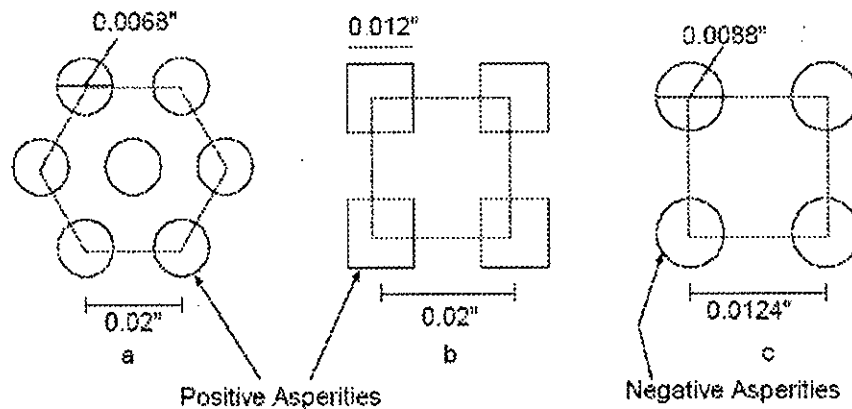
Asperity Area Fraction: a) 0.052   b) 0.36   c) 0.40

Projected Area Fraction: a) 0.052   b) 0.36   c) 0.60

Figure 1.2: Patterns showed in Anno et al. [7]

Sneak [8-9] showed in his investigation that misalignment and surface waviness are found to affect face seal performance in the same order the clearance changes affect the performance of the aligned seal surfaces. It was found in his works that variations in surface flatness of the magnitude which are likely to occur during manufacturing process or as a result of thermal distortion can result in increase in leakage rate. Waviness and misalignment are found to have a negligible effect on separating force in absence of cavitation.

Findlay [10] in his research showed how the cavitation affect the load on mechanical face seals operating on a thin hydrodynamic film containing gas cavity. Cheng et al.[11] did an extensive research on the behavior of hydrostatic and hydrodynamic

noncontacting face seals. They mentioned in their paper that even unplanned unevenness such as circumferential waviness or microirregularities help to generate significant hydrodynamic pressure. It was also found that the shape of film gap has a very critical influence on film stability, stiffness and leakage rate. Snegovsky et al. [12] and Lai [13] showed that microcavities or grooves with small depth may also keep the parallel faces apart.

The early findings on negative asperities have lately revived interest among the researchers, partly due to the developments in microfabrication techniques such as laser ablation. The studies are also influenced by increasingly stricter environmental controls on permissible emissions. Most noticeable contribution on analysis and experimental work on laser-textured surfaces is done by Etsion, I. and his group.

In one of their earlier papers in 1996 [14], Etsion and Burstein developed a mathematical model for hemispherical pores arranged in a rectangular array. Numerical methods using finite differences were employed to solve Reynolds Equation with Half Sommerfeld condition. The range of pore diameters and pore ratios used were 5μm to 200μm and 2.5% to 20% respectively. They found that pore size and pore ratio influences the seal performance significantly only in a certain range. An optimum value for a pore size was found to be dependent upon sealed pressure, viscosity and pore ratio. It decreased with lower viscosities, higher sealed pressures and lower pore ratios. Subsequently, in 1997, Etsion, I., Halperin, G., and Greenberg, Y. have presented experimental results to show the enhancement of mechanical face seal's life with laser textured seal faces [15].

1.3 OBJECTIVE OF THE PRESENT RESEARCH

With the current trend toward higher speed and pressures, any rubbing contacts between seal faces are no longer tolerable, and more and more seals are designed to operate with a continuous fluid film at the expense of leakage. The performance parameter for a mechanical face seals are mainly friction, leakage, wear and its thermal characteristics. In the present research thermal characteristics are ignored.

The wear is not occurred here as the face seal is assumed non contacting type for the present case. The surface structure of the sliding faces of sealing rings plays an important role in the performance of mechanical face seals. Surfaces covered with micropores have recently become a topic of interest as an effective means for better lubrication and friction reduction in thrust bearings, mechanical seals, piston rings, and other machine parts [16-18]. The surface structure of the sliding faces plays a vital role in their performances. The present research concerns the performance of the face seals due to different geometries of micropores.

The central objective of the present research is to develop a mathematical model of face seals having pores of different geometries and to perform a parametric study using this mathematical model.

The specific objectives of the present research work are as follows:

(a) To develop a mathematical model for the performance prediction of non-contacting mechanical face seals with regular micro-surface structures.

(b) To develop a suitable numerical scheme for solving the 2-D Reynolds equation for the hydrodynamic pressure components over a single control cell with specific pore geometry and boundary conditions.

(c) To conduct a parametric analysis using the developed model. Pores/ asperities of rectangular and exponential shapes will be investigated.

1.4 OUTLINE OF SOLUTION METHODOLOGY

Negative microasperities/pores on sliding surface subject to hydrodynamic lubrication are considered in this work. Separate mathematical model is developed for the pore of rectangular shape as well as elliptical shape. It is assumed that the negative asperities/pores are evenly distributed on the seal surface and each pore is located in the center of an imaginary control cell. The pressure distribution in the

lubricant film over the control cell is given by Reynolds equation of hydrodynamic lubrication [19-22]. Hydrodynamic pressure over a single control cell is determined numerically by solving Reynolds equation through finite difference method [23-26]. To obtain the hydrodynamic pressure distribution over the control cell, the Reynolds equation is solved using Successive Over Relaxation (SOR) method. Then total pressure over the control cell is calculated by adding hydrostatic pressure to it. Once a control cell with a positive pressure over its entire area is found, the search along a radial line is ended and the next radial line is examined. By iterative technique, the seal clearance is found by comparing the closing force and the opening force. Once the operating clearance is found, the friction torque and the leakage are then calculated.

Chapter 2

HYDRODYNAMIC LUBRICATION

2.1 HYDRODYNAMIC THEORY

The presence of a viscous fluid film such as lubricating oil, in between any two sliding solid surfaces is known to reduce frictional resistance and wear occurring at the surfaces. Apart from carrying away a major portion of the heat generated by friction, it also supports a part of the normal load. Design of hydrodynamic bearings such as thrust and journal bearings is carried out to ensure the presence of a fluid film. In non- conformal bearings, for example, gears and rolling bearing elements, elastic distortion of metal gives rise to the development of a fluid film. In machine tool slide ways a wedge is produced by the thermal distortion of metals to provide space for lubricant. In all these cases the fluid film may not carry the full load, but it relieves the metal of carrying most of it. The rest of the load is carried by the metal-to-metal asperity contacts. Generally, a convergent wedge along with speed and viscosity produces fluid film pressure.

Additives in lubricant, those have high endurance to extreme conditions created by temperature, help in forming a protective layer of surface-active molecules and thus prevent the chance of welding of asperities that can lead to the breakdown of the system. In fluid film lubrication, a very thin layer of fluid separates the two sliding surfaces completely, preventing the asperity contacts. Therefore, the frictional resistance to the motion is reduced to the level of shear forces experienced by the fluid. In order to support a normal load, pressures have to be developed in this fluid film. In hydrostatic lubrication, the lubricant is pressurized externally to achieve this. But, in boundary lubrication, the sliding faces are not completely separated and so wear takes place at the contacting points. An example of such type of lubrication is the operation of low speed bearings that are small in size. In comparison, with hydrodynamic or thick film lubrication, pressure is developed internally by the combined action of speed of the moving surfaces and the viscosity of the lubricant. If the surfaces are smooth and parallel, no pressures are developed and if irregularities are present on the surfaces, pressures are formed in the fluid film. The mechanism of this type of lubrication can be better understood by studying the action of a converging wedge of sliding surfaces on an interfacial fluid film (see figure 2.1). Convergence of a fluid film is formed either due to natural profile of asperities and surfaces or due to created profiles, as in the case of thermal distortion. Such converging wedge occurs in every lubricated pair of materials and produces pressure proportional to the viscosity and the sliding speed. As a result, the lubricated sliding pair carries a certain load.
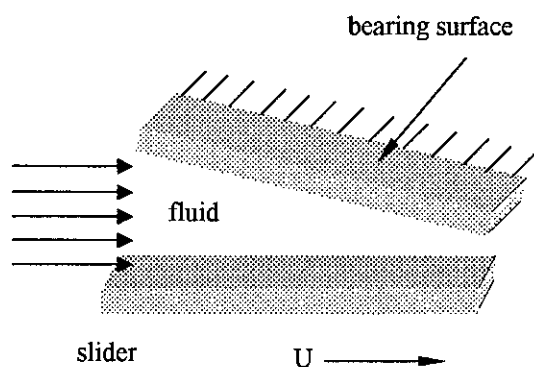
Figure 2.1: Convergent wedge [20]

2.2 STEADY STATE REYNOLDS EQUATION

The mathematical expressions for hydrodynamic conditions are given by the Reynolds equation (2.1), as given below. In simplifying the derivation of the mathematical expression, the following assumptions are made:

- The surfaces are smooth.
- The curvature of the surfaces is large compared to film thickness.
- The fluid flow is laminar.
- There is no slip at the boundaries.
- Body and inertia forces are neglected.
- The lubricant is Newtonian.
- Pressure is constant across the thin film.

Steady state Reynolds equation is developed by applying the continuity of flow and equilibrium of forces on a representative fluid element. The generalized expression is presented as,

$$\frac{\partial}{\partial x}\left(\frac{h^3}{\mu}\frac{\partial p}{\partial x}\right) + \frac{\partial}{\partial z}\left(\frac{h^3}{\mu}\frac{\partial p}{\partial z}\right) = 6(U_1 - U_2)\frac{\partial(\rho h)}{\partial x} + 6\rho h\frac{\partial(U_1 + U_2)}{\partial x} + 12\frac{\partial(ph)}{\partial t} \quad (2.1)$$

where U_1 and U_2 are velocities of the moving surfaces, the first term of the right hand side indicates wedge term, second term is the stretch term, and the third is the squeeze term.

The physical significance of Reynolds Equation is that the pressure generation in the fluid film is given as a composition of the wedge, stretch and squeeze contributions to the load support. The wedge effect is dependent on the variation of film thickness in the direction of the velocity. The stretch effect is caused due to the variation in the velocities of the moving surfaces as in the case of elastomeric surfaces. When rigid surfaces are considered for lubrication, stretch terms are of no significance. Finally, the squeeze effect is due to the impact or vibration of the surfaces relative to each other.

For rigid surfaces, if one of the sliding pairs is considered stationary and the other moving with a velocity, U and if density (ρ) and viscosity (μ) variations across the thin lubricant film are ignored (as a reasonable assumption), the above equation can be further simplified to

$$\frac{\partial}{\partial x}\left(\frac{h^3}{\mu}\frac{\partial p}{\partial x}\right) + \frac{\partial}{\partial z}\left(\frac{h^3}{\mu}\frac{\partial p}{\partial z}\right) = 6\left(U\frac{dh}{dx} + 2V\right) \tag{2.2}$$

where V is the vertical velocity of sliding surfaces relative to each other. If squeeze effects are absent and $\mu \neq \mu(x,z)$ then the above equation reduces to

$$\frac{\partial}{\partial x}\left(h^3\frac{\partial p}{\partial x}\right) + \frac{\partial}{\partial z}\left(h^3\frac{\partial p}{\partial z}\right) = 6U\mu\frac{dh}{dx} \tag{2.3}$$

This is the well-known Reynolds equation in two dimensions that is generally referred in most literature. Appendix B shows the derivation of equation (2.3).

2.3 MICROASPERITY LUBRICATION

Surfaces in reality are not smooth, as considered in the lubrication theory earlier. Irregularities are present in the form of surface roughness on the interfacial surfaces at microscopic levels. The generation of pressure in a fluid film due to the converging and diverging wedges of micro irregularities is classified as microasperity lubrication and experimental evidence has been presented in support of this theory [5].

The theory of microasperity lubrication can be better understood by an idealized one-dimensional model of a single irregularity. As an example, figure 2.3 shows a rectangular model paired with a flat slider in one dimension, in the presence of a fluid film. The moving surface produces antisymmetric pressure distribution around a single asperity. Positive pressure is developed towards the converging edge and negative in the diverging region. Since the load support is zero for an antisymmetric

pressure distribution, as is evident by the resulting net area under the graph, there would be no generation of thrust.

| Pressure distribution over a Single asperity | Net positive pressure distribution |

a) Ideal flow condition   b) Flow with cavitation
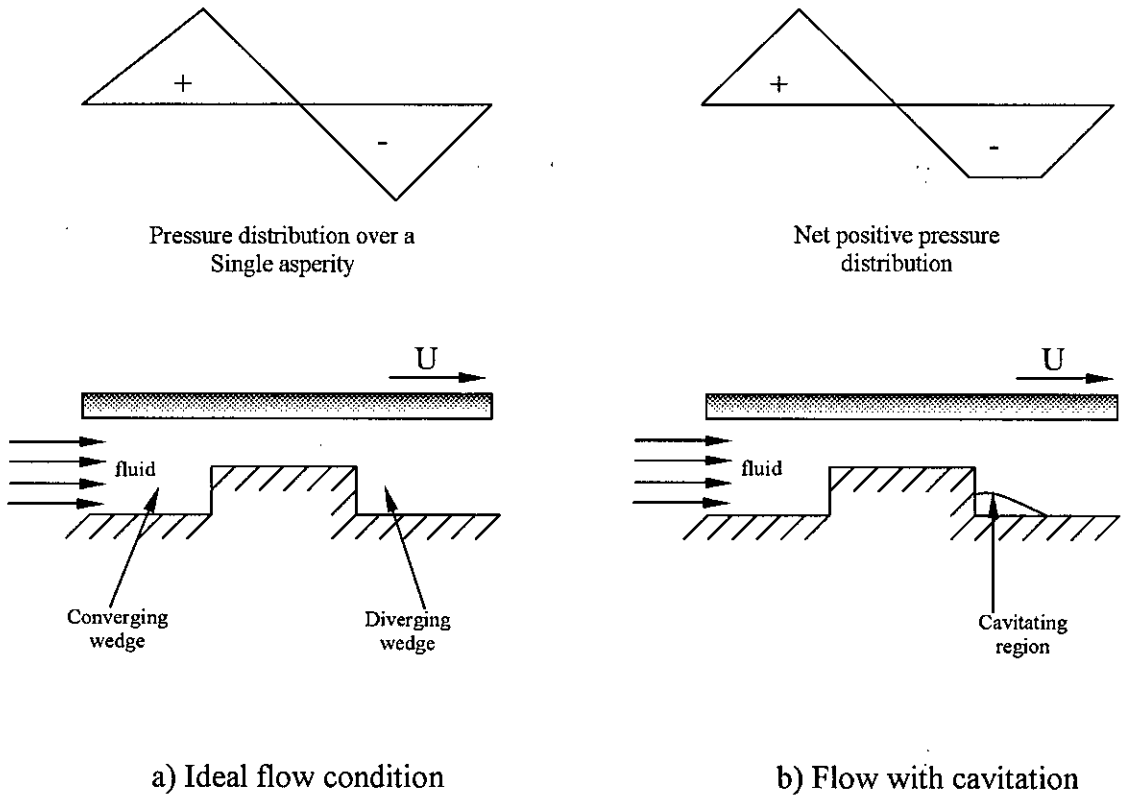
Figure 2.3: Couette flow over idealized asperity [5]

This contradiction to the experimental evidence is explained by the presence of a phenomenon known as cavitation, in the negative pressure zone of the lubricant [5]. Two types of cavitation in lubricants are generally observed. The first one, known as gaseous cavitation (in which gaseous bubbles are emanated by the lubricant when saturation pressures of dissolved gases are reached) is commonly found in bearings. The saturation pressures are generally near to the atmospheric pressure. Pure lubricants are generally free of dissolved gases, but most of the available lubricants are rarely pure. The second type called as vapor cavitation (in which liquid starts boiling when the pressure acting on it falls below the vapor pressure) is prevalent in hydraulic machinery. Due to the inability to withstand tensile forces, lubricant breaks

up into a cavitating region and a fluid flowing path. In the cavitating negative pressure region, isobaric pressure conditions prevail and thus, the net area under the graph as shown in figure (2.3-b) is no more zero, but positive. The integrated effect of the net positive pressure distribution of all the asperities on a sealing surface explains for the creation of thrust and hence, the otherwise mating surfaces.

2.4 MECHANISMS OF HYDRODYNAMIC LOAD SUPPORT

Load support with hydrodynamic lubrication can be achieved by both smooth and rough surfaces. Some of the familiar mechanisms of load support are given below.

2.4.1 Smooth Surfaces
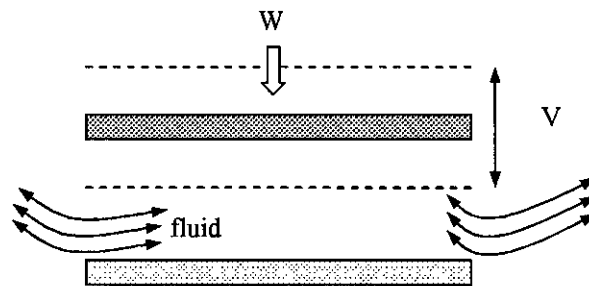
Figure 2.4: Squeeze effects [19]

In case of smooth surfaces, the load support mechanism is caused by three different phenomenon of the wedge, stretch and squeeze effects (as shown in figure 2.4). Stretch effects are found in the case of sliding tires. In case of a plain slider bearing with at least one elastomer surface, wedge and stretch effects are observed. In a journal bearing, wedge and squeeze effects are found

2.4.2 Rough Surfaces

There are four different phenomenon of load support mechanisms associated with rough surfaces [19]. In one of the mechanisms, roughness aligned in one particular direction generates more positive pressure zones than the negative ones and as a

15

result, net load support is observed (figure-2.5). Another mechanism is due to the combined effects of pressure and temperature. While pressure increases the viscosity and hence the load support, temperature has a reverse effect. These effects are assumed to be negligible in the thrust slider system used for this study.
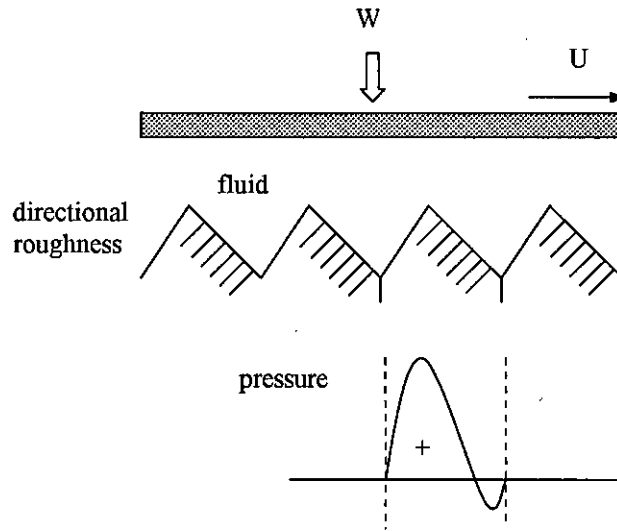
Figure 2.5: Directional roughness [19]
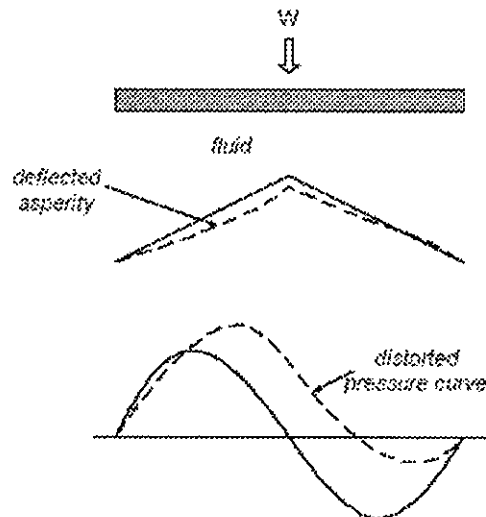
Figure 2.6: Elastohydrodynamic effects [19]

16

The other two mechanisms of load support due to net positive pressure effects are those commonly found with cavitation (as explained earlier) and elastohydrodynamic effects as shown in figure (2.6). Elastohydrodynamic lubrication occurs when at least one of the surfaces is elastic. Even rigid bodies when subjected to very high pressures (in order of thousands of *psi*) as in the case of non conformal bearings (e.g. roller bearings) undergo plastic deformation. As shown in the figure, due to deflection of the asperity, a shift in the pressure profile occur leading to the formation of a net positive pressure.

2.5 BOUNDARY CONDITIONS

2.5.1 Full Sommerfeld Condition
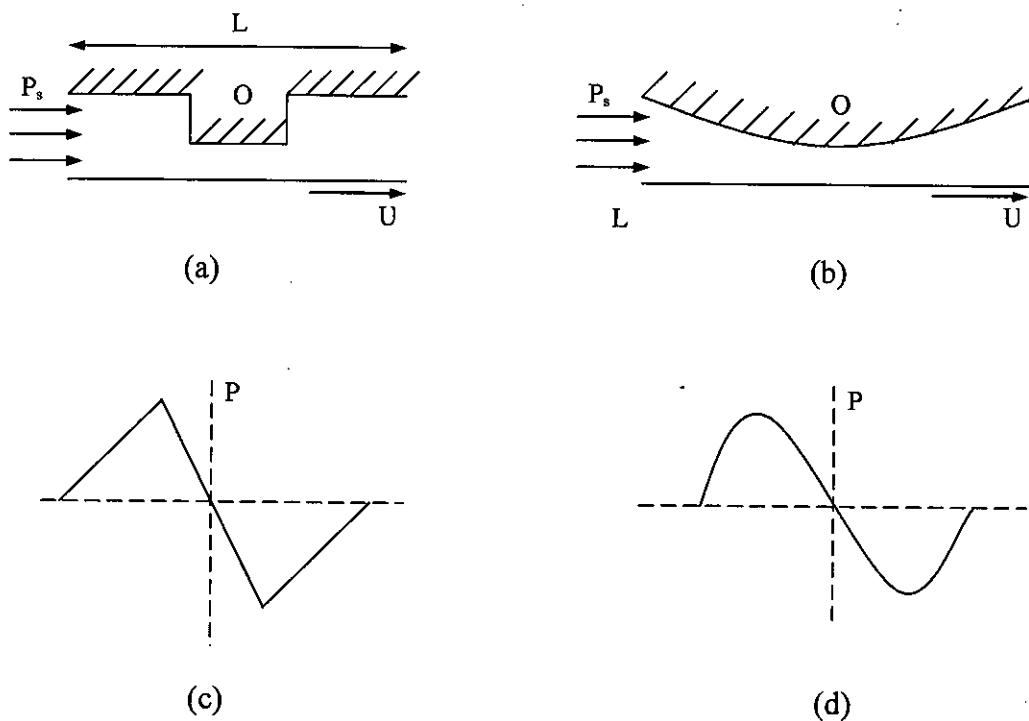
Figure 2.7: Full Sommerfeld pressure distribution.

By combining a converging wedge back to back with itself a converging-diverging wedge is formed. Two such examples are shown in figure 2.7. The first is an extension of a Rayleigh Step bearing and the second is the shape found generally in a journal bearing. Positive pressures are generated in the converging region and negative in the diverging region, giving an anti-symmetrical pressure distribution. Pressure boundary conditions at the entry, exit and the center of the wedge are each equal to zero and these conditions are known as Full Sommerfeld conditions. The resulting pressure curve is shown in figure 2.7-c&d. For low supply pressures, P_s, Reynolds equation predicts negative pressures that lead to erroneous results in load capacity.

Load carrying capacity is given as:

$$W = \int_{-L/2}^{+L/2} p\,dx \qquad\qquad (2.4)$$

2.5.2 Half Sommerfeld Condition
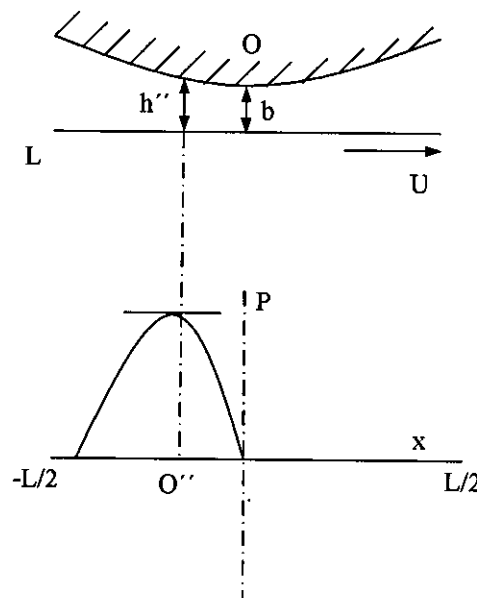
Figure 2.8: Half Sommerfeld pressure distribution [26]

This condition assumes that cavitation occurs over the entire diverging region and hence pressures are considered to be completely and continuously zero in the negative zone. However, this condition is rejected based on the continuity of flow. A typical pressure profile is shown in figure 2.8.

Load Carrying capacity is given as

$$W = \int_{-L/2}^{0} p\, dx \qquad (2.5)$$

2.6 Balance Ratio

An important parameter, well known in the sealing industry, is the balance ratio, which for an outside pressurized seal is defined as:

$$B_r = \frac{Hydraulic\ Loading\ Area}{Sealing\ Interface\ Area} = \frac{A_h}{A_f} = \frac{\left(D_o^2 - D_b^2\right)}{\left(D_o^2 - D_i^2\right)} \qquad (2.6)$$

For an inside pressurized seal the hydraulic loading area is given by $\frac{1}{4}\pi\left(D_b^2 - D_i^2\right)$, thus

$$B_r = \frac{A_h}{A_f} = \frac{\left(D_b^2 - D_i^2\right)}{\left(D_o^2 - D_i^2\right)} \qquad (2.7)$$

where, D_i is the seal inner diameter

D_o is the seal outer diameter

D_b balance diameter

The balance ratio controls the axial load, acting on the seal interface. When B_r is greater than 1, the seal is called *unbalanced*, whereas a *balanced* seal has a B_r-value lower than 1. Seals operating at high pressures are mostly of the balanced type, $B_r <$ 1, whereas many low-pressure seals operate at $B_r > 1$, the unbalanced type.

2.7 Arrays

In micropore (microasperity) lubrication, improvement in tribological performance depends upon the viscosity of the lubricant, the relative velocity of the moving surfaces and the geometries of both the micro pores and the face seal. Generally, for a given situation, the applied load, the viscosity (ignoring the temperature effects), velocity and the dimensions of the face seal are constant. The parameters then available for a designer to enhance the friction and leakage performance is the micro pores shape. An array refers to the way micropores are distributed in a layout. The most common array shapes are square, hexagonal and rectangular as shown in figure 2.9.

a) Square   b) Hexagon   c) Rectangular
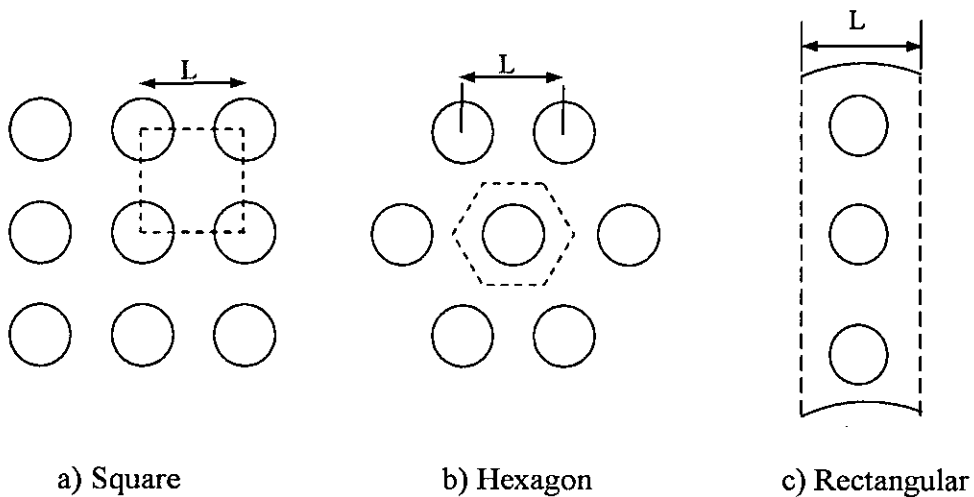
Figure 2.9: Types of arrays

2.8 LEAKAGE (BASED ON POISEUILLE FLOW)

Leakage occurs in the radial direction and is governed by the well-known Poiseulle's law given as

$$Q = \frac{h^3 \Delta p (2\pi r_m)}{12\mu(r_o - r_i)}$$

(2.8)

where Δp is the hydrostatic pressure difference across one unit cell [7]. Though this formula for leakage is in its simplified form, since other effects such as rotation and surface tension are not considered [7], a reasonable estimate of leakage can be expected, good enough for comparative studies.
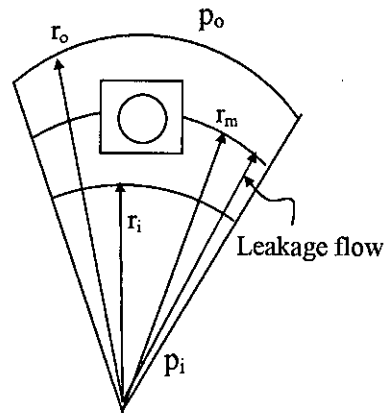
Figure 2.10: Leakage in a face seal with pores

Chapter 3

MATHEMATICAL MODELING

In the present model micropores are considered to be distributed along the mechanical face seal following a rectangular grid. Following figure depicts the distribution of micropores clearly. The pores can be produced by various methods and may have different geometries. The present work concentrates on rectangular pores and exponential pores evenly distributed over the surface area of the seal ring.
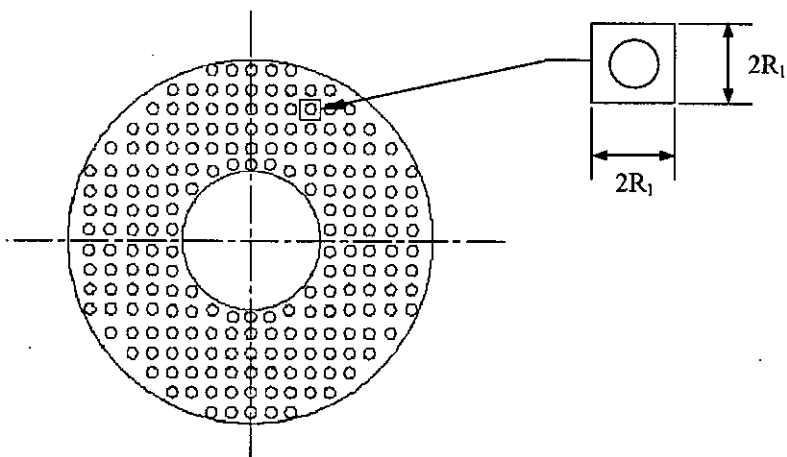
Figure 3.1: Pore distribution on sliding face of seal ring

3.1 ASSUMPTIONS FOR THE PRESENT WORK

The derivation of Reynolds equation is being done on the basis of few assumptions. Here in this work few more additional assumptions are made to facilitate the construction of the physical model with less complexity. The basic assumptions are:

- The seal is a all-liquid noncontacting seal, with parallel faces separated by a constant film thickness h_o.

- Curvature effects of the seal rings can be neglected. Hence, a uniform circumferential velocity U and linear pressure drop from the seal's outer to inner circumference are assumed.

- The sealed fluid is a Newtonian liquid having a constant viscosity, μ.

- Half Sommerfeld condition is assumed whenever cavitation occurs.

Although the last assumption introduces a certain error in the flow around the control cell, it saves computing time without altering the general trend of the solution for load capacity.

3.2 RECTANGULAR PORE GEOMETRY

The pore geometry is showed in the figure 3.2. Each pore is rectangular shaped with a pore depth of h_p. The pores are evenly distributed with an area ratio, S. the distance between neighboring pores, $2R_1$, is large enough to justify the assumption of negligible interaction between the pores. Each pore is located in the center of an imaginary "control cell" of side $2R_1 \times 2R_1$, as shown in the figure 3.2-b. The control cell is the basic unit for the calculations. The hydrodynamic pressure distribution over each control cell is exactly the same.
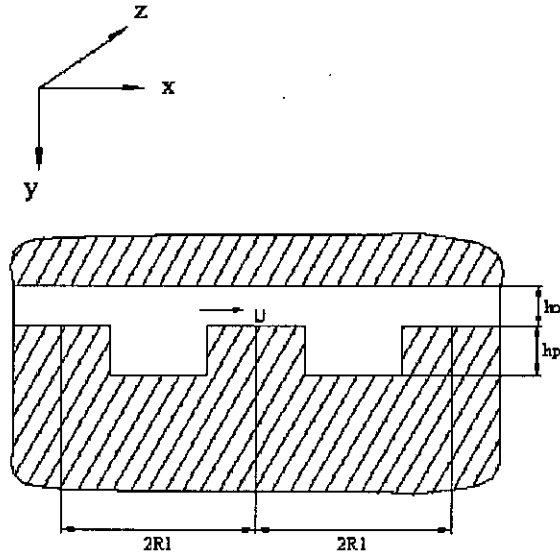
Figure 3.2(a): Pore geometry
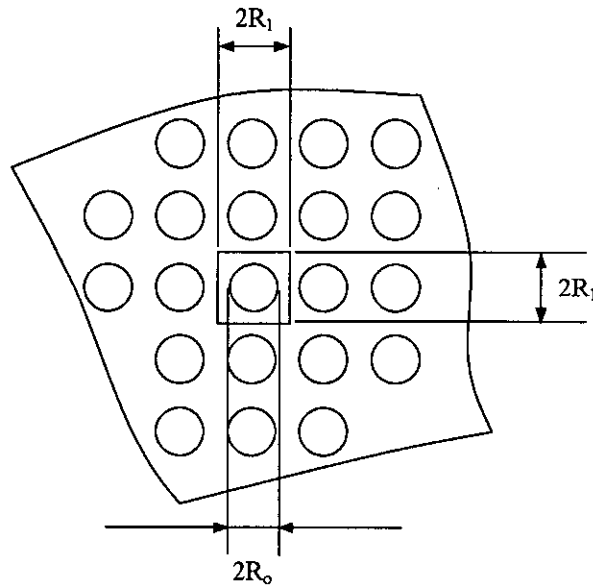
Figure 3.2(b): Control cell with coordinate system

The Reynolds equation (obtained from equation 2.3) for the hydrodynamic pressure component over a single control cell is:

$$\frac{\partial}{\partial x}\left(h^3 \frac{\partial p}{\partial x}\right) + \frac{\partial}{\partial z}\left(h^3 \frac{\partial p}{\partial z}\right) = 6\mu U \frac{\partial h}{\partial x}$$ (2.3)

The local film thickness h in the region $2R_1 \times 2R_1$ of a control cell is:

$$h = h_0$$ (3.1.1)

at outside the pore where, $\left(x^2 + z^2\right)^{\frac{1}{2}} > R_0$

Over the pore area the film thickness is:

$$h = h_0 + h'$$
$$h = h_0 + h_p \qquad [h' = h_p, \text{ for rectangular profile}]$$ (3.1.2)

The boundary conditions of Reynolds equation (2.3) are $p = 0$ at $x = \pm R_1$ and $z = \pm R_1$. After using the dimensionless variables in the following form

$$X = \frac{x}{R_0} \qquad Z = \frac{z}{R_0} \qquad \xi = \frac{R_1}{R_0} \qquad H = \frac{h}{h_0} \qquad \psi = \frac{h_p}{h_o} \qquad \Lambda = \frac{6\mu U R_0}{h_o^2} \qquad P = \frac{p}{\Lambda}$$

The equation (2.3) becomes

$$\frac{\partial}{\partial X}\left(H^3 \frac{\partial P}{\partial X}\right) + \frac{\partial}{\partial Z}\left(H^3 \frac{\partial P}{\partial Z}\right) = \frac{\partial H}{\partial X}$$ (3.2)

where, $H = 1$; at out side the pore (3.3.1)

and, $H = 1 + \psi$, over the pore where $\left(X^2 + Z^2\right)^{\frac{1}{2}} \leq 1$ (3.3.2)

The dimensionless boundary conditions are:

$$P = 0 \quad at \ X = \pm \xi$$
$$P = 0 \quad at \ Z = \pm \xi$$

The dimensionless size of the control cell can be found from the pore ratio S. For a particular control cell of size $2R_1 \times 2R_1$, if the pore size is S portion of $4R_1^2$ then it can be written as,

$$4R_1^2 S = \pi R_0^2 \qquad\qquad [R_0 \text{ is the pore radius}]$$

$$\text{or,} \quad \left(\frac{R_1}{R_0}\right)^2 = \frac{1}{4}\frac{\pi}{S}$$

$$\text{or,} \quad \xi = \frac{1}{2}\left(\frac{\pi}{S}\right)^{\frac{1}{2}}$$

The total dimensionless local pressure at each of the control cell is

$$P_t = P + P_s \qquad\qquad (3.4)$$

where, P_s is the dimensionless local hydrostatic pressure component. The hydrostatic pressure component over each control cell can be found from the following equation

$$p_s = p_i + (p_0 - p_i)\frac{r - r_i}{r_0 - r_i} \qquad\qquad (3.5)$$

where, p_i is the pressure at the seal inner radius

p_0 is the pressure at the seal outer radius

$p_0 > p_i$

The dimensionless local hydrostatic pressure that is obtained from the equation (3.5) is

$$P_s = \frac{P_s}{\Lambda} \qquad [\Lambda \text{ is bearing number}] \qquad\qquad (3.5.1)$$

The hydrodynamic load support provided by the cavitating n-th control cell or the average load per unit area of control cell can be calculated from

$$\overline{W}_n = \int_{-\xi}^{\xi}\int_{-\xi}^{\xi} P\, dX\, dZ \qquad\qquad (3.6)$$

Equation (3.6) will be evaluated numerically using Simpson's 1/3 rd rule in order to calculate the non-dimensional hydrodynamic load support over a control cell.

Now the dimensional load support over the n-th cell is given by

$$W_n = \overline{W_n} \times \Lambda \times R_0^2 \tag{3.7}$$

The total dimensional opening force tending to separate the seal ring is

$$W = \pi \left(r_o^2 - r_i^2 \right)\left(p_o - p_i \right) + \sum_{n=1}^{N_c} W_n \tag{3.8}$$

The $\overline{W_n}$ and hence the W is found for a given Ψ which depends on the seal clearance h_o that is actually unknown a priory. This clearance is the result of a balance between the opening force W and the closing force F_c given by

$$F_c = \pi \left(r_o^2 - r_i^2 \right)\left[p_f + B_r \left(p_o - p_i \right) \right] \tag{3.9}$$

where, p_f is the spring force

B_r is the balance ratio

3.2.1 Friction Torque Calculation

The total friction over area A of the sealing dam is:

$$F = \int \tau . dA \tag{3.10}$$

Neglecting the effect of pressure gradient the above equation can be written as

$$F = \int \mu \frac{U}{h} . dA$$

or, $\quad F = \int_{\substack{over\,nonpore \\ area}} \mu \frac{U}{h} dA + \int_{\substack{over\,pore \\ area}} \mu \frac{U}{h} dA \tag{3.10.1}$

or, $\quad F = I_1 + I_2 \tag{3.10.2}$

Using Equation (3.1.1) the first integral equation can be written as

$$I_1 = \int_0^{2\pi} \int_{r_i}^{r_o} (1-S)\mu \frac{U}{h_0} r.dr.d\theta \tag{3.11.1}$$

or, $$I_1 = \pi\mu U \frac{\left(r_o^2 - r_i^2\right)(1-S)}{h_0} \tag{3.11.2}$$

The second integral of equation (3.10.2) can be written using the equation (3.1.2)

$$I_2 = \int_0^{2\pi} \int_0^{R_0} N\mu \frac{U}{h_0 + h_p} R.dR.d\theta \tag{3.12.1}$$

where, N is the total number of pores, $N = \dfrac{r_0^2 - r_i^2}{R_0^2} S$

   R is the seal radial coordinate

or, $$I_2 = \pi\mu U \frac{\left(r_0^2 - r_i^2\right)S}{h_0(1+\psi)} \tag{3.12.2}$$

The friction force can be obtained by substituting I_1 and I_2 of equation (3.10.2) by the equations (3.11.2) and (3.12.2) respectively. Thus the friction force is

$$F = \pi\mu U\left(r_0^2 - r_i^2\right)\left[\frac{1-S}{h_0} + \frac{S}{h_0(1+\psi)}\right] \tag{3.13}$$

We can write the dimensionless friction force in the form

$$\overline{F} = \frac{F.h_p}{\pi\mu U\left(r_0^2 - r_i^2\right)} \tag{3.14.1}$$

or, $$\overline{F} = (1-S)\psi + \frac{S.\psi}{1+\psi} \tag{3.14.2}$$

So the friction torque of the seal is

$$T = F.r_m \tag{3.15}$$

where, $r_m = \dfrac{r_0 + r_i}{2}$

3.2.2 Leakage

Leakage loss is obtained using the leakage formula based on Poiseuille's law (equation 2.8 of chapter 2). The dimensional leakage across the seal is

$$Q = \frac{\pi h_o^3 r_m}{6\mu} \frac{p_o - p_i}{r_o - r_i} \tag{3.16}$$

3.3 EXPONENTIAL PORE GEOMETRY

The pore geometry is shown in figure 3.3-a. Each pore has exponential shaped cross section with a pore depth of h_p. The pores are evenly distributed with an area ratio, S. The distance between neighboring pores, $2R_1$, is large enough to justify the assumption of negligible interaction among the pores. Each pore is located at the center of an imaginary "control cell" of side $2R_1 \times 2R_1$, as shown in figure 3.3-b. The control cell is the basic unit for the calculations. The hydrodynamic pressure distribution over each control cell is exactly the same.
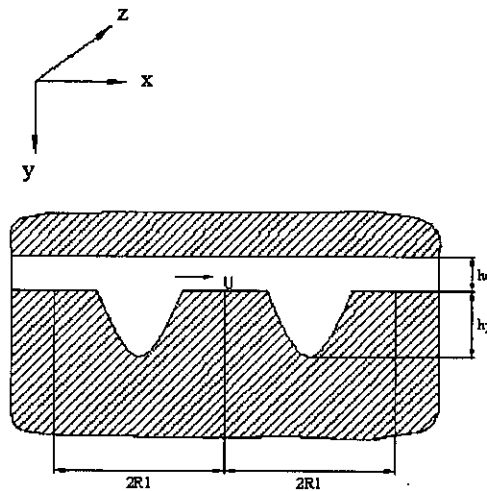
Figure 3.3(a): Pore geometry
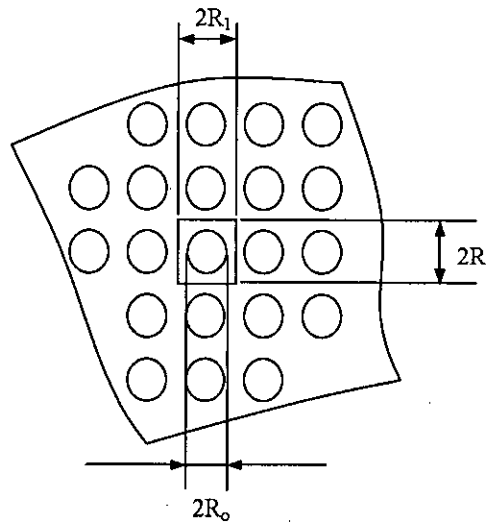
Figure 3.3(b): Control cell with coordinate system

The Reynolds equation for the hydrodynamic pressure component over a single control cell is:

$$\frac{\partial}{\partial x}\left(h^3\frac{\partial p}{\partial x}\right)+\frac{\partial}{\partial z}\left(h^3\frac{\partial p}{\partial z}\right)=6\mu U\frac{\partial h}{\partial x} \qquad (2.3)$$

The local film thickness h in the region $2R_1 \times 2R_1$ of a control cell is:

$$h = h_0 \qquad (3.17.1)$$

at outside the pore where, $\left(x^2+z^2\right)^{\frac{1}{2}} > R_0$

Over the pore area the film thickness is:

$$h = h' e^{k\rho} \qquad (3.17.2)$$

where h' and k are two constants, $\rho = \dfrac{R}{R_0}$ and $0 \le \rho \le 1$

From the geometry of the exponential pore shown in the figure (3.3-b),

at $\rho = 0$

$$h = h_0 + h_p$$

or, $\qquad h_0 + h_p = h' e^{k.0}$

or, $\qquad h' = h_0 + h_p \qquad (3.18)$

at $\rho = 1$

$$h = h_0$$

or, $\qquad h_0 = h' e^{k.1}$

or, $\qquad k = \ln\dfrac{h_0}{h_0 + h_p} \qquad (3.19)$

Combining equations (3.17.2), (3.18) and (3.19) we get

$$h = \left(h_0 + h_p\right)e^{\ln\left(\frac{h_0}{h_0+h_p}\right)\rho} \qquad (3.20)$$

or, $H = Ae^{B\rho}$ (3.21)

where, $A = 1 + \psi$ and $B = -\ln(A)$

The non dimensional form of equation (2.3) becomes

$$\frac{\partial}{\partial X}\left(H^3 \frac{\partial P}{\partial X}\right) + \frac{\partial}{\partial Z}\left(H^3 \frac{\partial P}{\partial Z}\right) = \frac{\partial H}{\partial X}$$ (3.22)

where, $H = 1$; at out side the pore where $\left(X^2 + Z^2\right)^{\frac{1}{2}} > 1$ (3.23)

and, $H = Ae^{B\rho}$, over the pore where $\left(X^2 + Z^2\right)^{\frac{1}{2}} \leq 1$ (3.24)

The dimensionless boundary conditions are:

$P = 0 \quad at \; X = \pm \xi$
$P = 0 \quad at \; Z = \pm \xi$

The dimensionless size of the control cell can be found from the pore ratio S. For a particular control cell of size $2R_1 \times 2R_1$, if the pore size is S portion of $4R_1^2$ then it can be written as,

$4R_1^2 S = \pi R_0^2$ [R$_0$ is the pore radius]

or, $\left(\frac{R_1}{R_0}\right)^2 = \frac{1}{4}\frac{\pi}{S}$

or, $\xi = \frac{1}{2}\left(\frac{\pi}{S}\right)^{\frac{1}{2}}$

The total dimensionless local pressure at each of the control cell is

$P_t = P + P_s$ (3.25)

where, P_s is the dimensionless local hydrostatic pressure component. The hydrostatic pressure component over each control cell can be found from the following equation

$$p_s = p_i + (p_0 - p_i)\frac{r - r_i}{r_0 - r_i} \tag{3.26}$$

where, p_i is the pressure at the seal inner radius

p_0 is the pressure at the seal outer radius

$p_0 > p_i$

The dimensionless local hydrostatic pressure that is obtained from the equation (3.26) is

$$P_s = \frac{p_s}{\Lambda} \tag{3.26.1}$$

The hydrodynamic load support provided by the cavitating n-th control cell or average load per unit area of control cell can be calculated from

$$\overline{W_n} = \int_{-\xi}^{\xi} \int_{-\xi}^{\xi} P dX dZ \tag{3.27}$$

Equation (3.27) will be evaluated numerically using Simpson's 1/3 rd rule in order to calculate the non-dimensional hydrodynamic load support over a control cell.

Now the dimensional load support over the n-th cell is given by

$$W_n = \overline{W_n} \times \Lambda \times R_0^2 \tag{3.28}$$

Similarly we get $\overline{W_n}$ and hence W is found for a given Ψ which depends on the seal clearance h_o that is actually unknown a priory. This clearance is the result of a balance between the opening force W and the closing force F_c given by

$$F_c = \pi(r_o^2 - r_i^2)[p_f + B_r(p_o - p_i)] \tag{3.29}$$

3.3.1 Friction Torque Calculation

The total friction over area A of the sealing dam is:

$$F = \int \tau . dA$$

Neglecting the effect of pressure gradient the above equation can be written as

$$F = \int \mu \frac{U}{h} . dA$$

or, $$F = \int_{\substack{over\ nonpore \\ area}} \mu \frac{U}{h} dA + \int_{\substack{over\ pore \\ area}} \mu \frac{U}{h} dA \qquad (3.30.1)$$

or, $$F = I_1 + I_2 \qquad (3.30.2)$$

Using Equation (3.14.11) the first integral equation can be written as

$$I_1 = \int_0^{2\pi} \int_{r_i}^{r_0} (1 - S) \mu \frac{U}{h_0} r . dr . d\theta$$

or, $$I_1 = \pi \mu U \frac{(r_o^2 - r_i^2)(1 - S)}{h_0} \qquad (3.31.1)$$

The second integral of equation (3.30.1) can be written using equation (3.14.2)

$$I_2 = \int_0^{2\pi} \int_0^{R_0} N\mu \frac{U}{(h_0 + h_p) e^{\ln\left(\frac{h_0}{h_o + h_p}\right)\frac{R}{R_0}}} R . dR . d\theta$$

where, N is the total number of pores, $N = \dfrac{r_0^2 - r_i^2}{R_0^2} S$

        R is the pore radial coordinate

Integrating from 0 to 2π and then simplifying the above equation yield

$$I_2 = 2\pi N\mu U \int_0^{R_0} \frac{R . dR}{h(R)} \qquad (3.31.2)$$

Putting, $R/R_o = \overline{R}$ the equation (3.31.2) becomes

34

$$I_2 = 2\pi N \mu U \int_0^1 \frac{\overline{R} d\overline{R} R_o^2}{(h_o + h_p)e^{\ln\left(\frac{h_o}{h_o + h_p}\right)\overline{R}}} \tag{3.32.1}$$

or, $$I_2 = 2\pi N \mu U \int_0^1 \frac{\overline{R} d\overline{R} R_0^2}{h_0(1+\psi)e^{\ln\left(\frac{1}{1+\psi}\right)\overline{R}}}$$

or, $$I_2 = \frac{2\pi \mu U S \left(r_0^2 - r_i^2\right)}{h_0} \int_0^1 \frac{\overline{R} d\overline{R}}{H(\overline{R})} \tag{3.32.2}$$

Let's denote the integral part of the equation (3.32.2) as I_3. That means we get

$$I_3 = \int_0^1 \frac{\overline{R} d\overline{R}}{H(\overline{R})} \tag{3.32.3}$$

The above integration is the function of $\overline{R}$. We can write equation (3.32.3) in the following form

$$I_3 = \int_0^1 \frac{\overline{R} d\overline{R}}{(1+\psi)e^{\ln\left(\frac{1}{1+\psi}\right)\overline{R}}} \tag{3.32.4}$$

or, $$I_3 = \int_0^1 \frac{\overline{R} d\overline{R}}{A e^{B\overline{R}}} \tag{3.32.5}$$

Putting, $B\overline{R} = t$ yields, $\quad$ $t = 0$ at $\overline{R} = 0$

$$t = B \text{ at } \overline{R} = 1$$

After substituting and transforming the limit, the equation (3.32.5) becomes

$$I_3 = \frac{1}{A} \int_0^B \frac{t \, dt}{B^2 e^t} \tag{3.32.6}$$

Integrating the above equation yield

$$I_3 = \frac{1}{AB^2}\left[1 - A(B+1)\right] \tag{3.32.6}$$

Combining equations (3.32.2) and (3.32.6), we get

$$I_2 = \frac{2\pi\mu U S\left(r_0^2 - r_i^2\right)}{h_0} \times \frac{\left[1 - A(B+1)\right]}{AB^2} \tag{3.32.7}$$

The friction force can be obtained by substituting I_1 and I_2 of equation (3.30.2) by the equation (3.31.1) and (3.32.7) respectively. Thus the friction force is

$$F = \pi\mu U\left(r_0^2 - r_i^2\right)\left[\frac{1-S}{h_0} + \frac{2S}{h_0} \times \left\{\frac{1-(1+\psi)\left[1-\ln(1+\psi)\right]}{(1+\psi)\left[-\ln(1+\psi)\right]^2}\right\}\right] \tag{3.33}$$

We can write the dimensionless friction force in the form

$$\overline{F} = \frac{F.h_p}{\pi\mu U\left(r_0^2 - r_i^2\right)} \tag{3.34.1}$$

or, $$\overline{F} = (1-S)\psi + 2S\psi\left[\left\{\frac{1-(1+\psi)\left[1-\ln(1+\psi)\right]}{(1+\psi)\left[-\ln(1+\psi)\right]^2}\right\}\right] \tag{3.34.2}$$

So the friction torque of the seal is

$$T = Fr_m \tag{3.35}$$

where, $r_m = \dfrac{r_0 + r_i}{2}$

3.3.2 Leakage

Leakage loss for the present case is obtained using the leakage formula based on Poiseuille's law (equation 2.8 of chapter 2). The formula is same for both cases. The dimensional leakage across the seal is (using same equation as before) given by

$$Q = \frac{\pi h_o^3 r_m}{6\mu} \frac{p_o - p_i}{r_o - r_i} \tag{3.12}$$

Chapter 4

NUMERICAL SOLUTION

The application of finite differences is commonly found in the numerical solution to elliptic partial differential equations such as a Laplacian, $\nabla^2 f = 0$ or a Poisson's equation, $\nabla^2 f = g(x, z)$. Finite difference method is preferable to Finite element method because of the advantages of less computational time and simplified model.

4.1 FINITE DIFFERENCE EQUATIONS

The hydrodynamic pressure distribution within the lubricated face seal interface can be determined from the numerical solution of the Reynolds equation. The numerical analysis starts with the following non dimensional Reynolds equation

$$\frac{\partial}{\partial X}\left(H^3 \frac{\partial P}{\partial X}\right) + \frac{\partial}{\partial Z}\left(H^3 \frac{\partial P}{\partial Z}\right) = \frac{\partial H}{\partial X} \qquad (3.2)$$

$$H^3 \frac{\partial^2 P}{\partial X^2} + \frac{\partial P}{\partial X}\frac{\partial}{\partial X}\left(H^3\right) + H^3 \frac{\partial^2 P}{\partial Z^2} + \frac{\partial P}{\partial Z}\frac{\partial}{\partial Z}\left(H^3\right) = \frac{\partial H}{\partial X} \qquad (4.1)$$

$$H^3\left(\frac{\partial^2 P}{\partial X^2}+\frac{\partial^2 P}{\partial Z^2}\right)+3H^2\left(\frac{\partial H}{\partial X}\frac{\partial P}{\partial X}+\frac{\partial H}{\partial Z}\frac{\partial P}{\partial Z}\right)=\frac{\partial H}{\partial X}$$

(4.2)

$$\frac{\partial^2 P}{\partial X^2}+\frac{\partial^2 P}{\partial Z^2}+\frac{3}{H}\left(\frac{\partial H}{\partial X}\frac{\partial P}{\partial X}+\frac{\partial H}{\partial Z}\frac{\partial P}{\partial Z}\right)=\frac{1}{H^3}\frac{\partial H}{\partial X}$$

(4.3)

$$\frac{\partial^2 P}{\partial X^2}+\frac{\partial^2 P}{\partial Z^2}+f_1(X,Z)\frac{\partial P}{\partial X}+f_2(X,Z)\frac{\partial P}{\partial Z}=f_3(X,Z)$$

(4.4)

Here for the rectangular pore,

The value of H outside the pore is

$$H=1$$

(4.5)

Over the pore,

$$H=1+\psi$$

(4.6)

$$f_1(X,Z)=\frac{3}{H}\frac{\partial H}{\partial X}$$

(4.7)

$$f_2(X,Z)=\frac{3}{H}\frac{\partial H}{\partial Z}$$

(4.8)

$$f_3(X,Z)=\frac{1}{H^3}\frac{\partial H}{\partial X}$$

(4.9)

For the exponential pore

Outside the pore

$$H=1$$

(4.10)

over the pore

$$H = A e^{B\rho} \tag{4.11}$$

$$H = (1+\psi)e^{-\ln(1+\psi)\sqrt{X^2+Z^2}} \tag{4.12}$$

$$f_1(X,Z) = \frac{3}{H}\frac{\partial H}{\partial X} = 3\ln(1+\psi) \times \frac{-X}{\sqrt{X^2+Z^2}} \tag{4.13}$$

$$f_2(X,Z) = \frac{3}{H}\frac{\partial H}{\partial Z} = 3\ln(1+\psi) \times \frac{-Z}{\sqrt{X^2+Z^2}} \tag{4.14}$$

$$f_3(X,Z) = \frac{1}{H^3}\frac{\partial H}{\partial X} = \frac{1}{H^2} \times \ln(1+\psi) \times \frac{-X}{\sqrt{X^2+Z^2}} \tag{4.15}$$

Now equation (4.4) can be written as

$$\frac{P_{i+1,j} - 2P_{i,j} + P_{i-1,j}}{\Delta X^2} + \frac{P_{i,j+1} - 2P_{i,j} + P_{i,j-1}}{\Delta Z^2} + f_1(X_i,Z_i)\frac{P_{i+1,j} - P_{i-1,j}}{2\Delta X}$$
$$+ f_2(X_i,Z_i)\frac{P_{i,j+1} - P_{i,j-1}}{2\Delta Z} = f_3(X_i,Z_i) \tag{4.16}$$

Assuming same step size for both directions, i.e., $\Delta X = \Delta Z = \Delta$

$$P_{i+1,j} - 2P_{i,j} + P_{i-1,j} + P_{i,j+1} - 2P_{i,j} + P_{i,j-1} + f_1(X_i,Z_i)\frac{\Delta}{2}(P_{i+1,j} - P_{i-1,j})$$
$$+ f_2(X_i,Z_i)\frac{\Delta}{2}(P_{i,j+1} - P_{i,j-1}) = \Delta^2 f_3(X_i,Z_i) \tag{4.17}$$

Putting,

$$f_1(X_i,Z_i)\frac{\Delta}{2} = a_1 \tag{4.18}$$

$$f_2(X_i, Z_i)\frac{\Delta}{2} = a_2 \qquad (4.19)$$

$$f_3(X_i, Z_i)\Delta^2 = a_3 \qquad (4.20)$$

Equation (4.17) can be rewritten as

$$P_{i+1,j} - 2P_{i,j} + P_{i-1,j} + P_{i,j+1} - 2P_{i,j} + P_{i,j-1} + a_1(P_{i+1,j} - P_{i-1,j}) + a_2(P_{i,j+1} - P_{i,j-1}) = a_3$$

$$(4.21)$$

$$(1 + a_1)P_{i+1,j} + (1 - a_1)P_{i-1,j} - 4P_{i,j} + (1 + a_2)P_{i,j+1} + (1 - a_2)P_{i,j-1} = a_3 \qquad (4.22)$$

The boundary condition for the above equation is

$$\begin{aligned} X &= \pm\xi & P &= 0 \\ Z &= \pm\xi & P &= 0 \end{aligned} \qquad (4.23)$$

4.2 SOLUTION METHOD

Equation (4.21) is a linear system of algebraic equations expressed as

$$\sum_{j=1}^{n} a_{ij}x_j = b_i \qquad i = 1,2,3,\ldots\ldots n$$

The coefficient matrix obtained for lubrication applications is not only large and sparse, but also amenable for iterative methods. It addition, it is computationally advantageous to solve the set of equations by an iterative method rather than by direct calculations. The iterative method produces a sequence of solution vectors,

$$x^1, x^2, x^3, x^4, \ldots\ldots\ldots x^k, x^{k+1}, \ldots\ldots\ldots$$

The system of equations, given in equation (4.21) above, can be solved by Jacobi iteration, Gauss-Seidel iteration or by Successive over relaxation methods

In Jacobi iteration, the values obtained in any iteration are based entirely on the values of the previous iteration. This is given as:

$$x_i^{k+1} = x_i^k - \frac{1}{a_{ii}}\left(b_i - \sum_{j=1}^{n} a_{ij} x_j^k\right) \qquad , i = 1,2,\ldots\ldots n$$

Gauss-Seidel method, on the other hand, uses the most recent computed values in the iteration. It is expressed as:

$$x_i^{k+1} = x_i^k + \frac{1}{a_{ii}}\left(b_i - \sum_{j=1}^{n} a_{ij} x_j^k - \sum_{j=i}^{n} a_{ij} x_j^k\right) \qquad , i = 1,2,\ldots\ldots n$$

The number of iterations in both of these methods is proportional to N^2, where N is the number of grid intervals in one dimension. However, with only a fewer iterations, a faster convergence to the correct solution is obtained by introducing a relaxation parameter, ω into the solution set, given as:

$$x_i^{k+1} = x_i^k + \omega\frac{1}{a_{ii}}\left(b_i - \sum_{j=1}^{n} a_{ij} x_j^k - \sum_{j=i}^{n} a_{ij} x_j^k\right) \qquad , i = 1,2,\ldots\ldots n$$

If the value of ω is unity, the above set of equations reduces to the Gauss-Seidel method. If $\omega < 1$, the method is slower and is called as under relaxation. When $1 \leq \omega \leq 2$, the method is called successive over relaxation (SOR). For values of $\omega > 2$, the method proves to be unstable. The optimal choice for ω, is obtained from the study of the eigen values of the iterative matrices. For lubrication problems, the values for ω in the range of 1.5 to 1.8 have been found to work well. In the present work, successive over relaxation method is used for the numerical solution.

Chapter 5

RESULTS AND DISCUSSION

Hydrodynamic pressure components at various grid points of a control cell are computed using the numerical scheme described in the previous chapter. This computed pressure components are identical for all control cells. Different input parameters for this computation are shown in table 1.

Table 1: Different input parameters

Name of Parameters	Symbol	Numerical Values	Unit
Seal inside radius	r_i	28.4	mm
Seal outer radius	r_o	31.1	mm
Spring pressure	p_f	0.415	MPa
Balance ratio	B_r	0.79	-
Mean sliding velocity	U	9.5	m/s
Viscosity	μ	25	m. Pa-s
Friction coefficient		0.1	

Seals are designed to operate with lubrication oil at a pressure variation from 0.5 MPa to 3.0 MPa. The iterative procedure to balance the opening force to the closing force is stopped when the seal clearance falls below certain limiting value. In the present work the limiting seal clearance is 0.01µm. Partial face contact is assumed when seal clearance becomes less than this limiting value and the friction force is no longer be calculated. Though seals are originally designed for water, it was found, however that because of low viscosity of water, the hydrodynamic effect on the pressure is too weak [6]. As a result it was impossible to find the clearance, h_o, at which the opening force would balance the closing force. Thus it may be concluded that when sealing water the designed seal selected here will operate as a contacting seal.

Different pore ratios are considered for the evaluation of the seal performance having pores of rectangular and exponential shapes. The pore ratios are 2.5%, 11.25%, 15% and 20%

Rectangular Pore

Figure 5.1 to figure 5.4 show the relation between the pore diameter and the seal clearance at different sealed pressures ranging from 0.5 MPa to 3.0 MPa for the rectangular pore geometry. The seal clearance exhibits almost same nature for different pore ratios. Considering figure 5.1, where pore ratio is S=0.025, the optimum pore size for the sealed pressure of 0.5 MPa is about 12.5 µm. At this size the seal clearance is the maximum and is about 3.3 µm. This is the point of operation where opening force tends to balance the closing force and hence the axial stiffness becomes maximum .Beyond this point, the seal clearance decreases rapidly. The figure further depicts change in seal clearance with an increase of sealed pressure. As the sealed pressure increases, the seal clearance decreases. The size of the pore diameter where the maximum seal clearance occurs reduces with sealed pressure. But as the pore ratio increase from 2.5% to 20% the seal clearance and hence the maximum seal clearance also increases.

Figures 5.5 to 5.8 present the relationship between friction torque and pore diameter at different sealed pressures for the rectangular pore. It is observed that the torque is at its minimum at the maximum clearance, as expected. The value of minimum friction

torque reduces with the increase of pore ratio. After the point of minimum friction torque, it again increases with pore diameter. That means the loss of energy due to friction increases with the increase of pore diameter after a certain point of pore diameter.

Figures 5.9 to 5.12 depict the relation between leakage and pore diameter for different sealed pressures. The leakage loss is of great importance in sealing purposes. The leakage is maximum while the seal clearance is maximum as well as the friction torque is minimum. The maximum leakage drops with an in increase of sealed pressure. It is clearly evident that the amount of leakage increases by a considerable amount for the pore ratio other than 2.5%. That indicates that the effect of pore ratio plays a vital role in the face seal performance regarding leakage.

Exponential Pore:

Figures 5.13 to 5.16 describe the relation of seal clearance with pore diameter at different sealed pressures for the pore of exponential shape. Here we find a similar behavior as rectangular pore. There is a optimum diameter at which seal clearance is maximum. Beyond that optimum pore diameter the seal clearance decreases. One interesting observation is that within a range of 10 micron to 20 micron of pore diameter maximum seal clearance is exhibited other than the sealed pressure of 0.5 MPa.

Figures 5.17 to 5.20 show the relationship between friction torque and pore diameter. Here friction torque exhibits minimum value at the point of maximum clearance. One thing is noticeable from these graphs that with the increase of pore ratio the friction torque for the sealed pressure of 0.5 MPa remain almost same beyond the optimum pore diameter. Almost same magnitude of friction torque is observed up to the optimum pore diameter for the pore ratio other than 2.5%. We can deduce from here that beyond the optimum pore diameter the friction will increase by a considerable amount while below that critical value the effect of seal clearance is insignificant for higher pore ratios.

Figures 5.21 to 5.24 indicate the relationship between leakage vs. pore diameter at different sealed pressures. Here leakage becomes maximum at the point of maximum seal clearance. Beyond the critical pore diameter the leakage drops sharply. The magnitude of leakage increases a considerable amount with the increase of pore ratio. That actually indicates that leakage will be important when higher pore ratios are considered.

In the figures 5.1 to 5.4 and figures 5.13 to 5.16, the relationship between seal clearance and pore diameter at different sealed pressures are shown for rectangular as well as exponential pores. It is observed in those figures that the seal clearance is higher for the lower sealed pressure and clearance is lower at higher sealed pressure. The increase of sealed pressure indicates larger hydrostatic effects at higher pressure. That means at lower sealed pressure the hydrostatic effect is lower and hydrodynamic effect plays dominant role That is why in lower sealed pressures higher seal clearances are observed for both the geometry.

Again in the above mentioned figures it is visible clearly that seal clearances increase with increase of pore ratio. This is because with the increase of pores on the sealing dam the effect of cavitation become more prominent and consequently the hydrodynamic load support becomes more. But this effect is not increasing continuously with the increasing pore ratio. This is because when number of pores increases the interaction between pores are more probable and the distinction between converging and diverging area diminishes which lead lower hydrodynamic effect.

In the figures, which depict the relationship between friction torque and pore diameter, the friction torque increases sharply after the optimum pore diameter. After the point of optimum pore size the pore diameter approaches to its critical value at which seal clearance falls below limiting value. As the film clearance diminishing the fluid film tends to collapse and consequently friction rises sharply.

Tables 2 to 13 show the three characteristics that have been discussed above. The tables show comparative results, between rectangular pore and exponential pore, of maximum

seal clearance, minimum friction torque and maximum leakage for different pore ratios. The tabular values are summarized and presented graphically in the figure 5.25 to 5.30. Figures 5.25 to 5.30 describe the relationships of maximum seal clearance, minimum friction torque, maximum leakage at different pore ratios for rectangular pores. It is being observed that the rate of performance improvement becomes smaller with the increased pore ratio. Figures 5.28 to 5.30 describe the same relationships for the exponential pores. Similar behavior is observed i.e., improvement decreases with the higher pore ratios.

Overall, in those figures it has been clearly visible that the rate of improvement in terms of seal clearance, friction torque or leakage decrease with the increasing percentage of pores. It has been concluded that a pore ratio of 20% is a preferable choice for enhanced performance of a mechanical face seal.

Table 2: Maximum seal clearance for pore ratio of 2.5%

Pore Geometry	0.5 MPa	1.0 MPa	1.5 MPa	2.0 MPa	2.5 MPa	3.0 MPa
Rectangular	3.36	2.105	1.79	1.58	1.46	1.31
Exponential	5.45	4.67	3.65	3.14	2.83	2.65

Table 3: Maximum seal clearance for pore ratio of 11.25%

Pore Geometry	0.5 MPa	1.0 MPa	1.5 MPa	2.0 MPa	2.5 MPa	3.0 MPa
Rectangular	5.11	3.88	2.94	2.48	2.21	1.96
Exponential	5.85	4.92	4.46	4.10	3.72	3.51

Table 4: Maximum seal clearance for pore ratio of 15%

Pore Geometry	0.5 MPa	1.0 MPa	1.5 MPa	2.0 MPa	2.5 MPa	3.0 MPa
Rectangular	5.46	3.98	2.95	2.62	2.36	2.16
Exponential	7.19	6.26	5.53	5.13	4.83	4.51

Table 5: Maximum seal clearance for pore ratio of 20%

Pore Geometry	0.5 MPa	1.0 MPa	1.5 MPa	2.0 MPa	2.5 MPa	3.0 MPa
Rectangular	5.51	4.00	2.96	2.63	2.42	2.24
Exponential	7.23	6.40	6.05	5.50	5.00	4.8

Table 6: Minimum friction torque for pore ratio of 2.5%

Pore Geometry	0.5 MPa	1.0 MPa	1.5 MPa	2.0 MPa	2.5 MPa	3.0 MPa
Rectangular	1.06	1.67	1.96	2.22	2.40	2.68
Exponential	0.651	0.759	0.972	1.130	1.255	1.340

Table 7: Minimum friction torque for pore ratio of 11.25%

Pore Geometry	0.5 MPa	1.0 MPa	1.5 MPa	2.0 MPa	2.5 MPa	3.0 MPa
Rectangular	0.646	0.851	1.127	1.33	1.49	1.705
Exponential	0.596	0.709	0.781	0.852	0.938	0.994

Table 8: Minimum friction torque for pore ratio of 15%

Pore Geometry	0.5 MPa	1.0 MPa	1.5 MPa	2.0 MPa	2.5 MPa	3.0 MPa
Rectangular	0.569	0.785	1.057	1.09	1.203	1.29
Exponential	0.471	0.547	0.621	0.668	0.713	0.764

Table 9: Minimum friction torque for pore ratio of 20%

Pore Geometry	0.5 MPa	1.0 MPa	1.5 MPa	2.0 MPa	2.5 MPa	3.0 MPa
Rectangular	0.519	0.722	0.978	1.089	1.203	1.293
Exponential	0.458	0.525	0.559	0.619	0.678	0.706

Table 10: Maximum leakage for pore ratio of 2.5%

Pore Geometry	0.5 MPa	1.0 MPa	1.5 MPa	2.0 MPa	2.5 MPa	3.0 MPa
Rectangular	3.50	1.94	1.85	1.73	1.72	1.50
Exponential	14.94	21.15	15.71	13.57	12.55	12.45

Table 11: Maximum leakage for pore ratio of 11.25%

Pore Geometry	0.5 MPa	1.0 MPa	1.5 MPa	2.0 MPa	2.5 MPa	3.0 MPa
Rectangular	12.31	12.13	8.21	6.69	5.98	5.04
Exponential	18.48	24.74	28.66	30.22	28.51	28.94

Table 12: Maximum leakage for pore ratio of 15%

Pore Geometry	0.5 MPa	1.0 MPa	1.5 MPa	2.0 MPa	2.5 MPa	3.0 MPa
Rectangular	15.03	13.09	8.29	7.89	7.28	6.74
Exponential	34.45	50.95	54.64	59.20	62.41	61.19

Table 13: Maximum leakage for pore ratio of 20%

Pore Geometry	0.5 MPa	1.0 MPa	1.5 MPa	2.0 MPa	2.5 MPa	3.0 MPa
Rectangular	15.44	13.29	8.38	7.97	4.57	6.74
Exponential	34.89	54.45	65.54	66.95	69.23	71.07

Considering the figures 5.31 to 5.35, we get some comparative results among pore geometries of hemispherical pores (delineated by Etsion at al [14]) and rectangular and exponential pores (present work) Figures 5.31 to 5.33 describe the behavior of maximum seal clearance with respect to pore ratio at sealed pressures of 1.0, 2.0 and 3.0 MPa respectively. The rate of increase of maximum seal clearance decreases with the increase of pore ratio for different sealed pressures. Its rate becomes narrower after the pore ratio of 20%. The same behavior we get in the figures 5.34 to 5.35 where the figures depict the behavior of minimum seal clearance with respect to pore ratio at sealed pressure of 1.0 and 2.0 MPa. Here we also find the decrease of rate with the increase of pore ratio and it also becomes narrower at the pore ratio of 20%.

This decrease of rate of performance of different parameters with the increase of pore ratio is observed because while pore ratio increases the possibilities of interaction between the pores become more evident. And the assumption of the negligible interaction between the pores become invalidate. That's why we get the performance reduction with the increased percentage of pore ratio.

In this present work, the pore depth to pore radius is taken unity. Average seal clearance for rectangular pore is:

$$h_{av} = h_0(1 + S\psi)$$ (5.1)

Average seal clearance for exponential pore is given by

$$h_{av} = h_0\left[1 + S\left(Ae^{B\rho} - 1\right)\right]$$ (5.2)

Average seal clearance for the hemispherical pore is given by

$$h_{av} = h_0\left[1 + S\psi\left(1 - \rho^2\right)^{1/2}\right]$$ (5.3)

Considering the above three equations for average seal, the average seal clearance for a control cell having pore of any geometry depends on the seal clearance, Ψ value and the shape of the geometry as well .For a given Ψ the average seal clearance for rectangular and hemispherical pore exhibit almost same numerical results. But the exponential pore geometry yields a higher value of h_{av} than the other two as the seal clearance found for the exponential pore is higher. That's why we get lower friction torque for exponential pore than the rectangular pore. The figures 5.31 to 5.35 thus depict a closer relation between the rectangular and hemispherical pores.

Figures 5.36 and 5.37 depict the effect of pore depth to seal clearance. In those figures maximum seal clearance at different sealed pressures are plotted against pore depth. The pore depth is made dimensionless by pore radius. The maximum seal clearance here is made dimensionless by pore depth and turned into $1/\psi$. Here it is observed that the seal clearance increases with the increase of pore depth. The increment rate of seal clearance diminishes after a pore depth ratio of 1.5 rectangular as well as exponential pore. That means the effect of pore depth is ineffectual after certain pore depths.

Chapter 6

CONCLUSIONS AND RECOMMENDATIONS

6.1 CONCLUSIONS

Mechanical face seals having pores of different geometries i.e., rectangular and exponential shape play an important role in the prediction of performance. Mathematical models are developed to allow the performance prediction of non-contacting mechanical seals having regular surface structure in the form of rectangular and exponential pores.

1. Seal clearance is higher in exponential pore geometry than that in rectangular pore geometry for a particular sealed pressure.

2. The optimum pore size decreases as the sealed pressure increases.

3. As the sealed pressure increases the seal clearance tends to decrease in accord.

4. Friction torque is minimum at the point of maximum seal clearance.

5. The friction torque remains almost same in lower sealed pressure (0.5 MPa) at pore ratio higher than 2.5%.

6. For exponential pore, the friction torque remains almost same up to the optimum pore diameter while increase a rapidly beyond the optimum value at pore ratio higher than 2.5%

7. Leakage is consequently the maximum at the point of minimum friction torque.

In a nutshell, it is shown that hydrodynamically induced load carrying capacity can be obtained due to cavitation over portions of the seal face area in and around pores. It is found that better performance in terms of higher clearance and smaller friction torque can be achieved with proper selection of pore size and pore ratio. The preferable percentage of pore ratio is 20 as performance improvement becomes negligible at higher values of pore ratio. The optimum pore diameter depends on sealed pressure and pore ratio. It is also concluded that for both geometries the effect of pore depth is negligible on seal clearance after the ratio of 1.5.

On the whole the hydrodynamic effect for the rectangular pore is weaker than for the exponential, and it seems more efficacious to use the exponential pore profile in surface design. The rectangular pore profile model is simpler for calculations and can be used for fast analysis or evaluation.

6.2 RECOMMENDATION

The research work can further be extended for different pore geometry. The effect of higher viscosity can also be another important part for the work which is ignored here. So the effect of higher viscosity can be another arena to extend this work.

Chapter 6

CONCLUSIONS AND RECOMMENDATIONS

6.1 CONCLUSIONS

Mechanical face seals having pores of different geometries i.e., rectangular and exponential shape play an important role in the prediction of performance. Mathematical models are developed to allow the performance prediction of non-contacting mechanical seals having regular surface structure in the form of rectangular and exponential pores.

1. Seal clearance is higher in exponential pore geometry than that in rectangular pore geometry for a particular sealed pressure.

2. The optimum pore size decreases as the sealed pressure increases.

3. As the sealed pressure increases the seal clearance tends to decrease in accord.

4. Friction torque is minimum at the point of maximum seal clearance.

5. The friction torque remains almost same in lower sealed pressure (0.5 MPa) at pore ratio higher than 2.5%.

6. For exponential pore, the friction torque remains almost same up to the optimum pore diameter while increase a rapidly beyond the optimum value at pore ratio higher than 2.5%

7. Leakage is consequently the maximum at the point of minimum friction torque.

In a nutshell, it is shown that hydrodynamically induced load carrying capacity can be obtained due to cavitation over portions of the seal face area in and around pores. It is found that better performance in terms of higher clearance and smaller friction torque can be achieved with proper selection of pore size and pore ratio. The preferable percentage of pore ratio is 20 as performance improvement becomes negligible at higher values of pore ratio. The optimum pore diameter depends on sealed pressure and pore ratio. It is also concluded that for both geometries the effect of pore depth is negligible on seal clearance after the ratio of 1.5.

On the whole the hydrodynamic effect for the rectangular pore is weaker than for the exponential, and it seems more efficacious to use the exponential pore profile in surface design. The rectangular pore profile model is simpler for calculations and can be used for fast analysis or evaluation.

6.2 RECOMMENDATION

The research work can further be extended for different pore geometry. The effect of higher viscosity can also be another important part for the work which is ignored here. So the effect of higher viscosity can be another arena to extend this work.
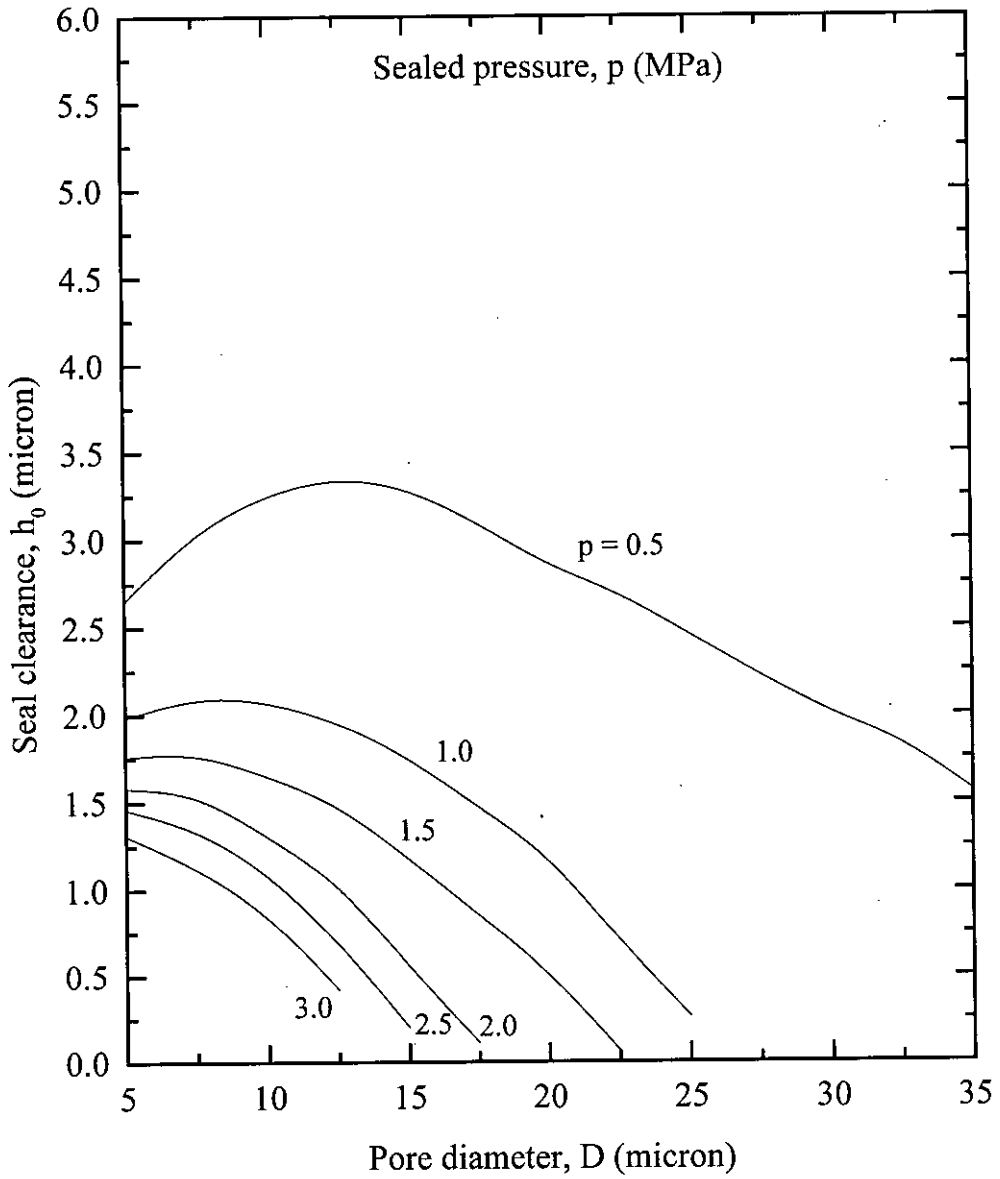
Figure 5.1: Seal clearance vs. pore diameter at different sealed pressures.
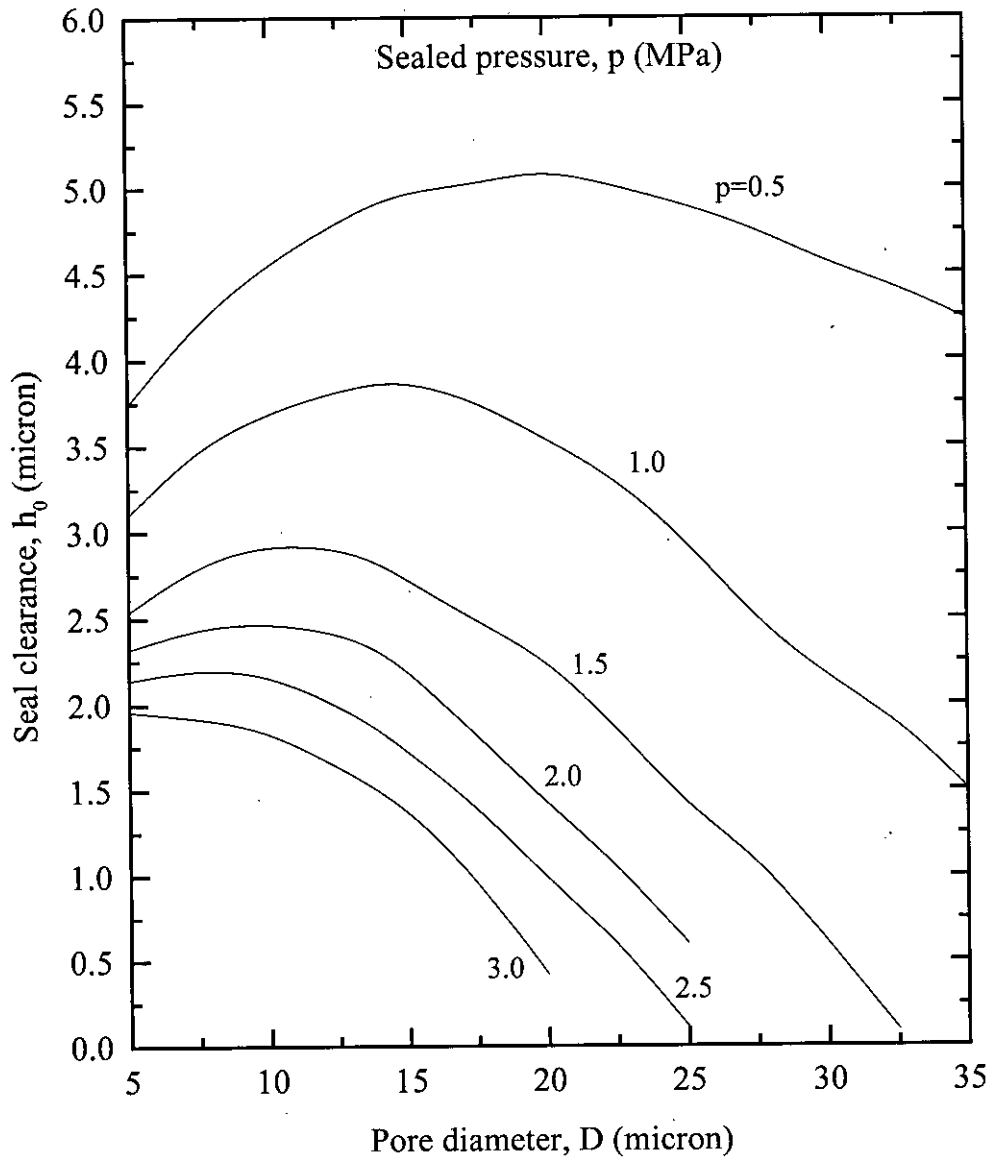Rectangular pore, pore ratio 2.5 % and viscosity 25 m.Pa-s

Figure 5.2: Seal clearance vs. pore diameter for different sealed pressures.
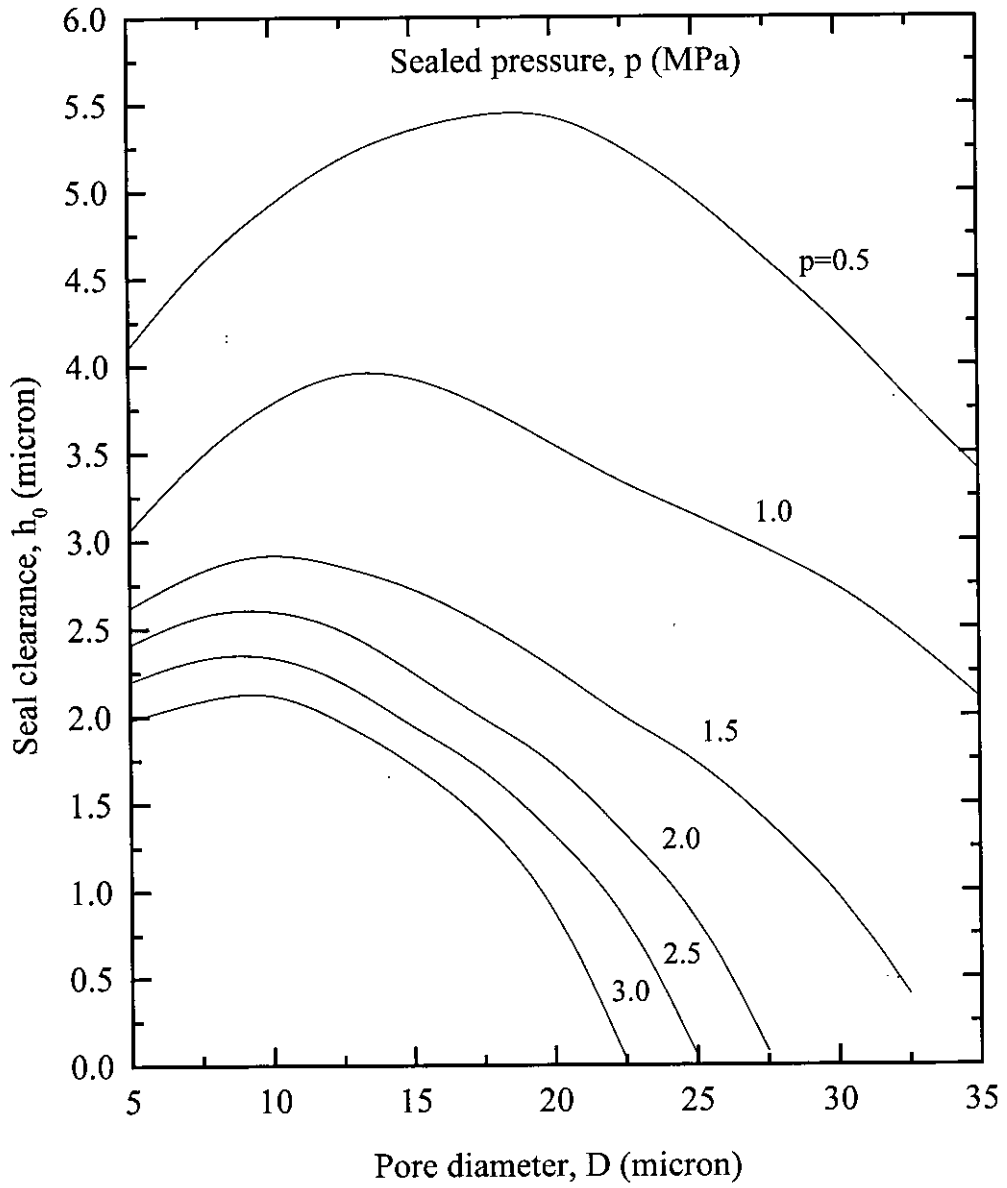Rectangular pore, pore ratio 11.25 % and viscosity 25 m.Pa-s

Figure 5.3: Seal clearance vs. pore diameter for different sealed pressures.
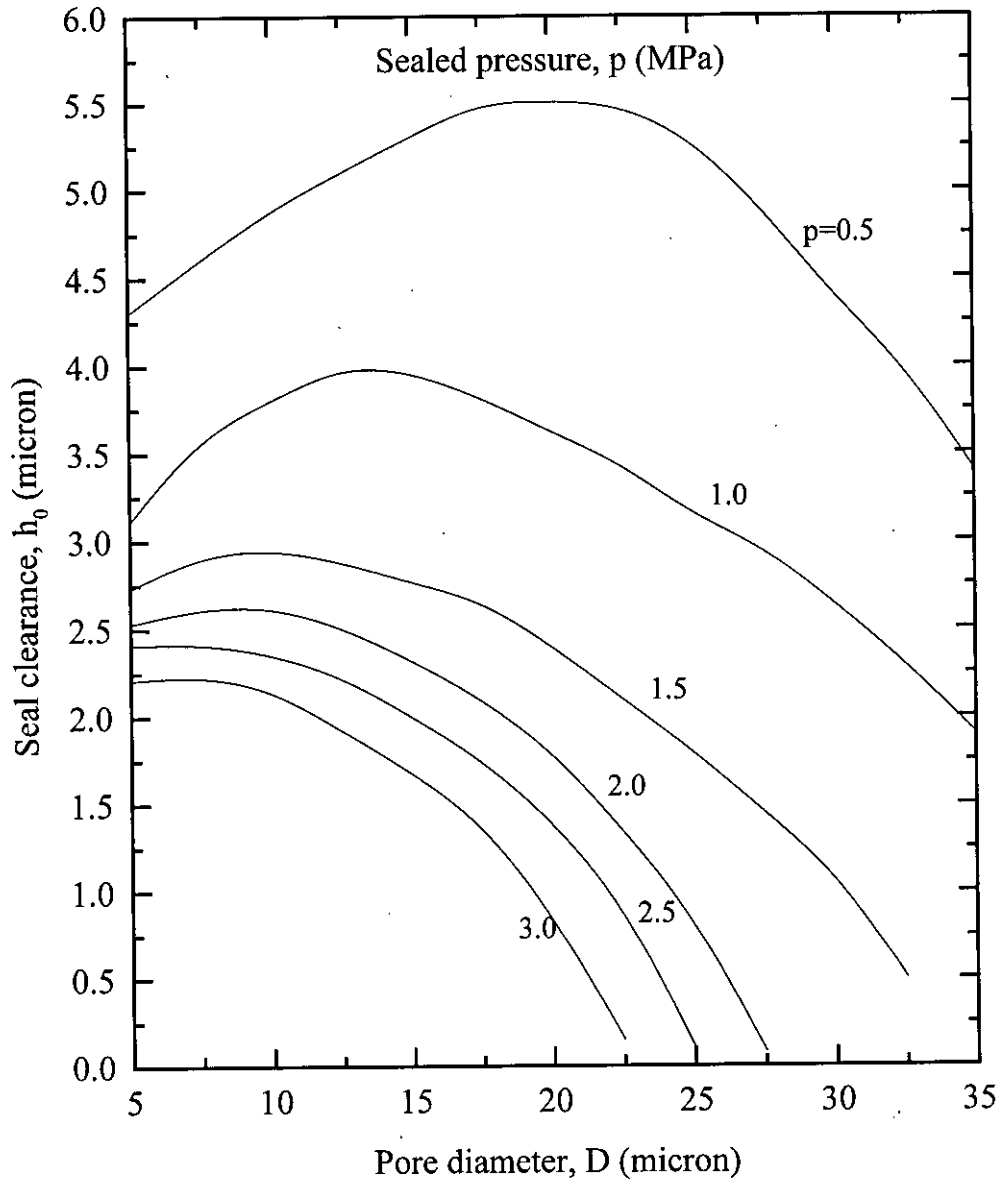Rectangular pore, pore ratio 15 % and viscosity 25 m.Pa-s

Figure 5.4: Seal clearance vs. pore diameter for different sealed pressures.
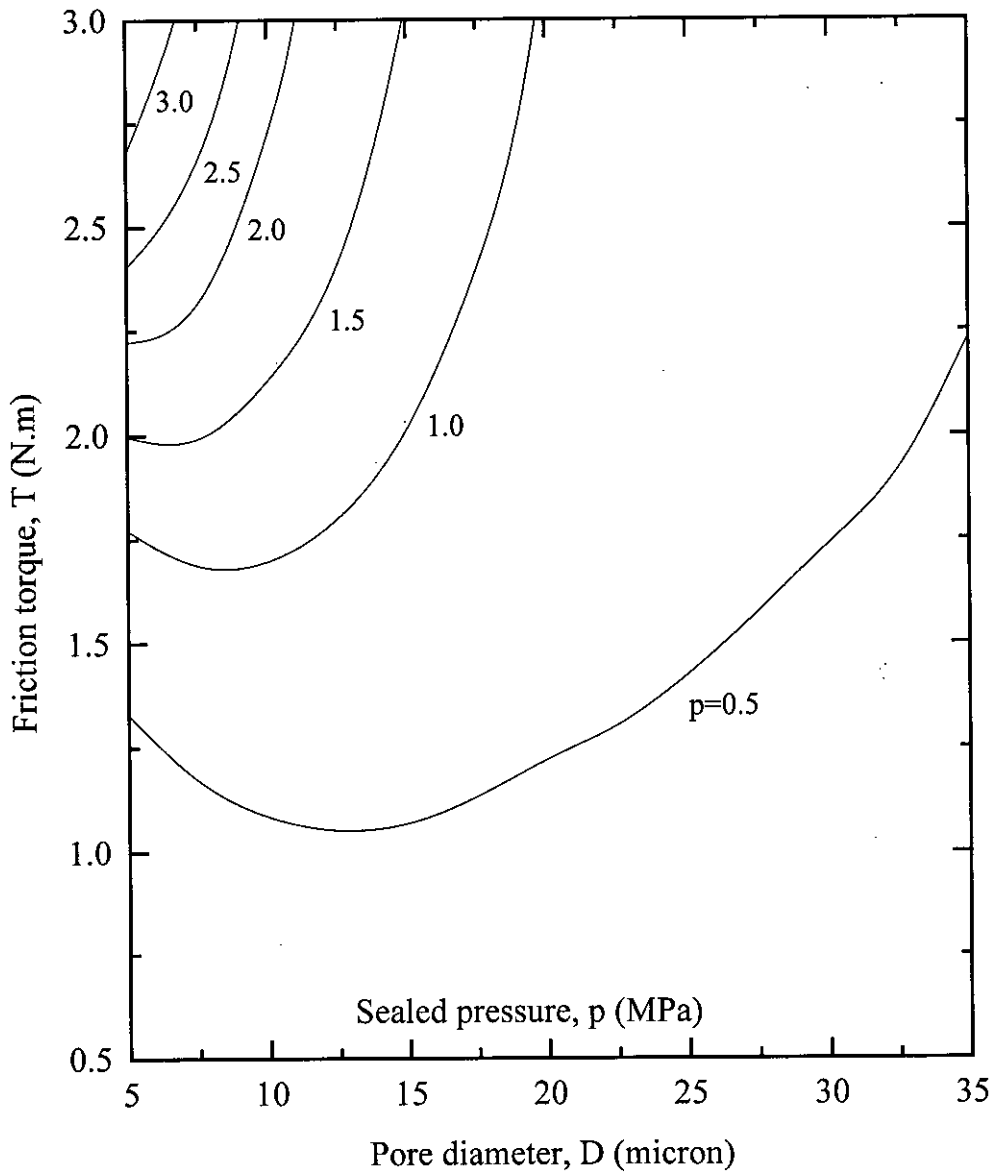Rectangular pore, pore ratio 20 % and viscosity 25 m.Pa-s

Figure 5.5: Friction torque vs. pore diameter at different sealed pressures. Rectangular pore, pore ratio 2.5 % and viscosity 25 m.Pa-s
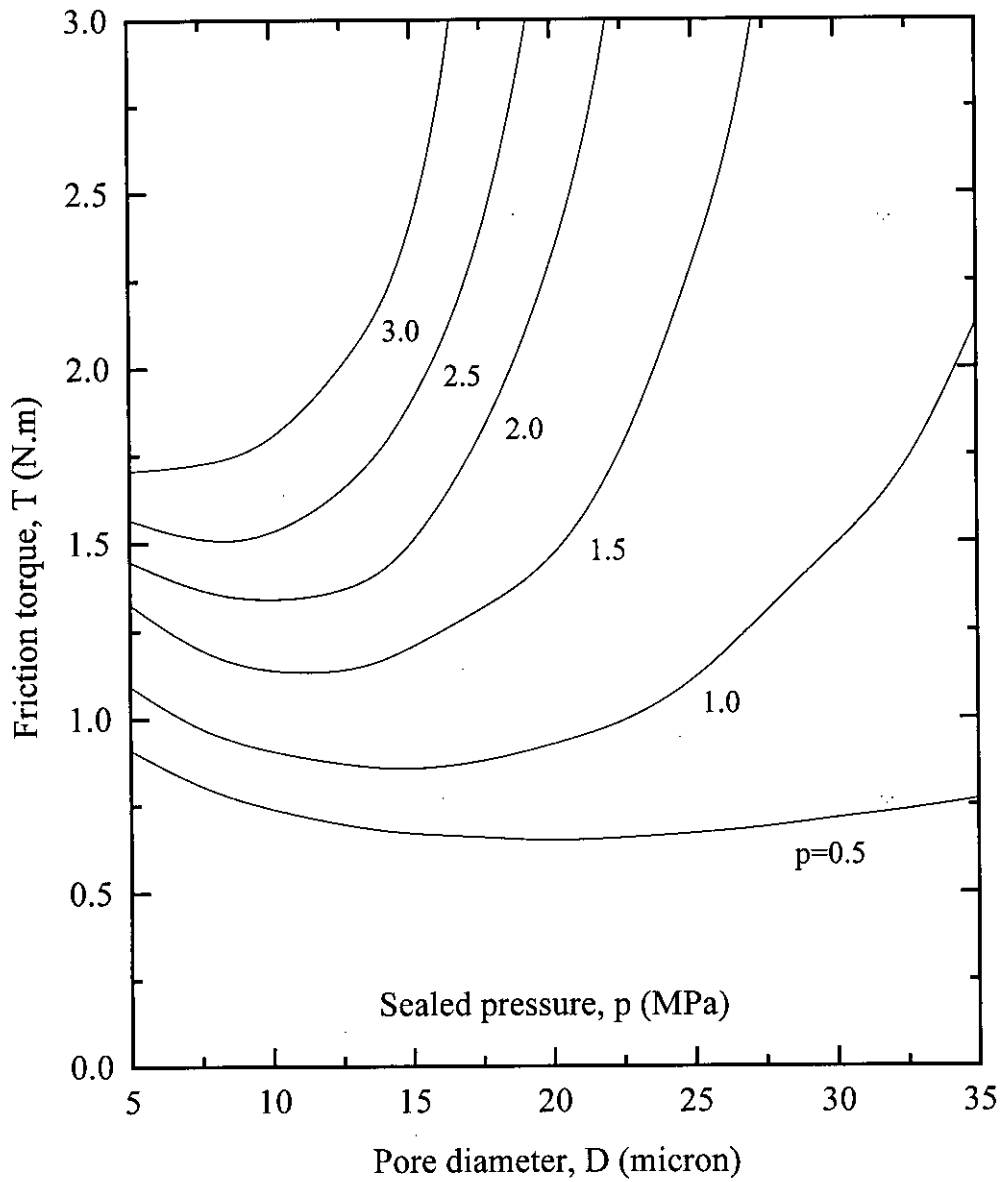
Figure 5.6: Friction torque vs. pore diameter at different sealed pressures. Rectangular pore, pore ratio 11.25 % and viscosity 25 m.Pa-s
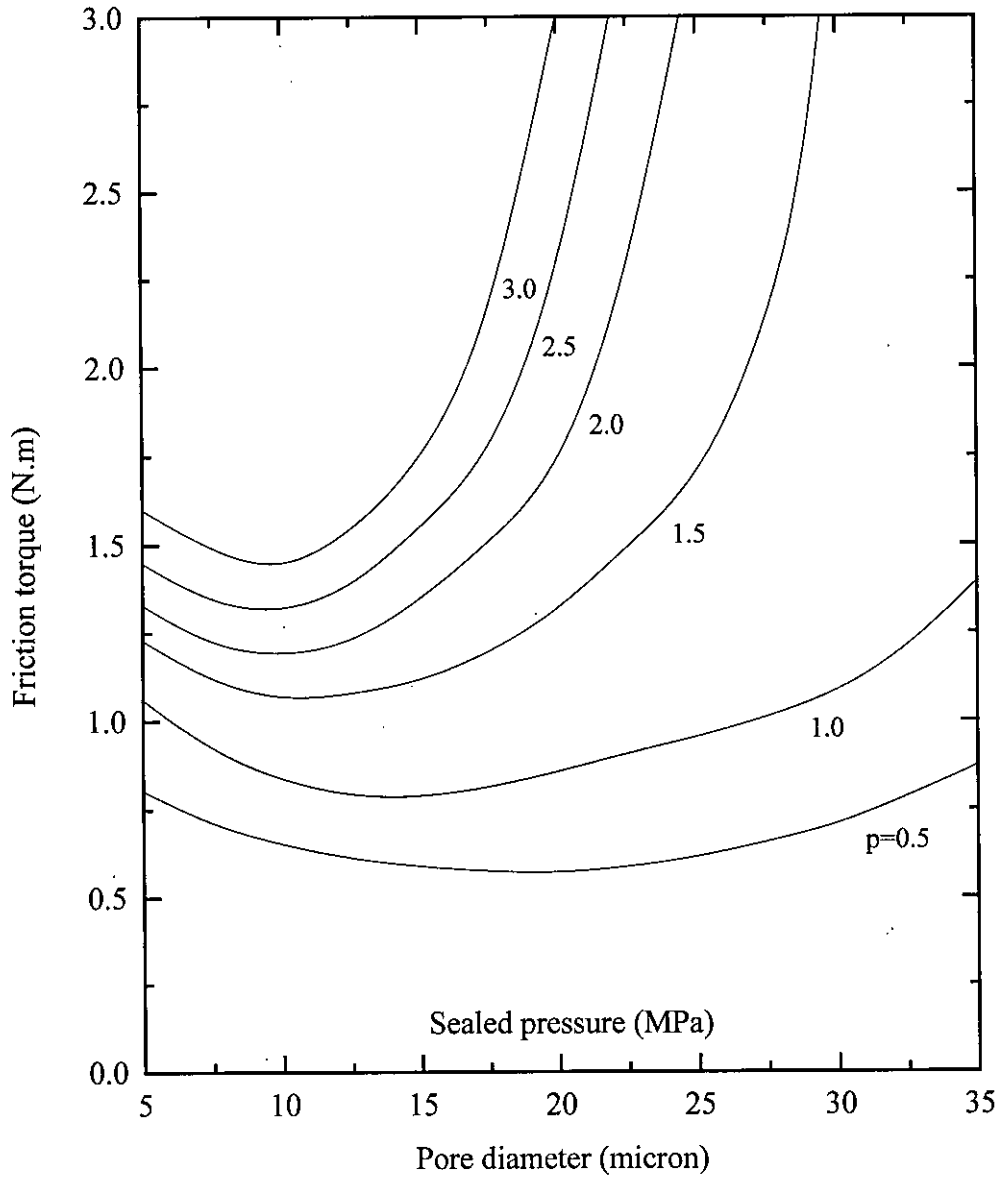
57

Figure 5.7: Friction torque vs. pore diameter at different sealed pressures.
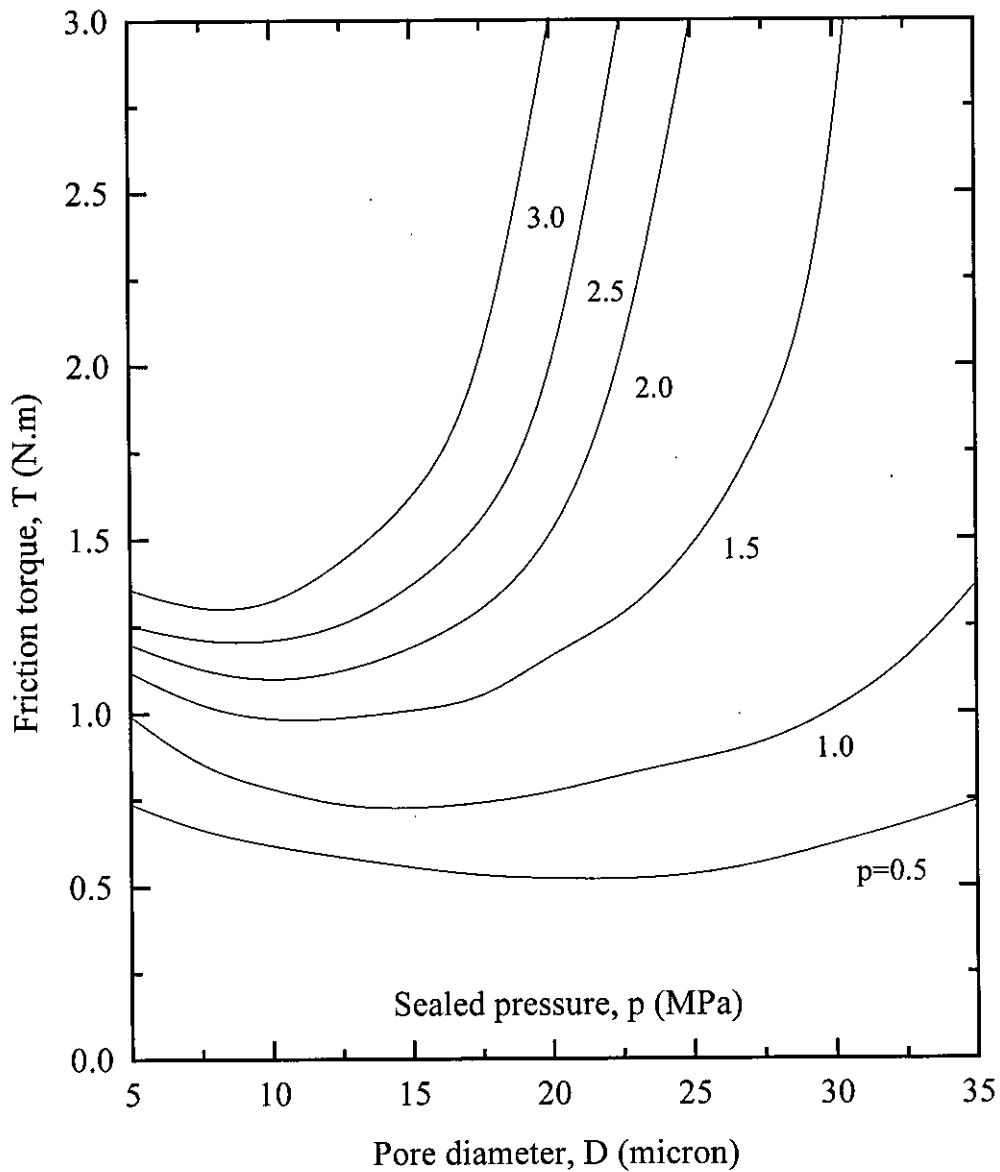Rectangular pore, pore ratio 15 % and viscosity 25 m.Pa-s

Figure 5.8: Friction torque vs. pore diameter at different sealed pressures.
Rectangular pore, pore ratio 20 % and viscosity 25 m.Pa-s

Figure 5.9: Leakage vs. pore diameter at different sealed pressures.
Rectangular pore, pore ratio 2.5 % and viscosity 25 m.Pa-s

Figure 5.10: Leakage vs. pore diameter at different sealed pressures.
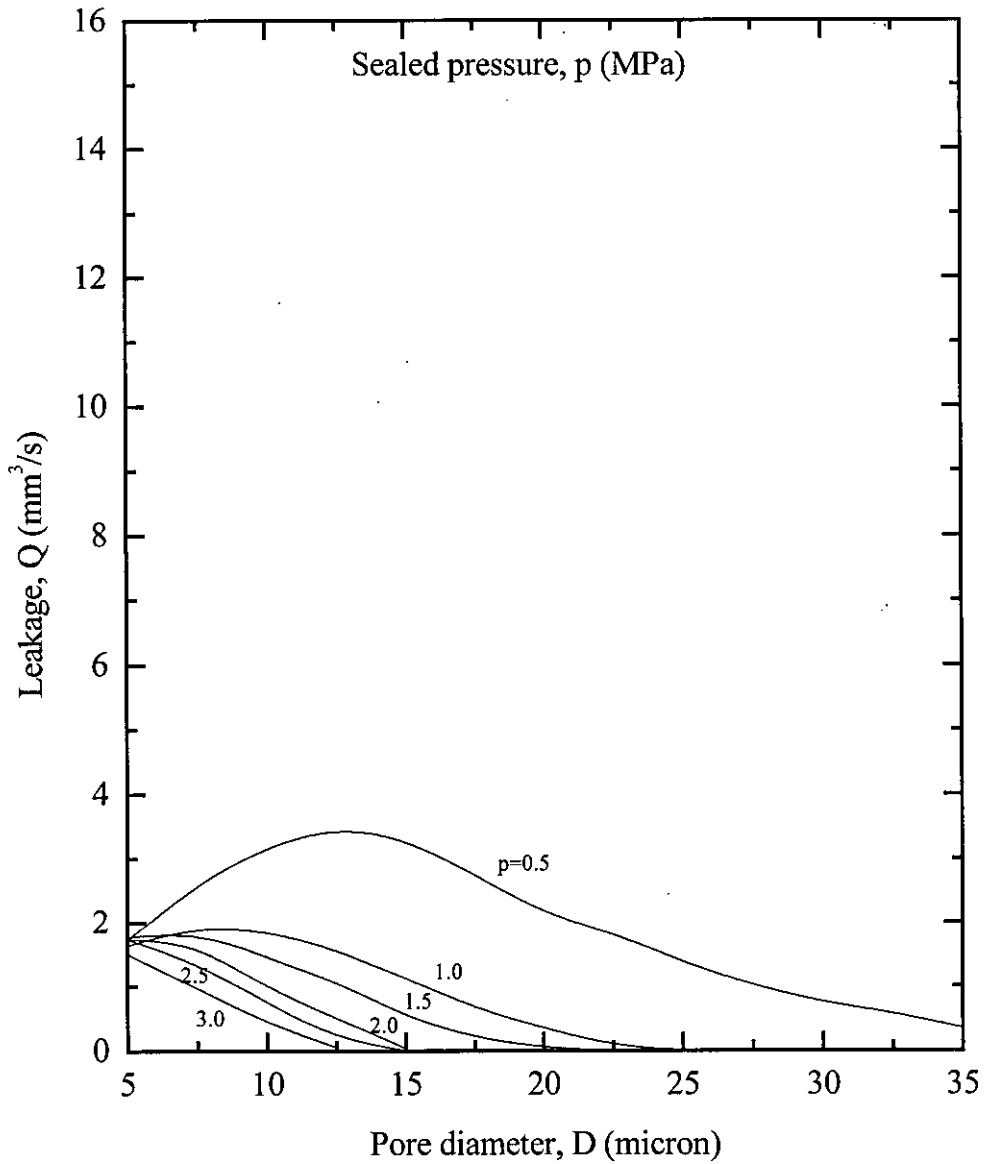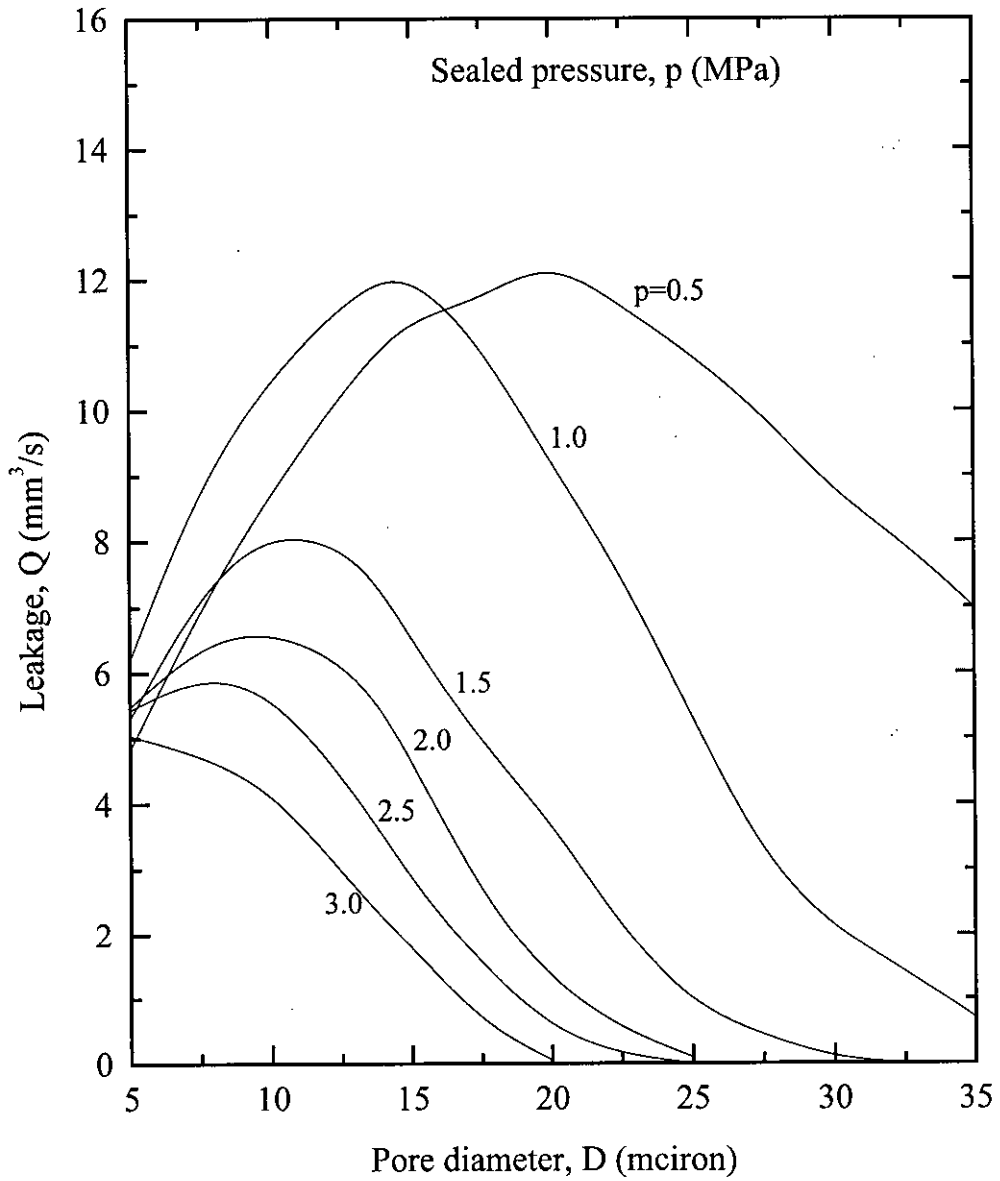Rectangular pore, pore ratio 11.25 % and viscosity 25 m.Pa-s

Figure 5.11: Leakage vs. pore diameter at different sealed pressures.
Rectangular pore, pore ratio 15 % and viscosity 25 m.Pa-s

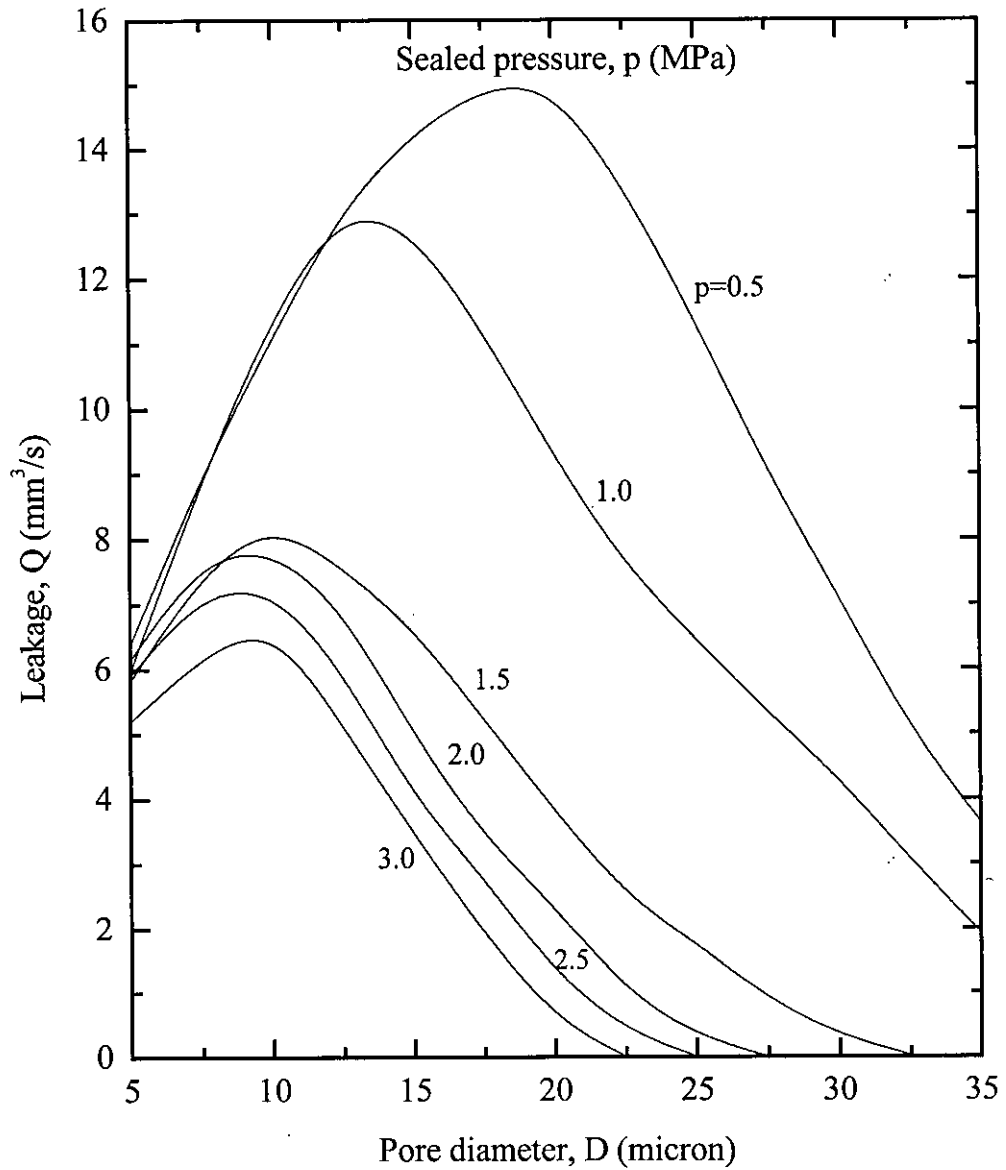Figure 5.12: Leakage vs. pore diameter at different sealed pressures.
Rectangular pore, pore ratio 20 % and viscosity 25 m.Pa-s

Figure 5.13: Seal clearance vs. pore diameter at different sealed pressures. Exponential pore, pore ratio 2.5 % and viscosity 25 m.Pa-s

Figure 5.14: Seal clearance vs. pore diameter at different sealed pressures.
Exponential pore, pore ratio 11.25 % and viscosity 25 m.Pa-s

Figure 5.15: Seal clearance vs. pore diameter at different sealed pressures. Exponential pore, pore ratio 15 % and viscosity 25 m.Pa-s

Figure 5.16: Seal clearance vs. pore diameter at different sealed pressures.
Exponential pore, pore ratio 20 % and viscosity 25 m.Pa-s

Figure 5.17: Friction torque vs. pore diameter at different sealed pressures. Exponential pore, pore ratio 2.5 % and viscosity 25 m.Pa-s
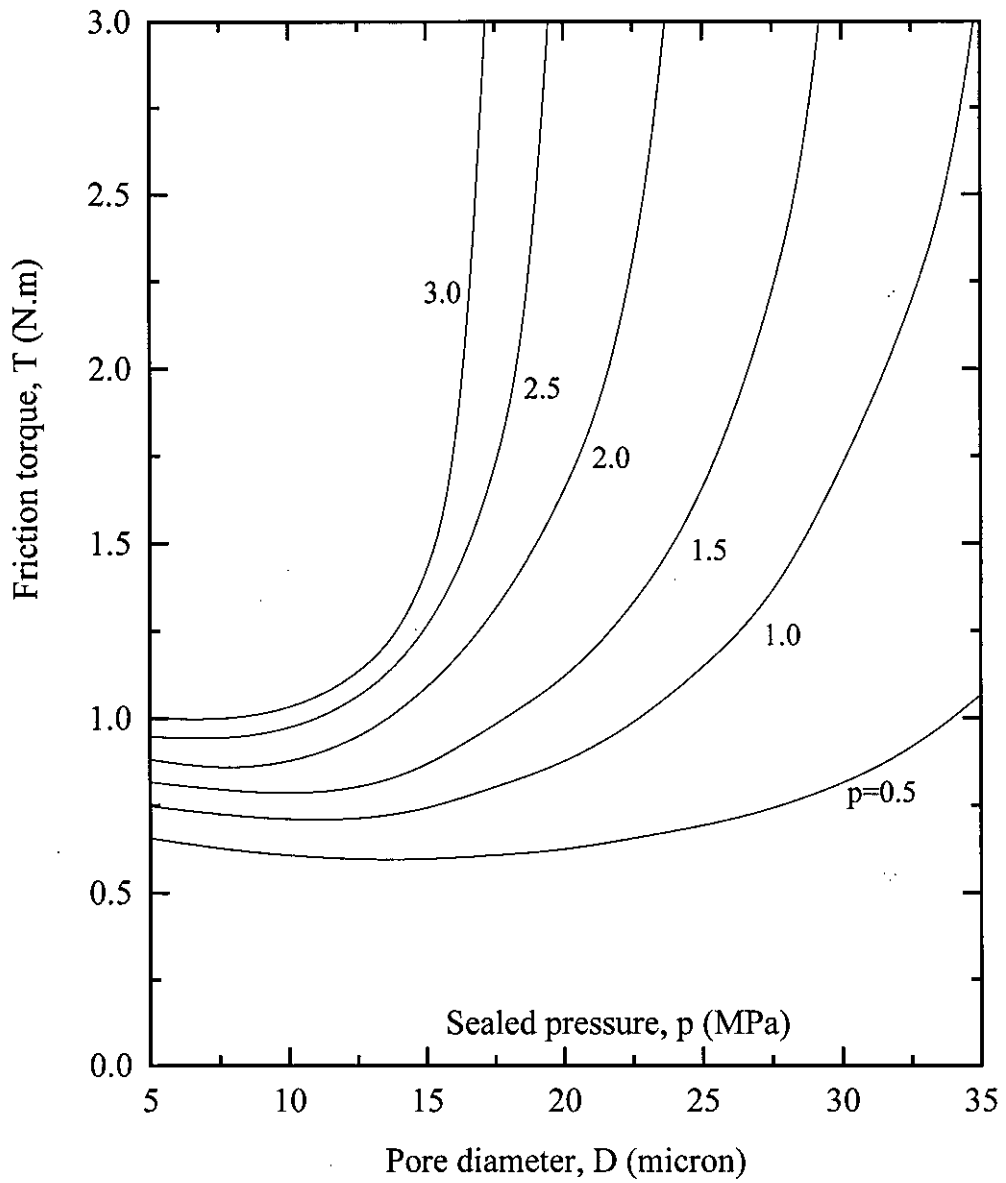
Figure 5.18: Friction torque vs. pore diameter at different sealed pressures.
Exponential pore, pore ratio 11.25 % and viscosity 25 m.Pa-s
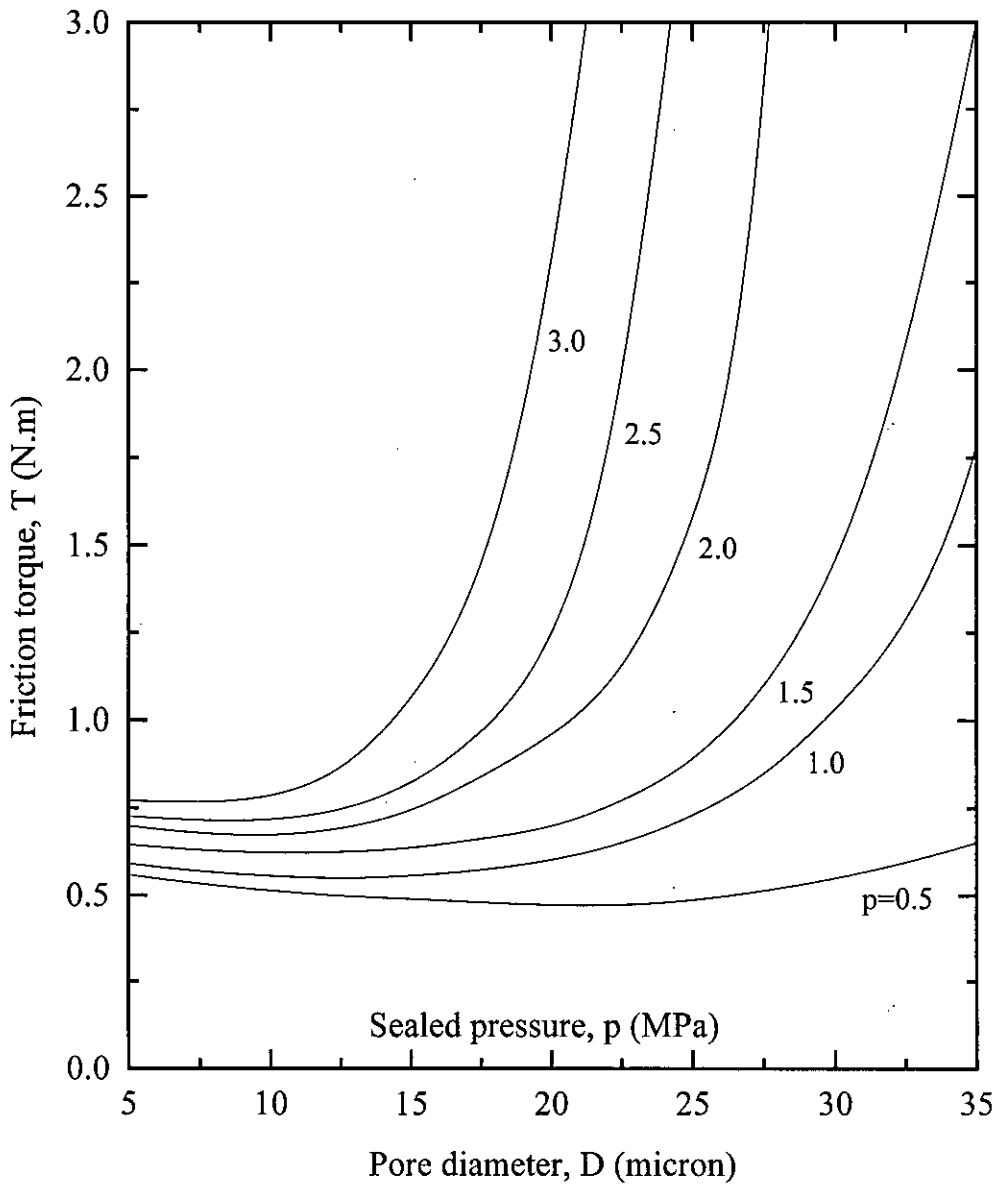
Figure 5.19: Friction torque vs. pore diameter at different sealed pressures.
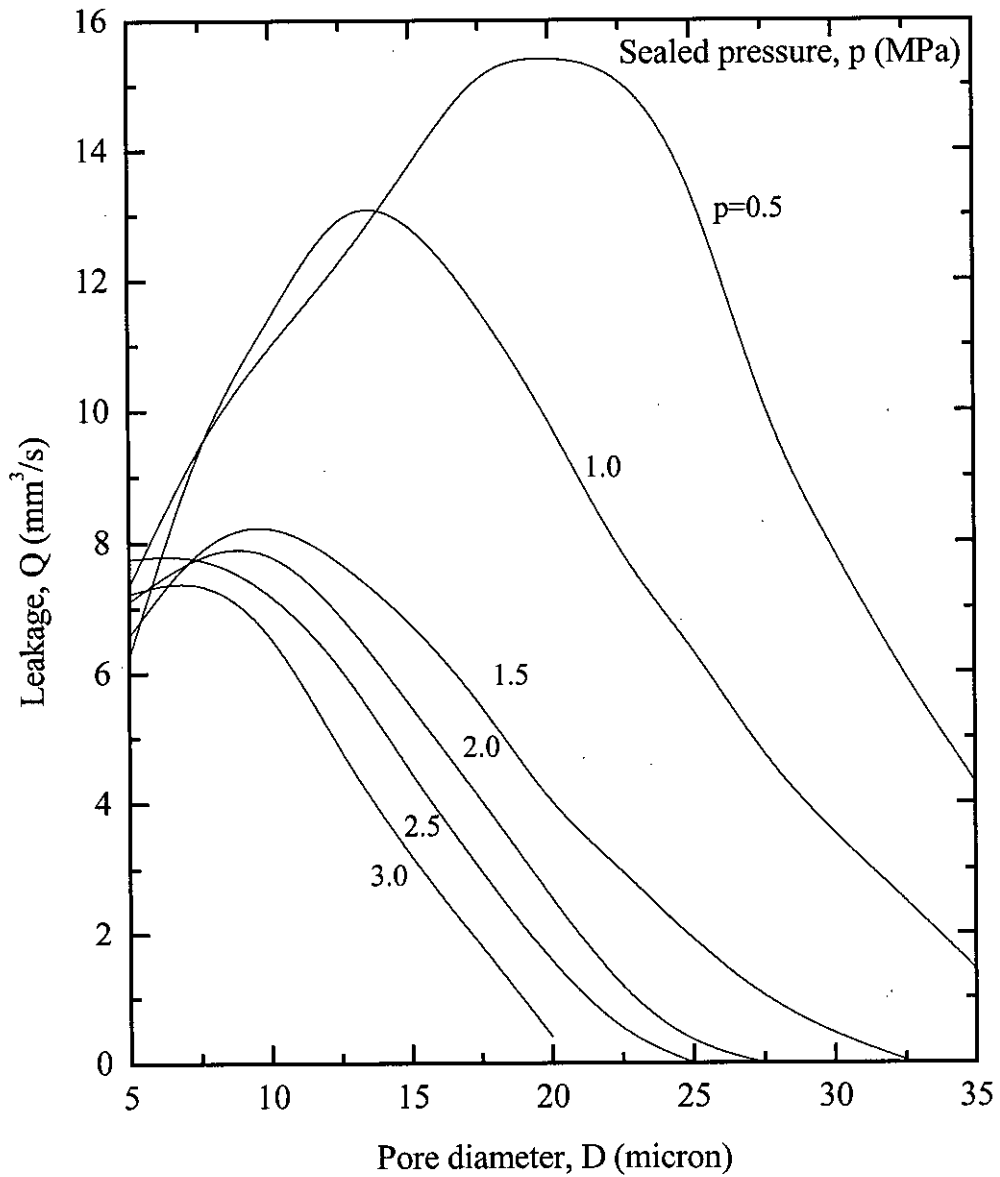Exponential pore, pore ratio 15 % and viscosity 25 m.Pa-s
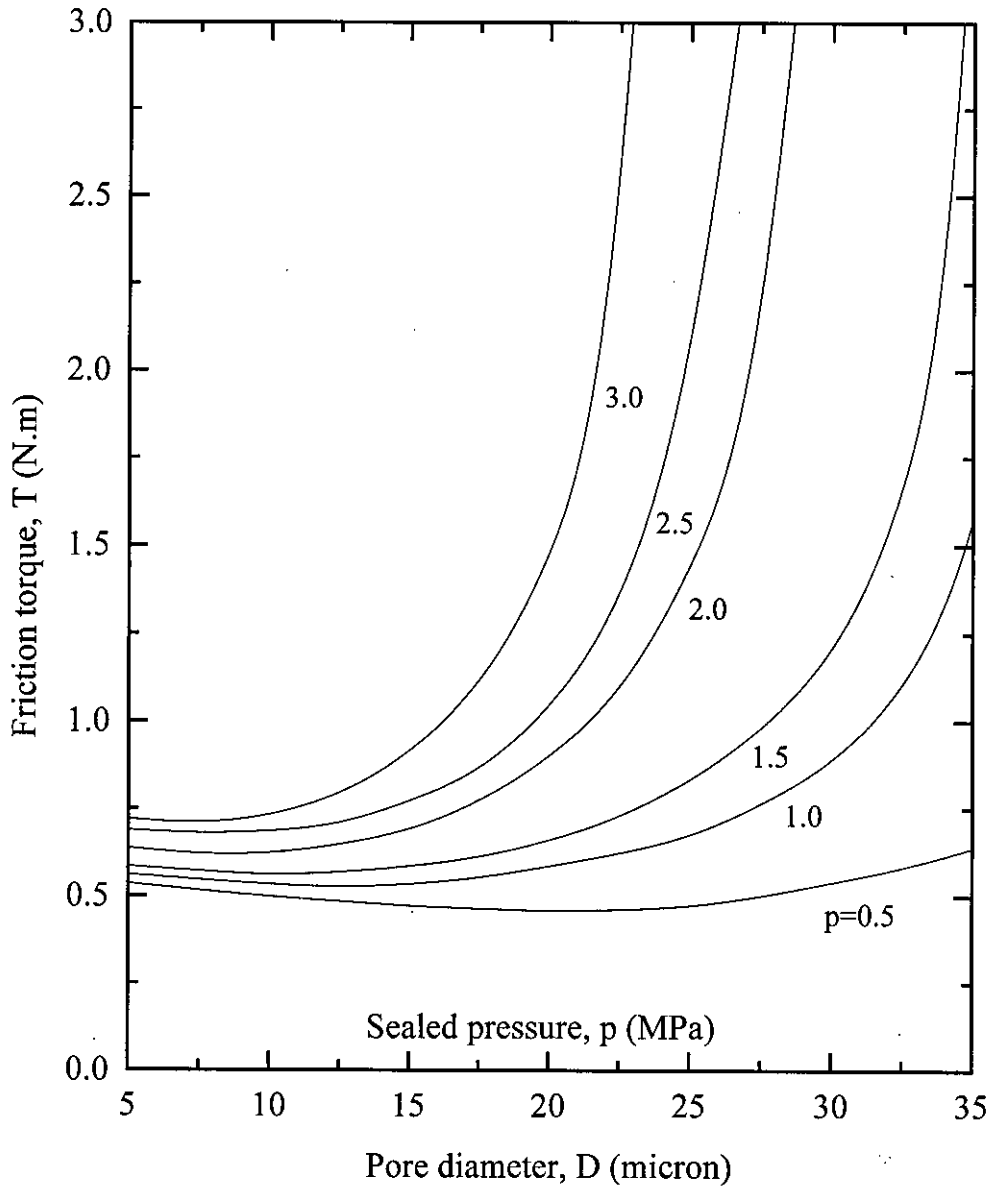
Figure 5.20: Friction torque vs. pore diameter at different sealed pressures.
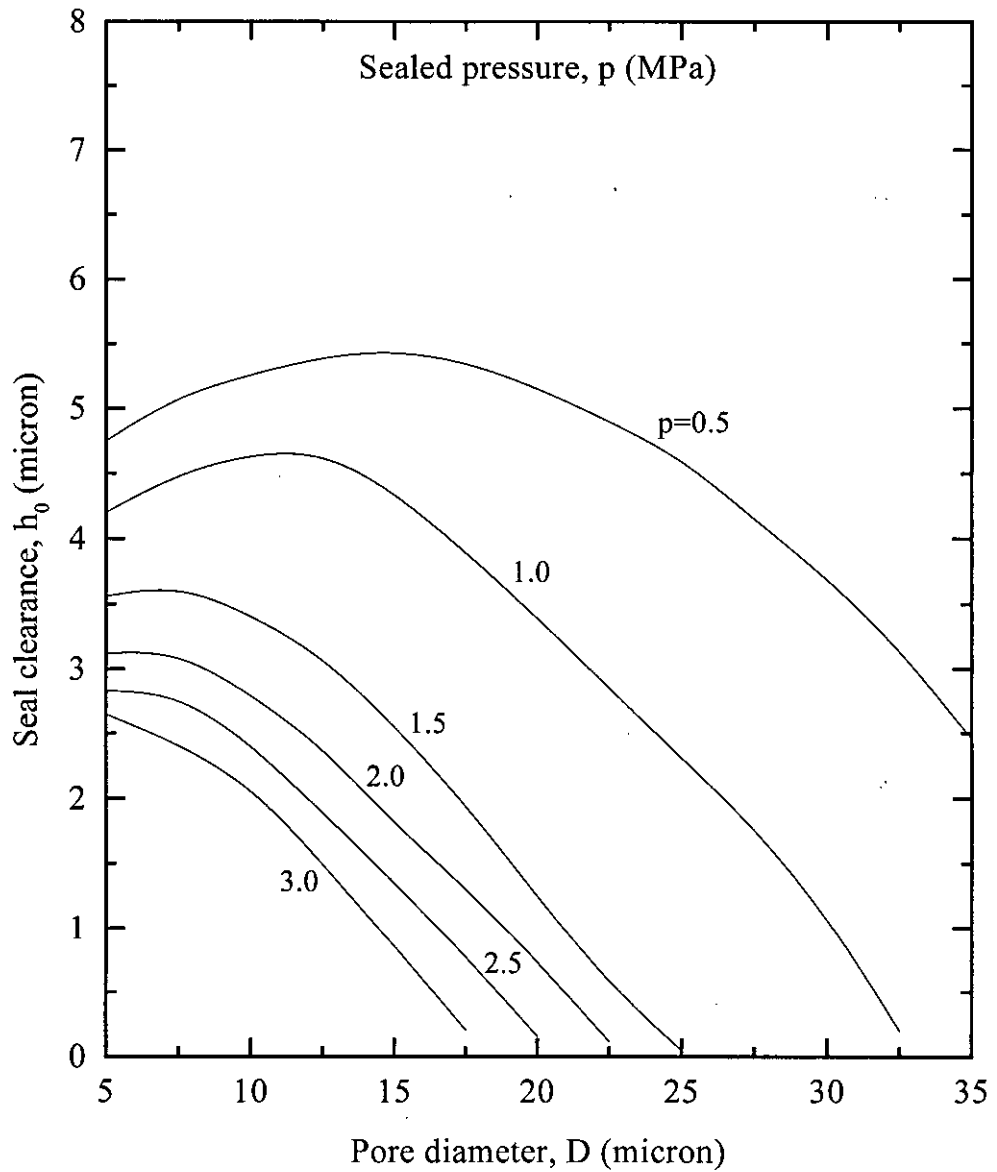Exponential pore, pore ratio 20 % and viscosity 25 m.Pa-s
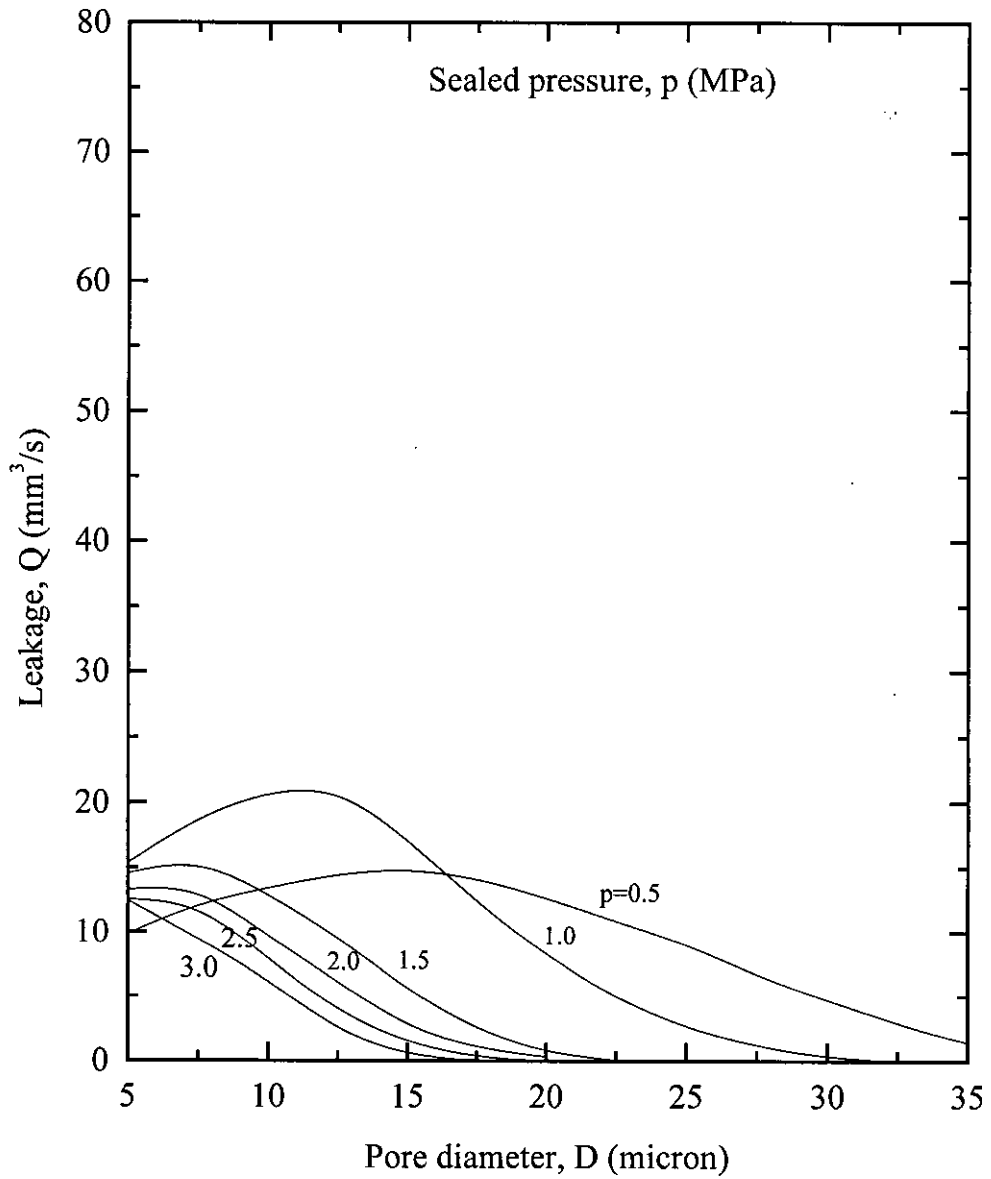
Figure 5.21: Leakage vs. pore diameter at different sealed pressures.
Exponential pore, pore ratio 2.5 % and viscosity 25 m.Pa-s
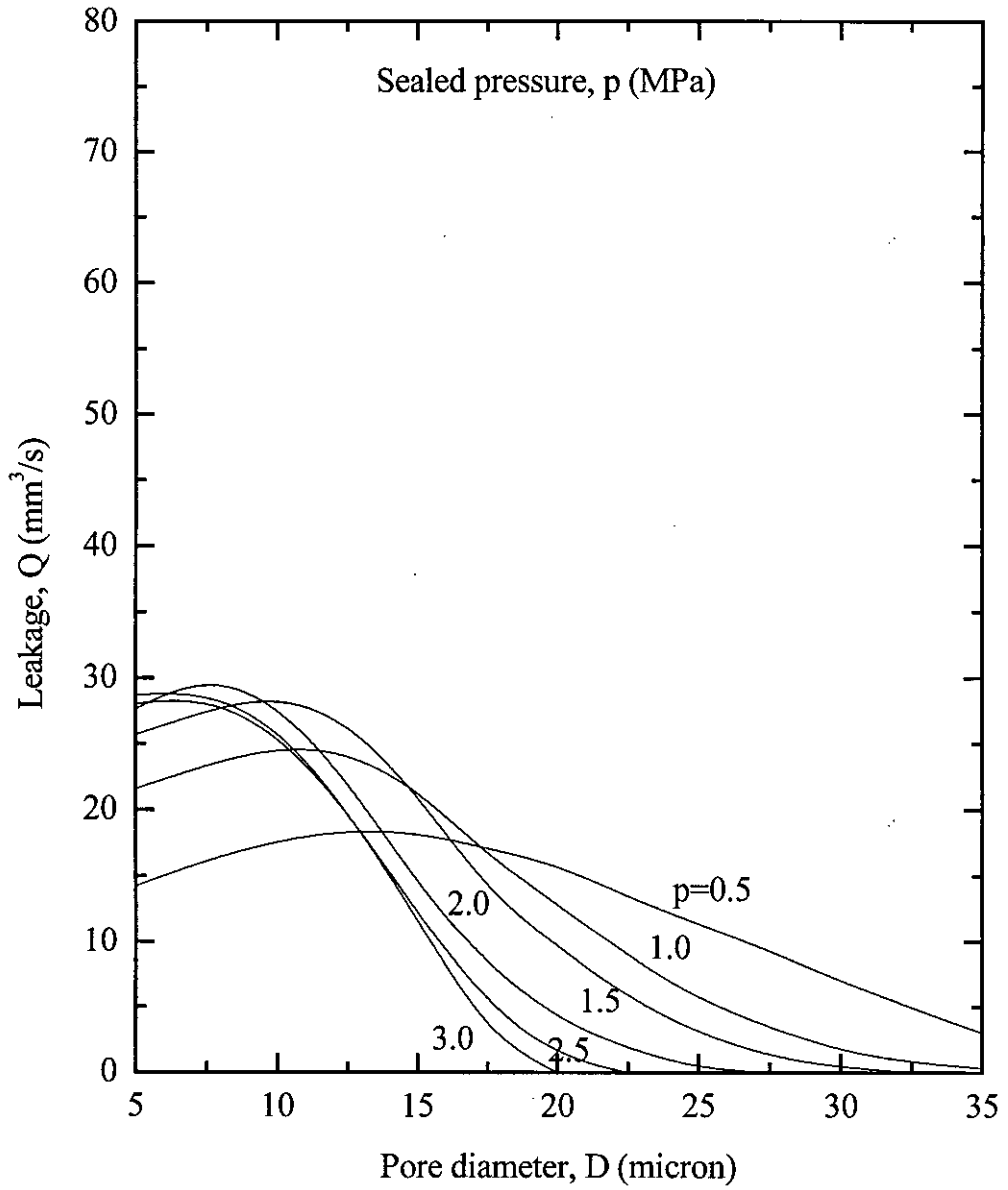
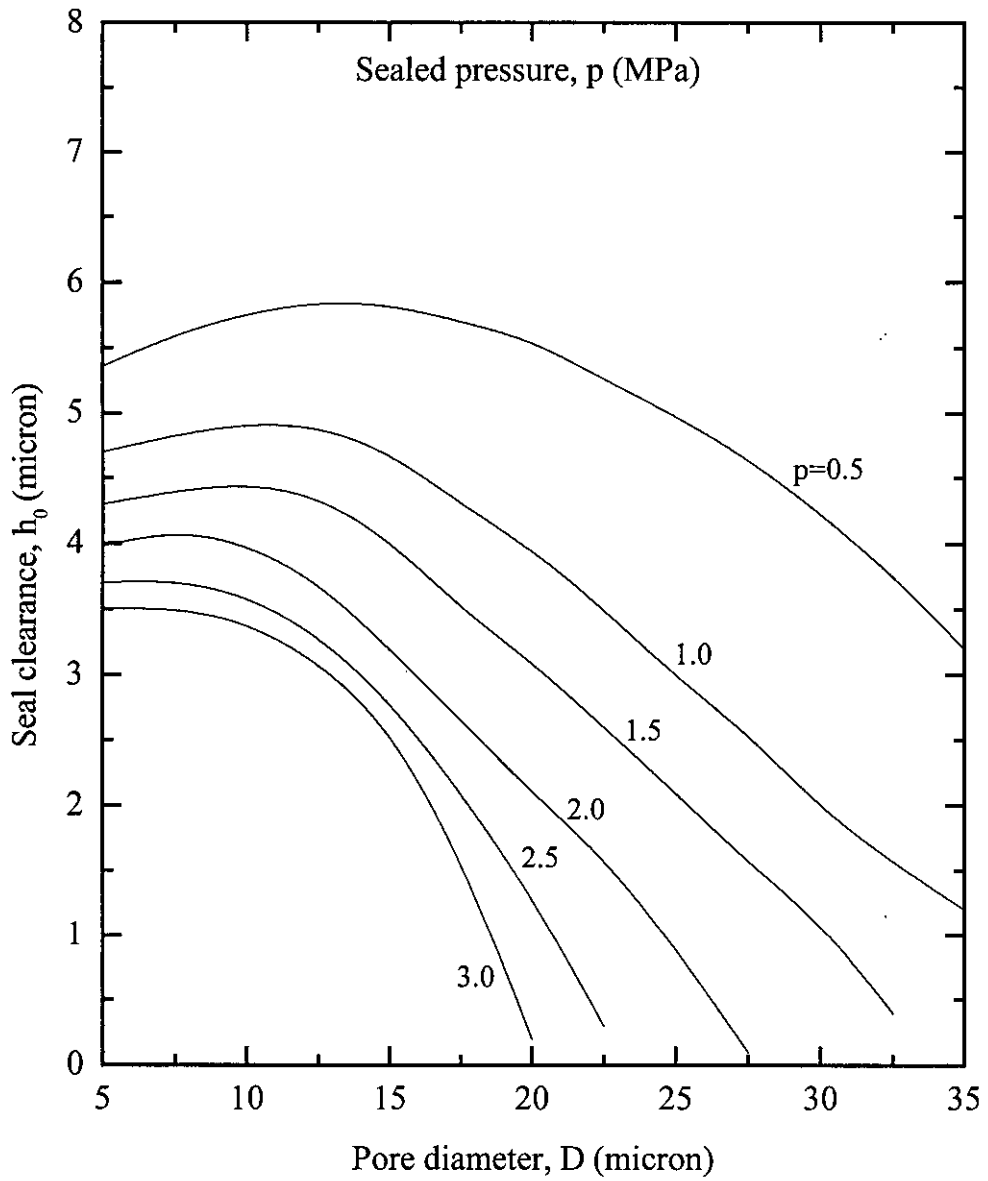Figure 5.22: Leakage vs. pore diameter at different sealed pressures.
Exponential pore, pore ratio 11.25 % and viscosity 25 m.Pa-s
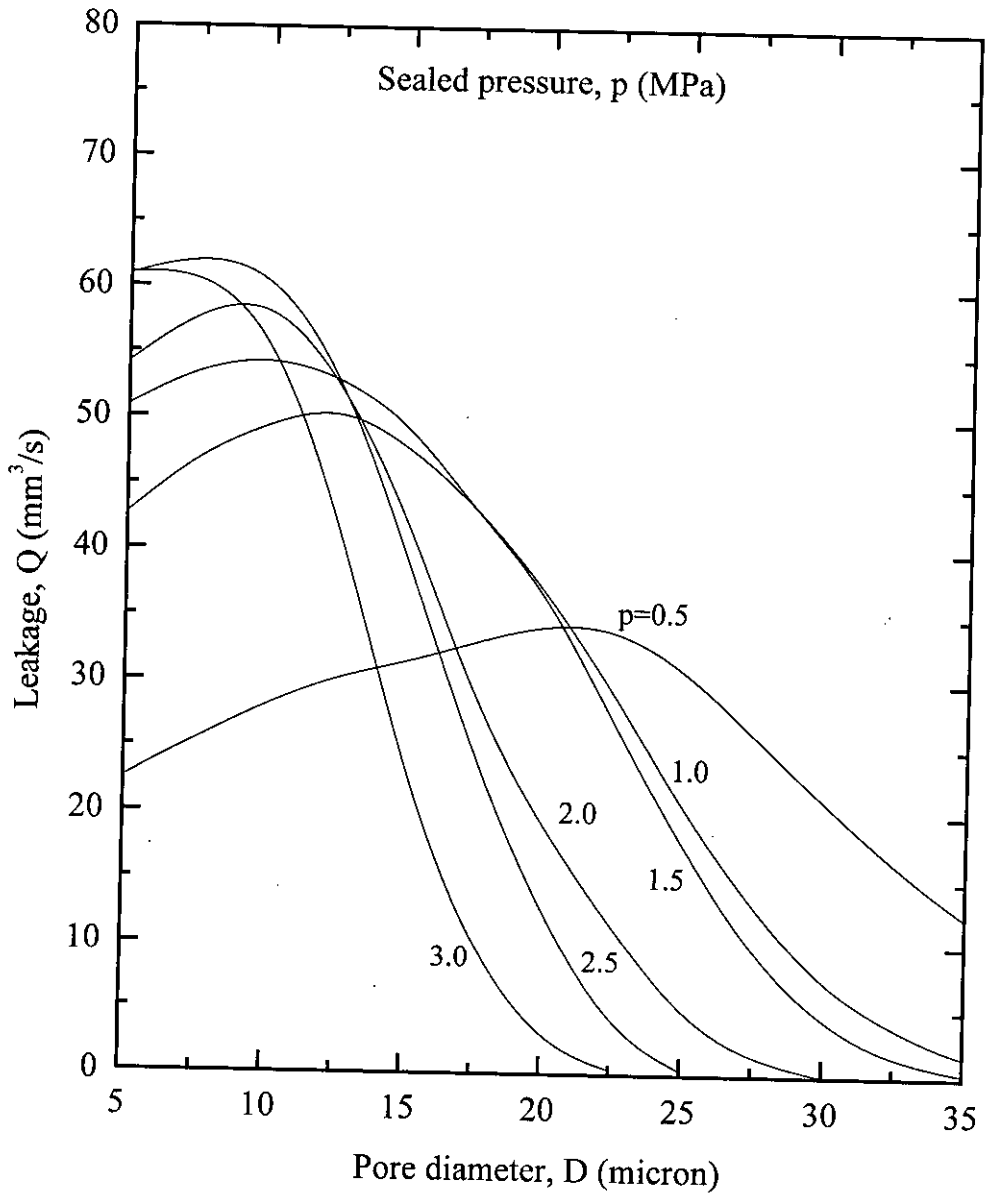
Figure 5.23: Leakage vs. pore diameter at different sealed pressures.
Exponential pore, pore ratio 15 % and viscosity 25 m.Pa-s
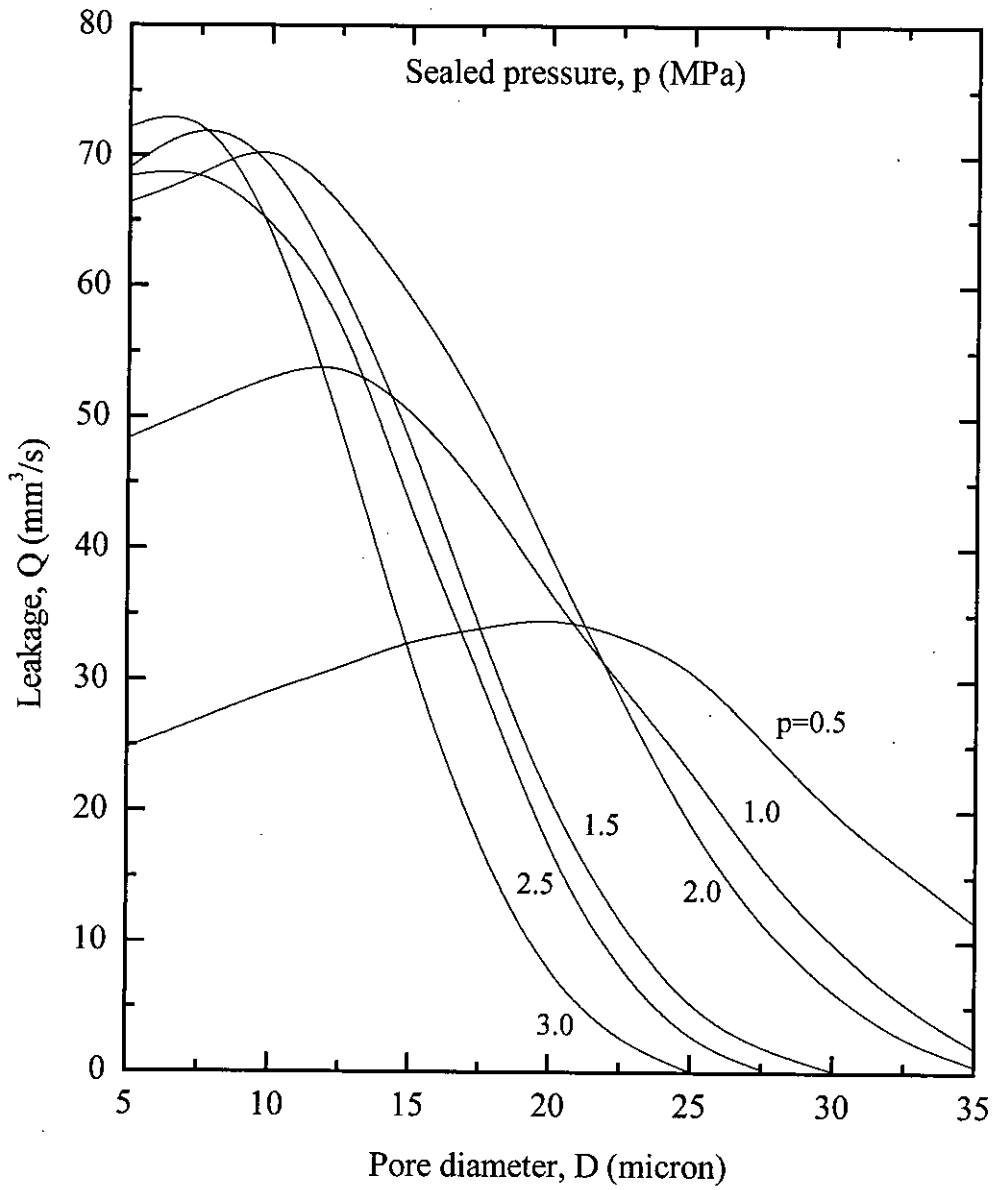
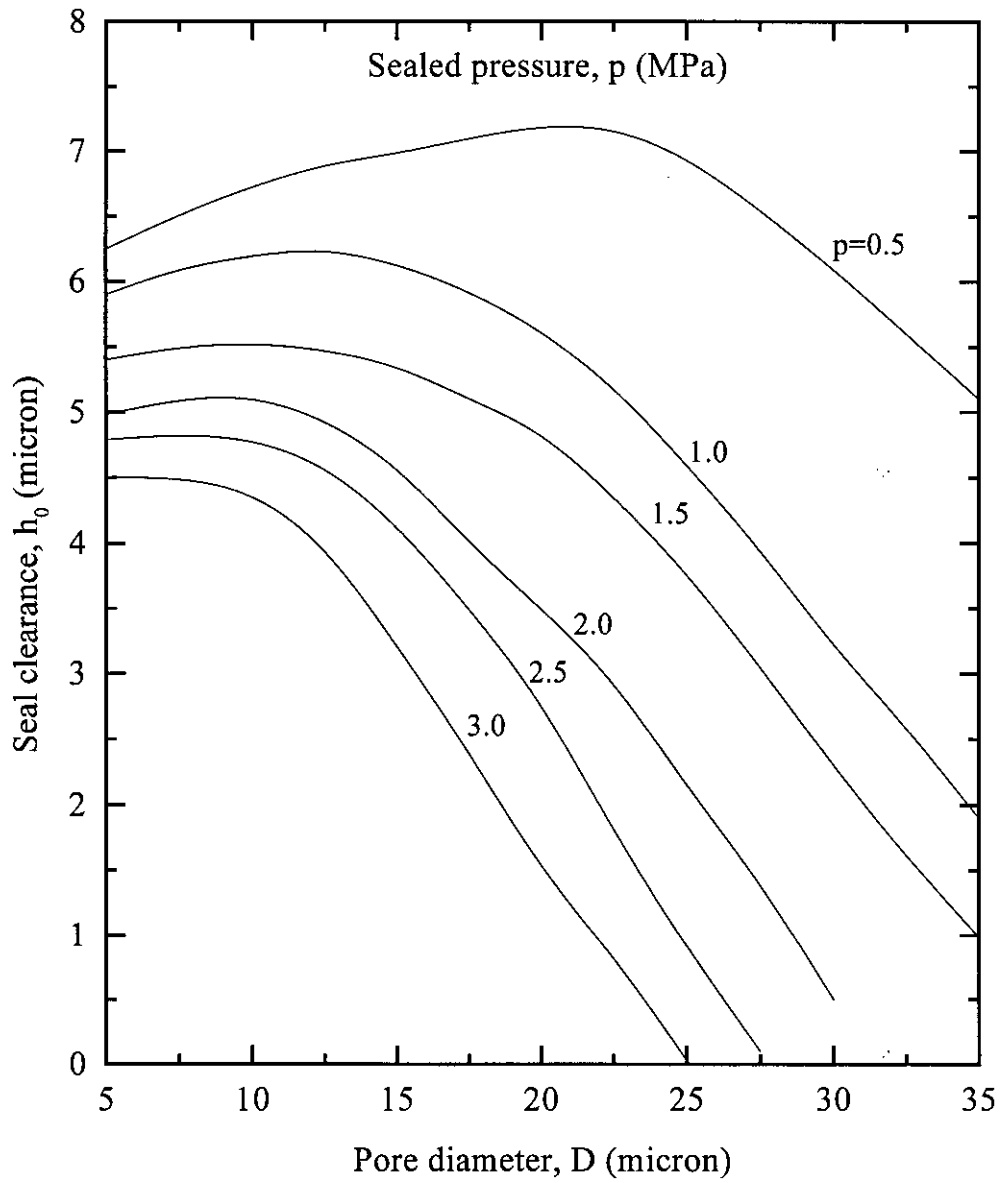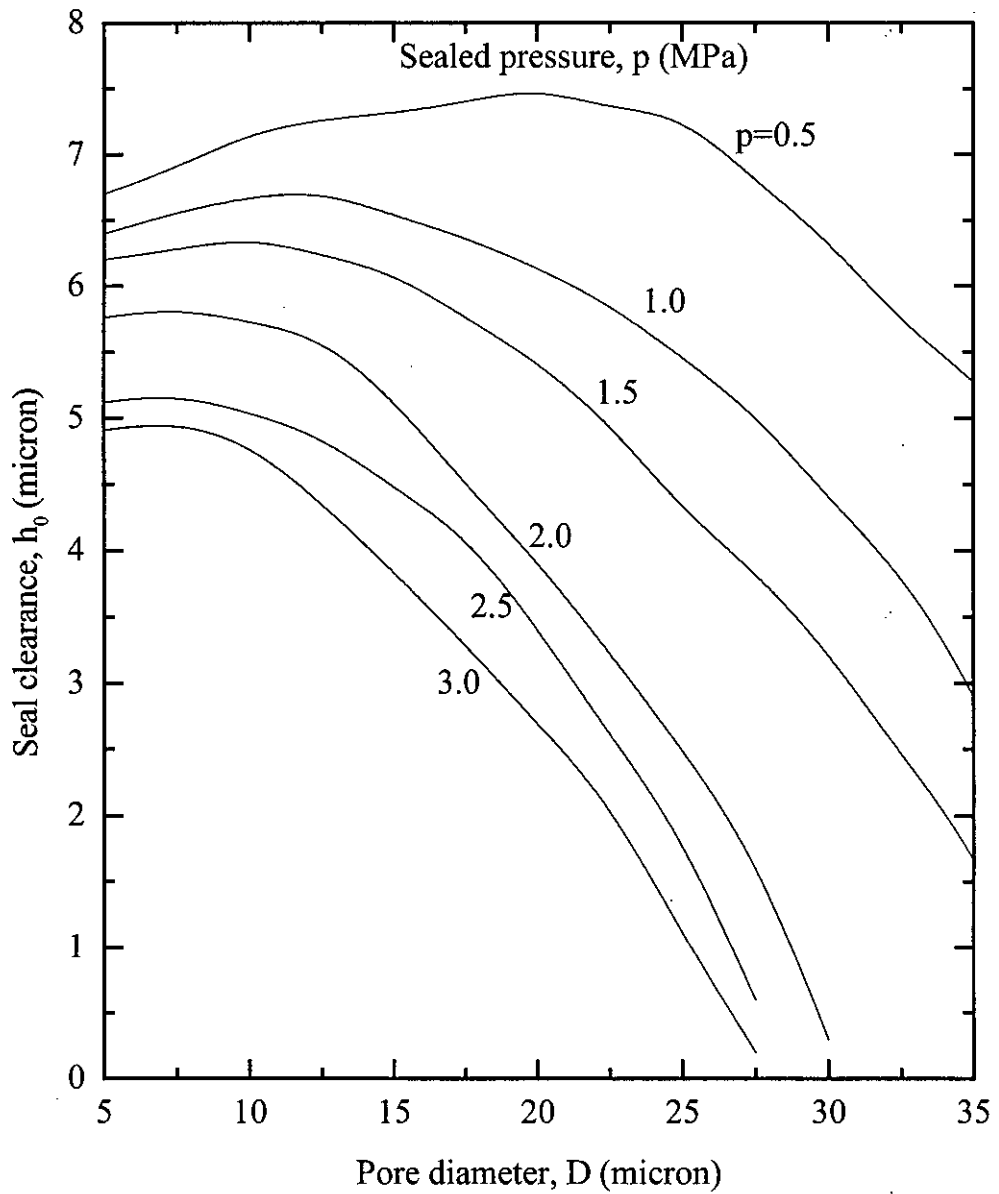Figure 5.24: Leakage vs. pore diameter at different sealed pressures.
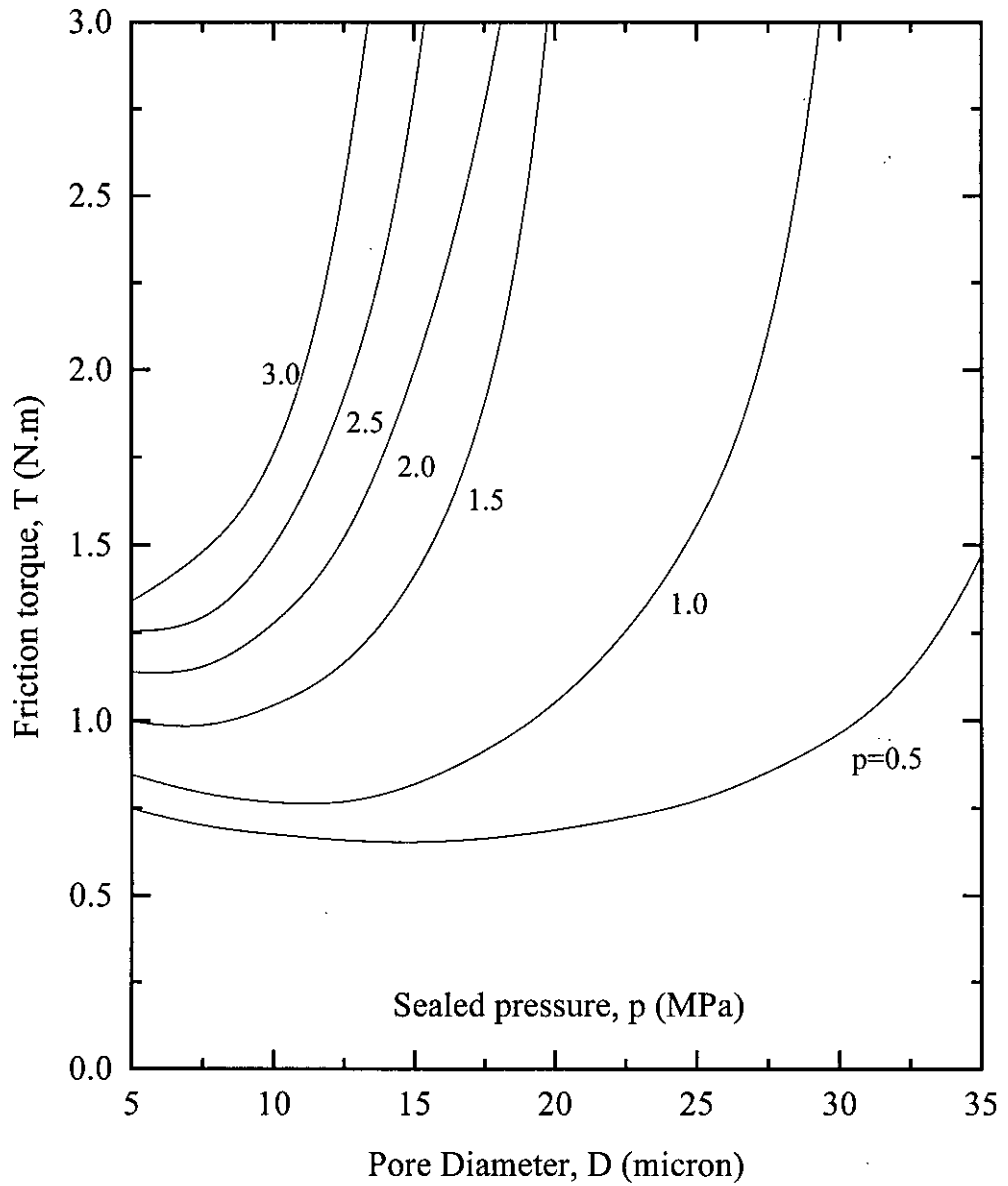Exponential pore, pore ratio 20 % and viscosity 25 m.Pa-s
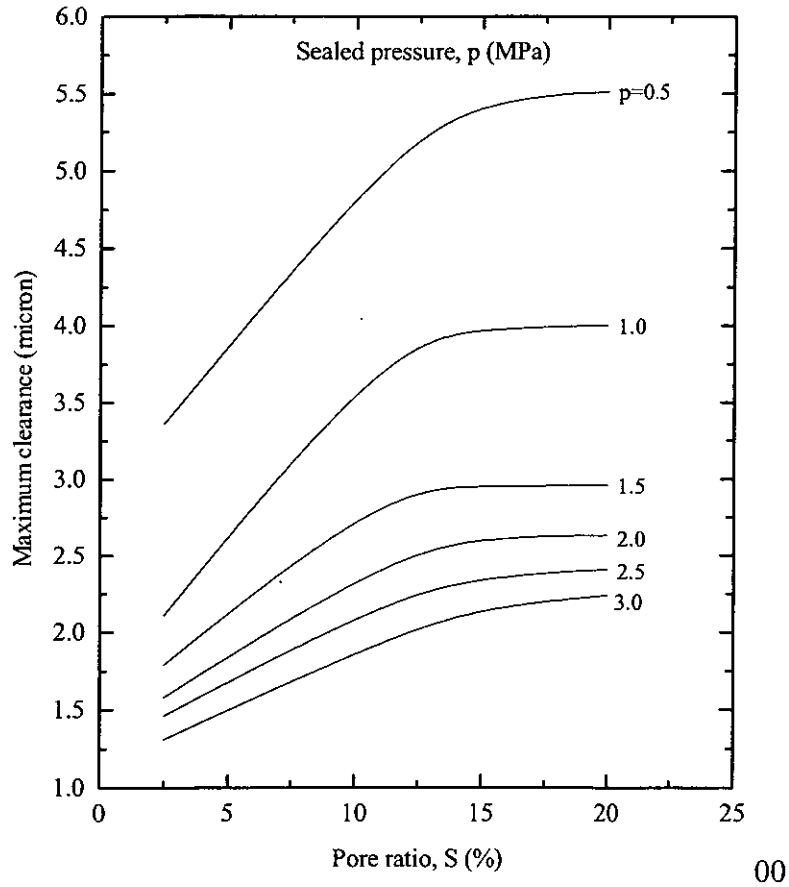
Figure 5.25: Maximum seal clearance vs. pore ratio at different sealed pressure for rectangular pore
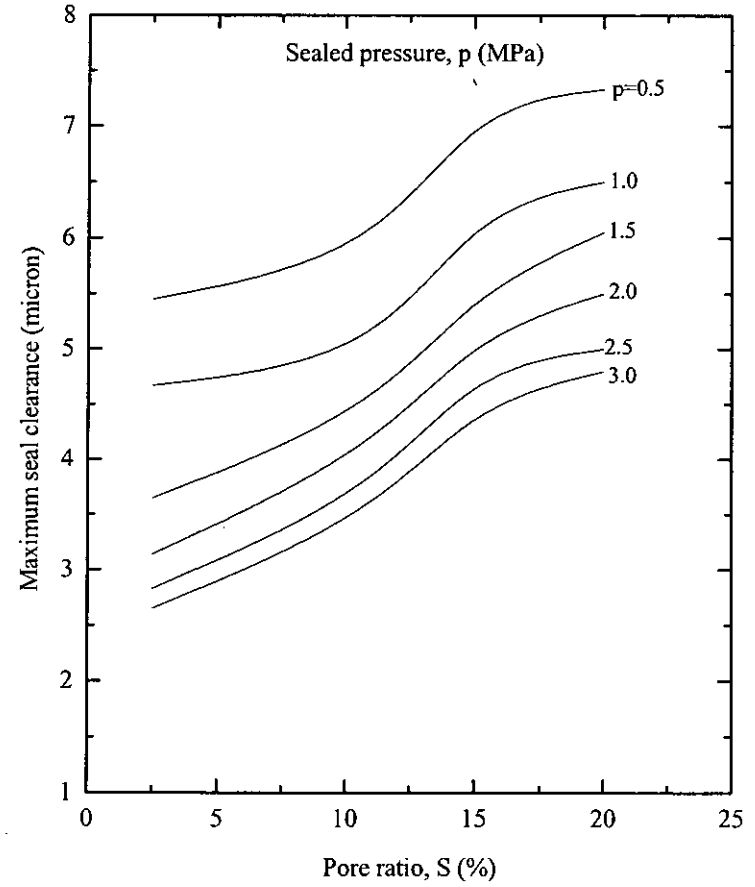
Figure 5.26: Maximum seal clearance vs. pore ratio at different sealed pressures for exponential pore
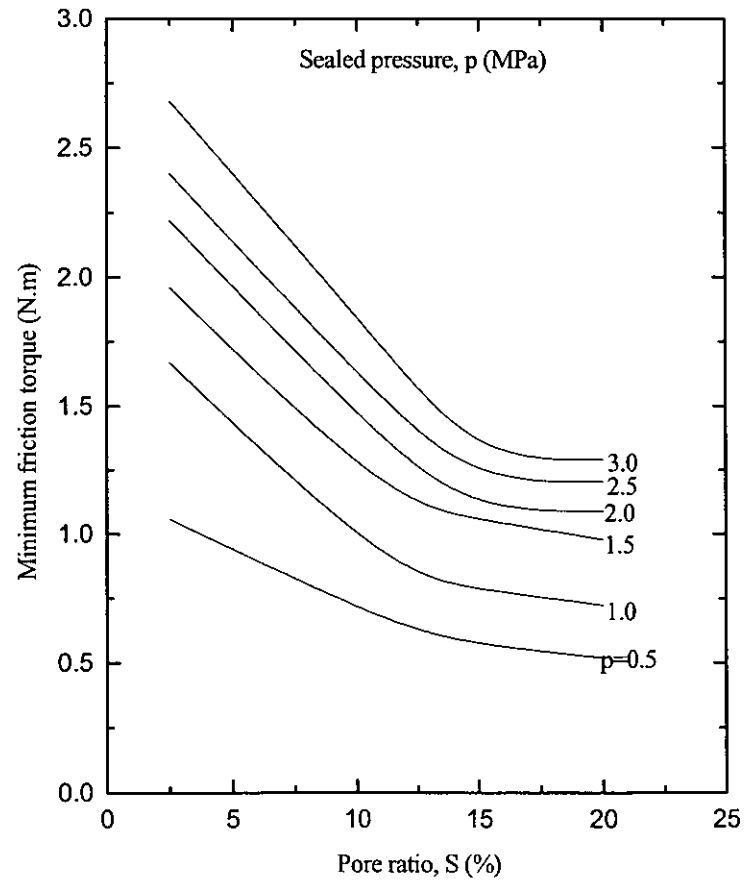
Figure 5.27: Minimum friction torque vs. pore ratio at different sealed pressures for rectangular pore
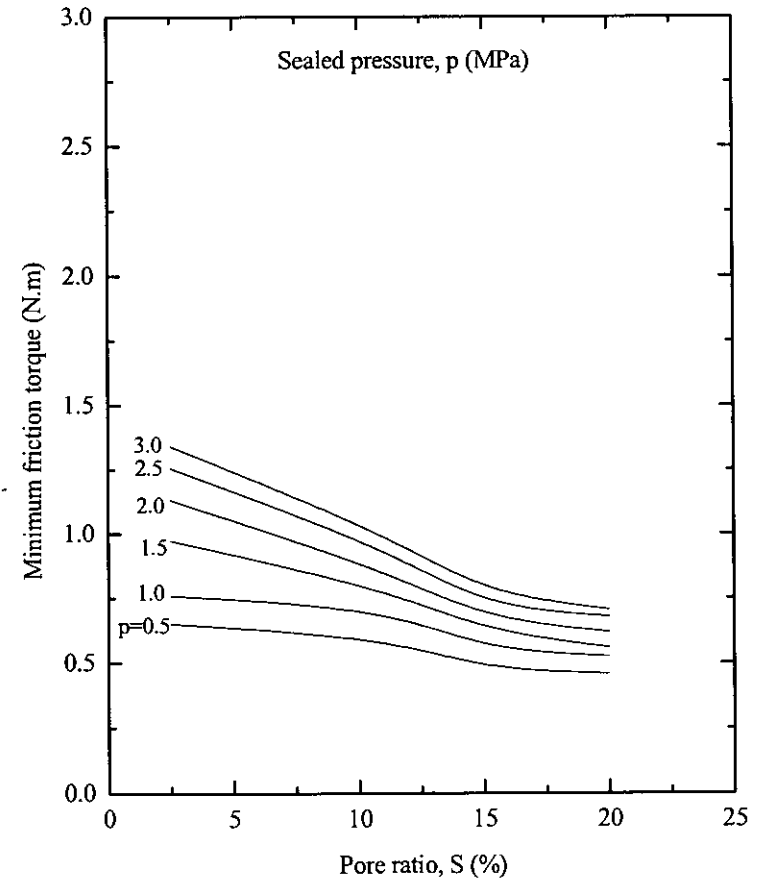
Figure 5.28: Minimum friction torque vs. pore ratio at different sealed pressures for exponential pore
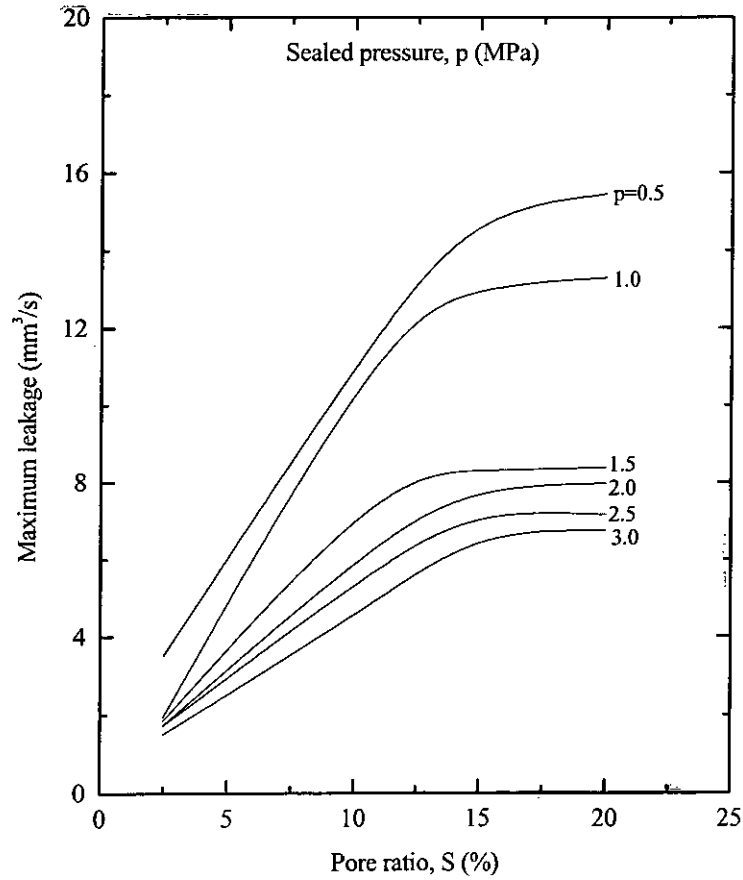
Figure 5.29: Maximum leakage vs. pore ratio at different sealed
pressures for rectangular pore
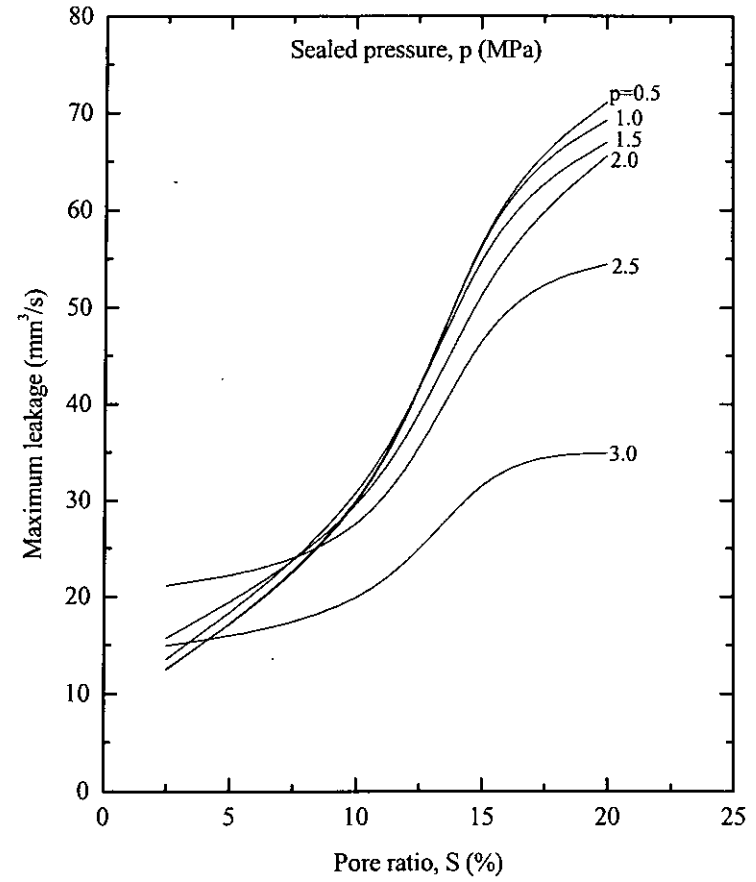
Figure 5.30: Maximum leakage vs. pore ratio at different sealed
pressures for exponential pore
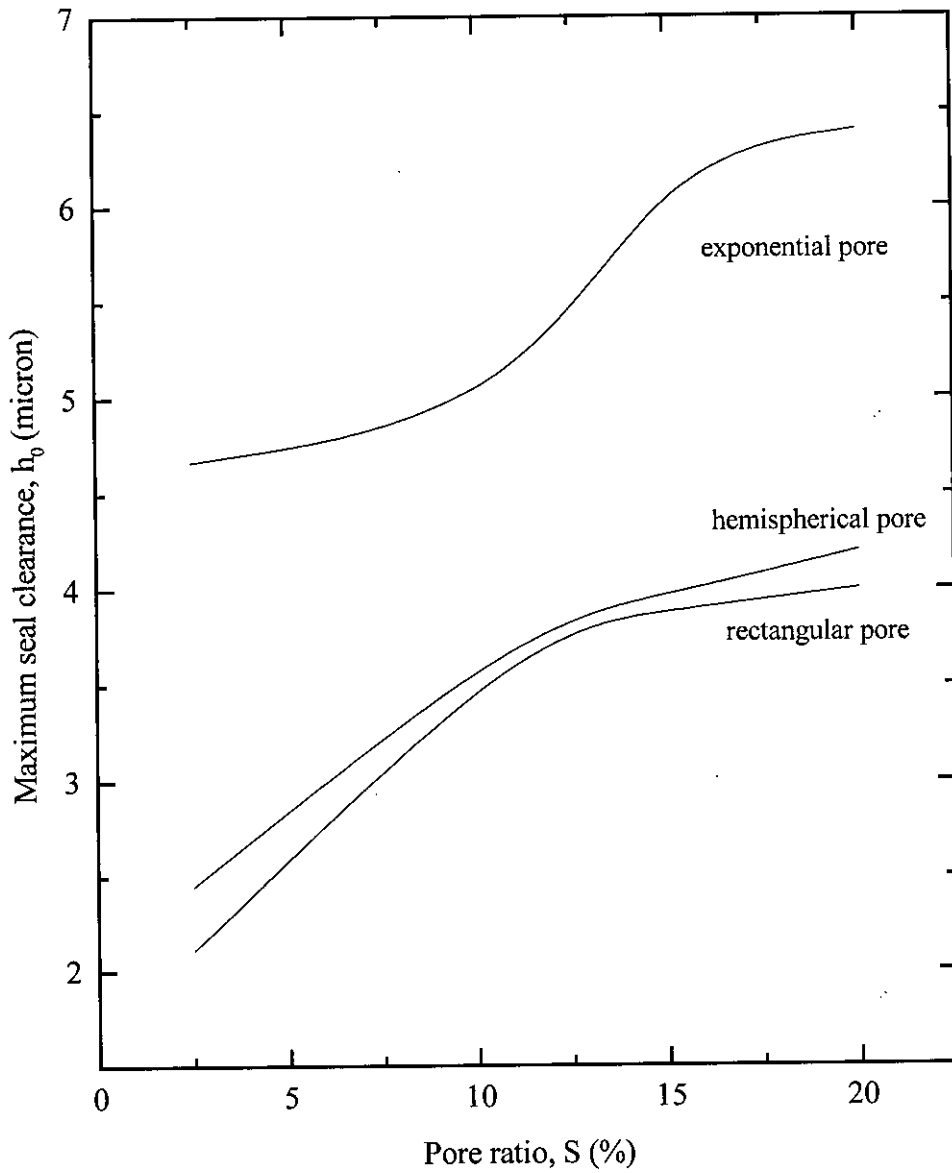
Figure 5.31: Relationship of maximum seal clearance vs. pore ratio among different pore geometries at sealed pressure of 1.0 MPa
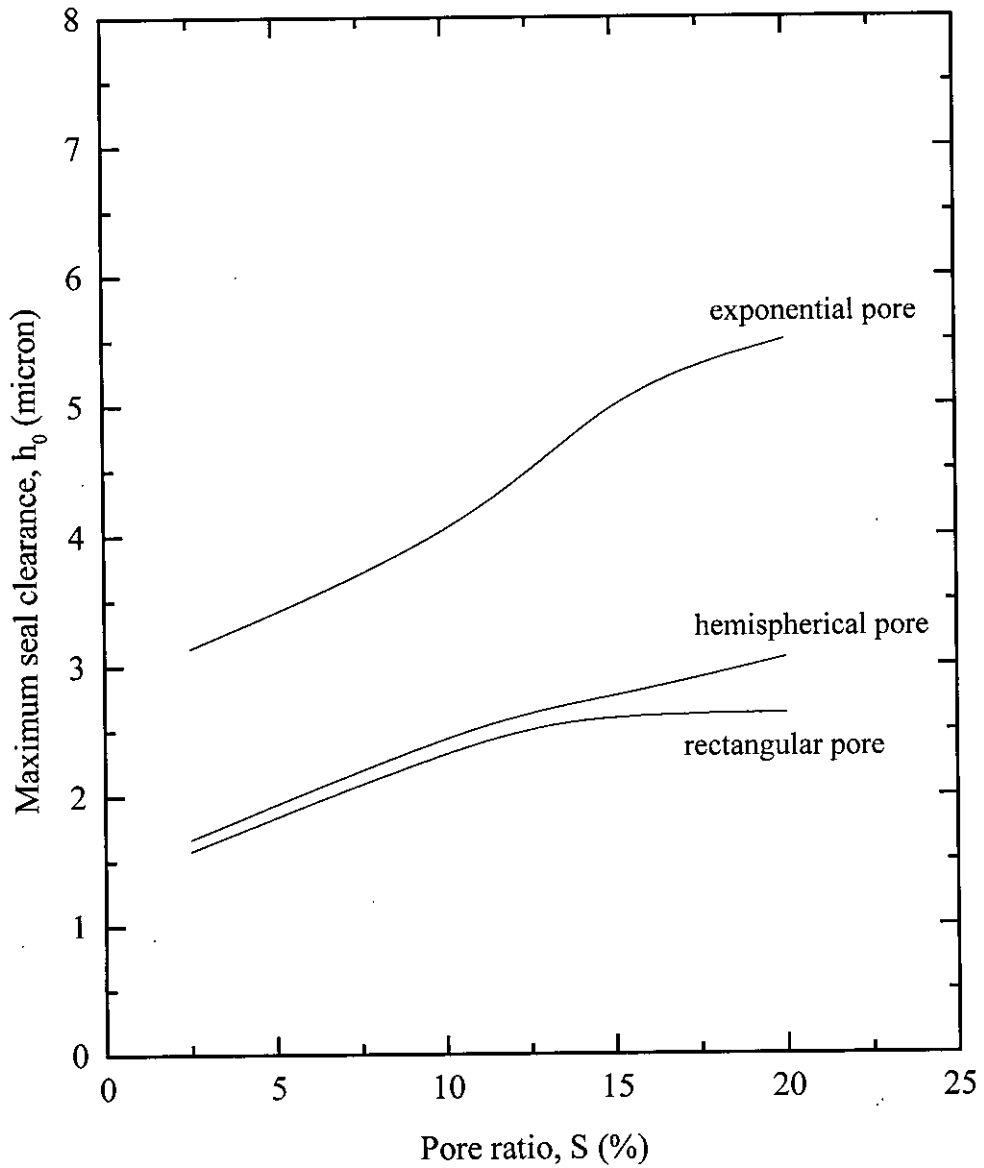
Figure 5.32: Relationship of maximum seal clearance vs. pore ratio among different
pore geometries at sealed pressure of 2.0 MPa
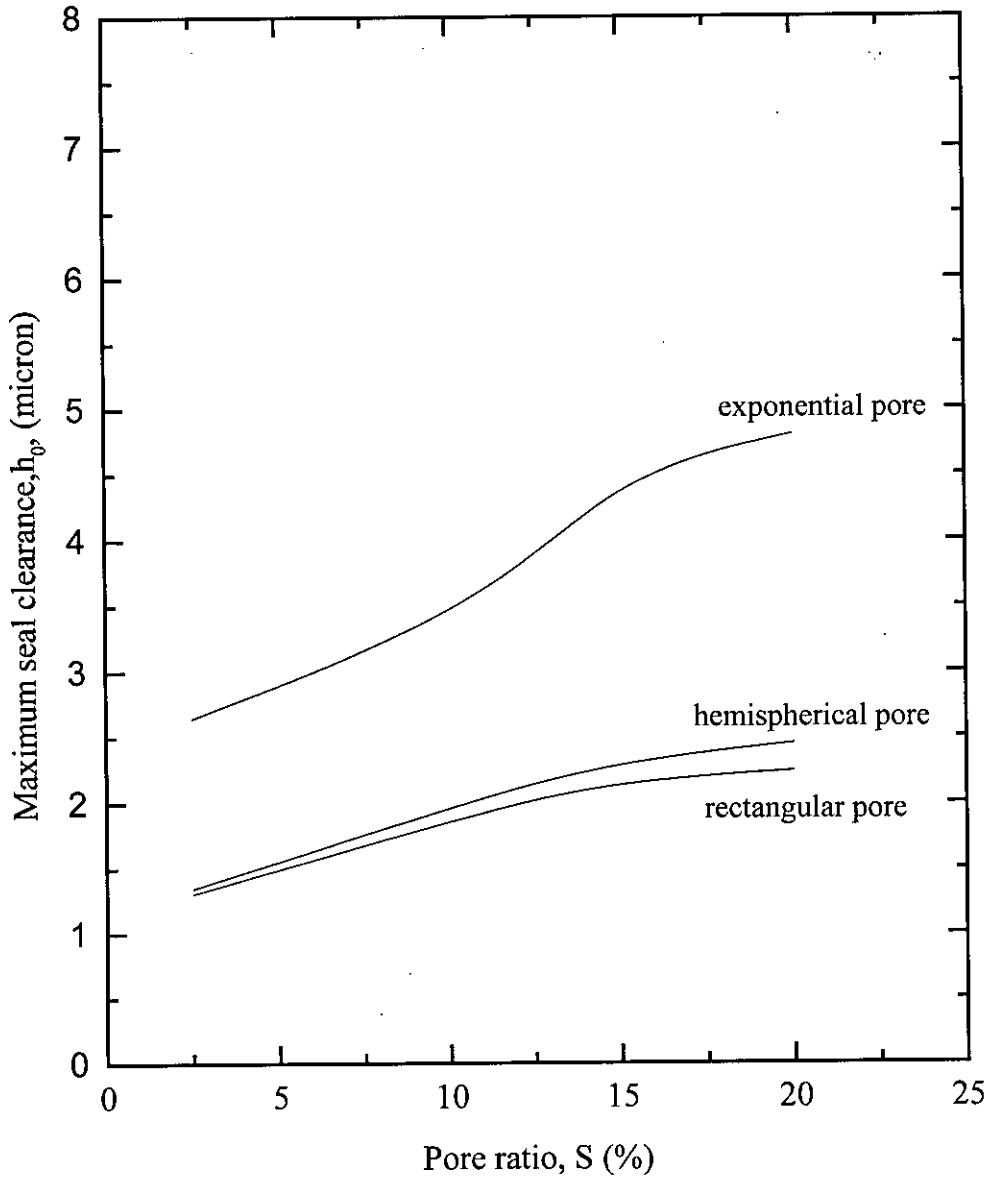
Figure 5.33: Relationship of maximum seal clearance vs. pore ratio among different pore geometries at sealed pressure of 3.0 MPa
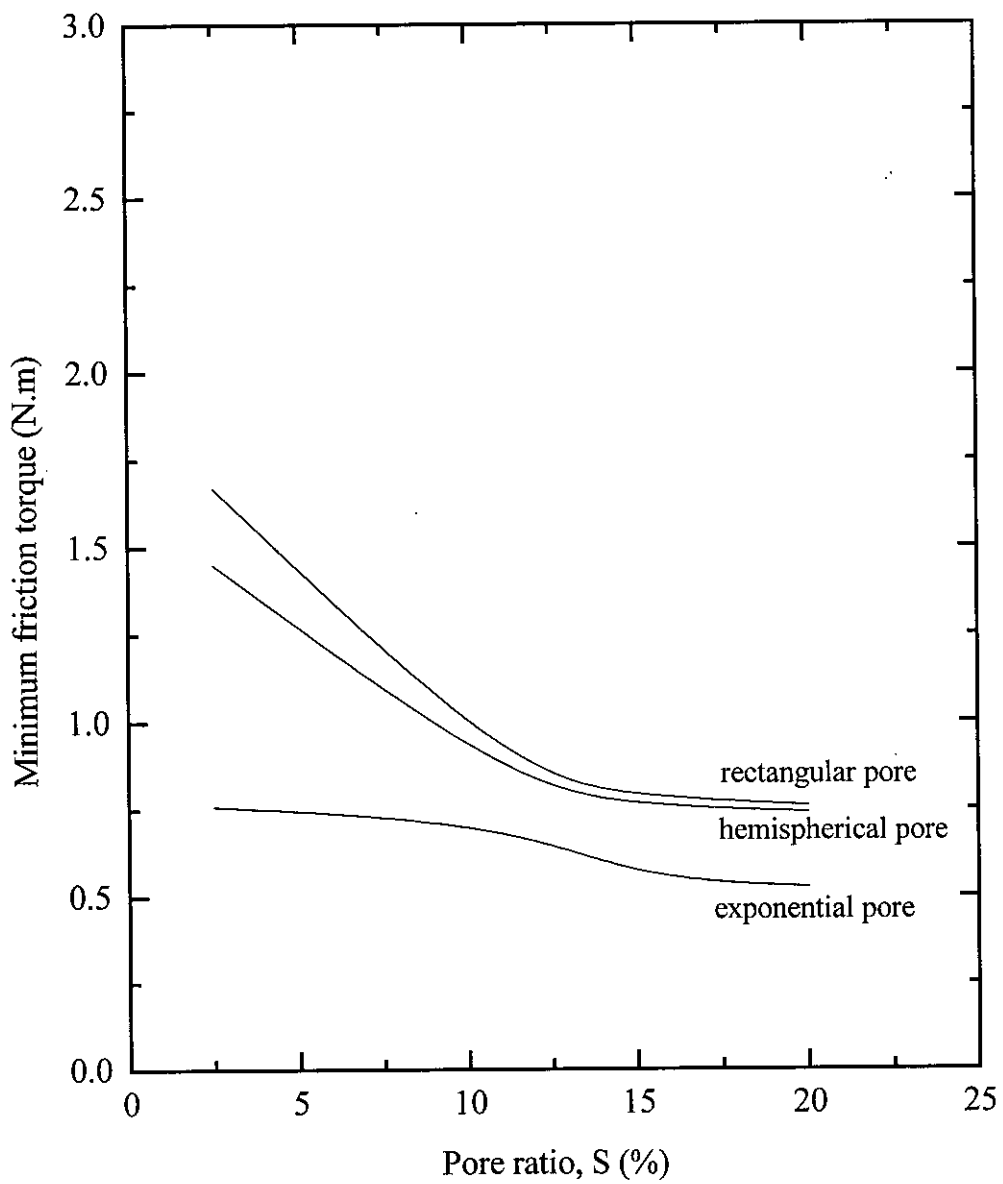
Figure 5.34: Relationship of minimum friction torque vs. pore ratio among different pore geometries at sealed pressure of 1.0 MPa
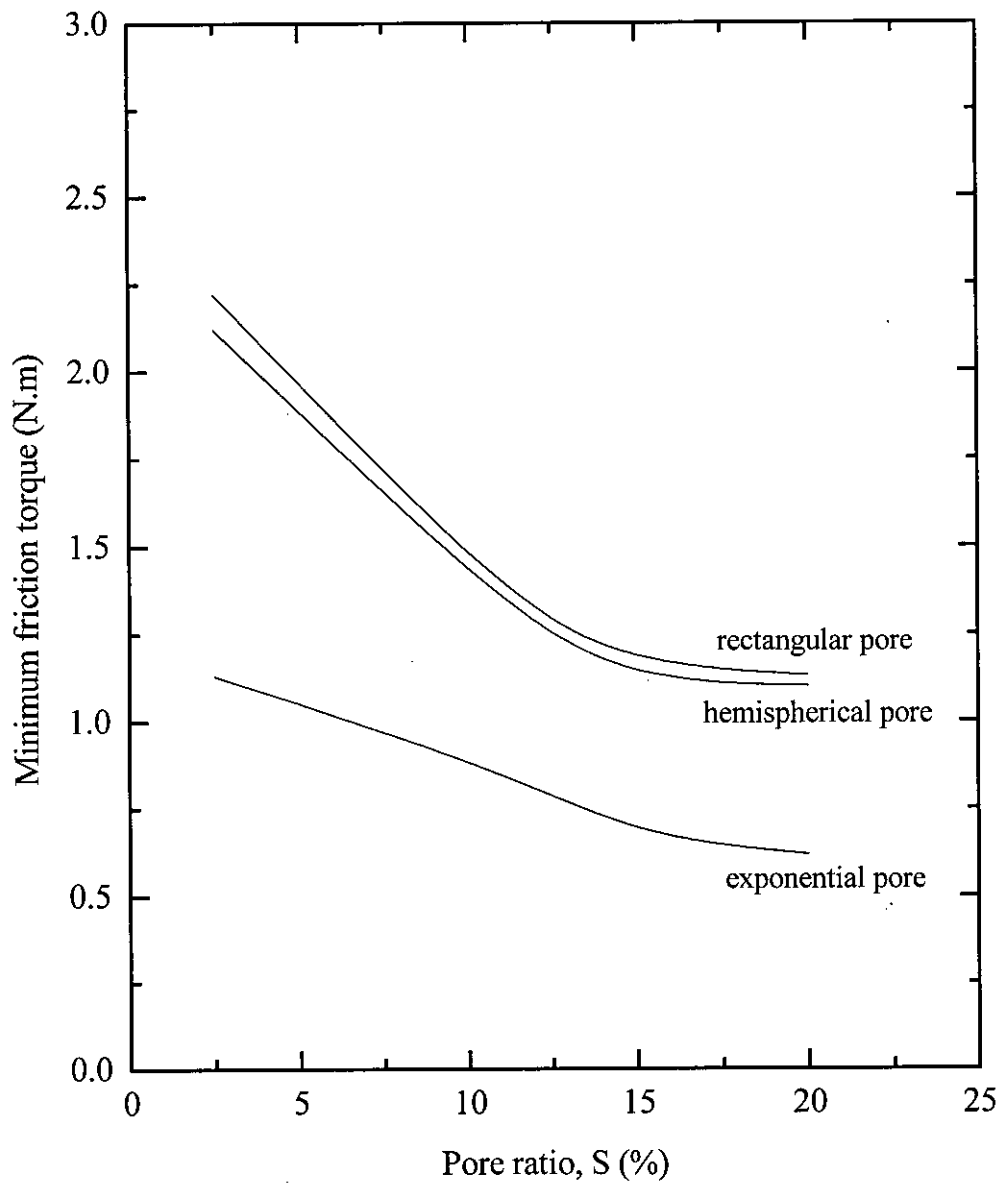
Figure 5.35: Relationship of minimum friction torque vs. pore ratio among different pore geometries at sealed pressure of 2.0 MPa
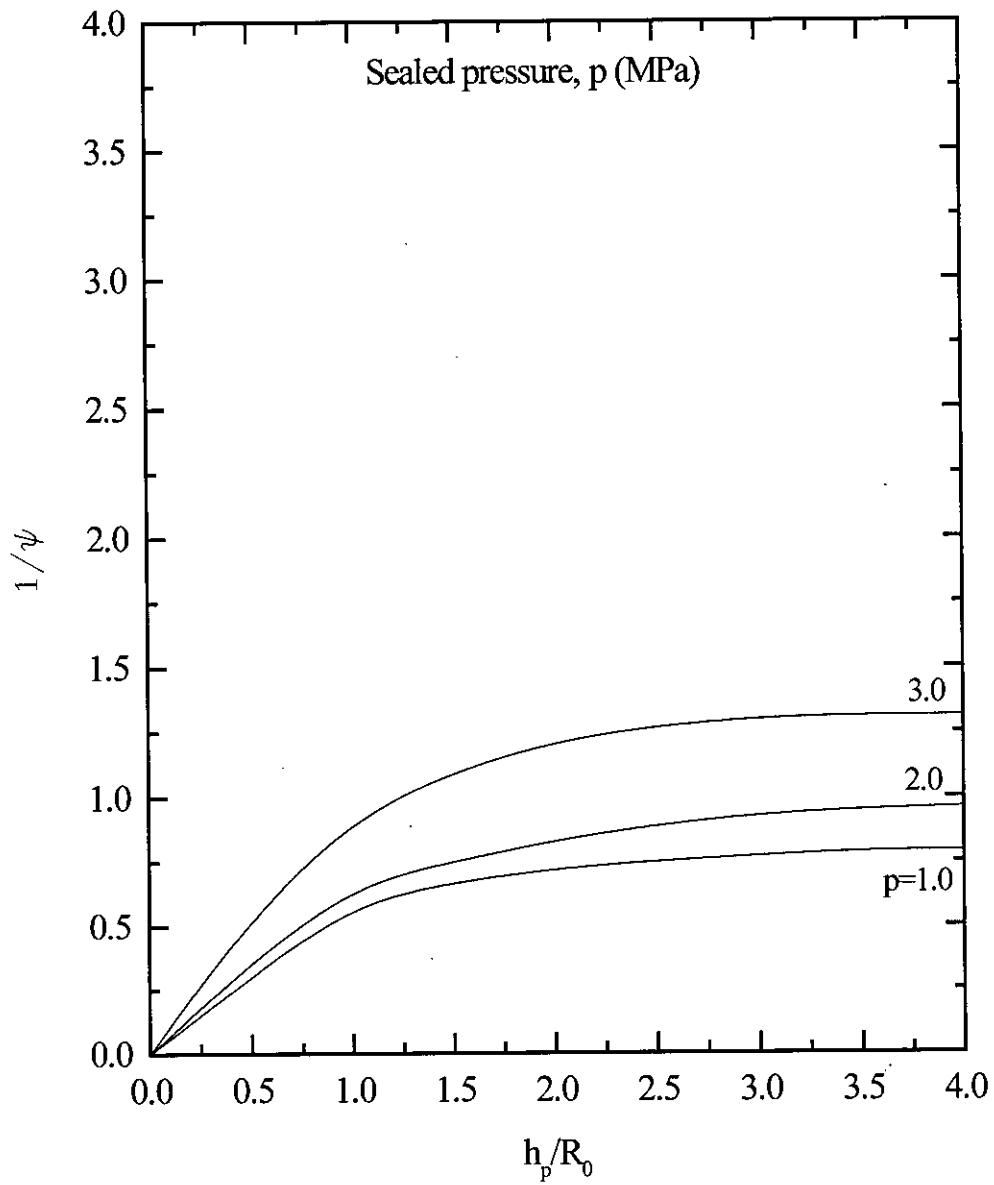
Figure 5.36: Relationship of $1/\psi$ vs. h_p/R_0 at different sealed pressures. Rectangular pore, pore ratio 20%
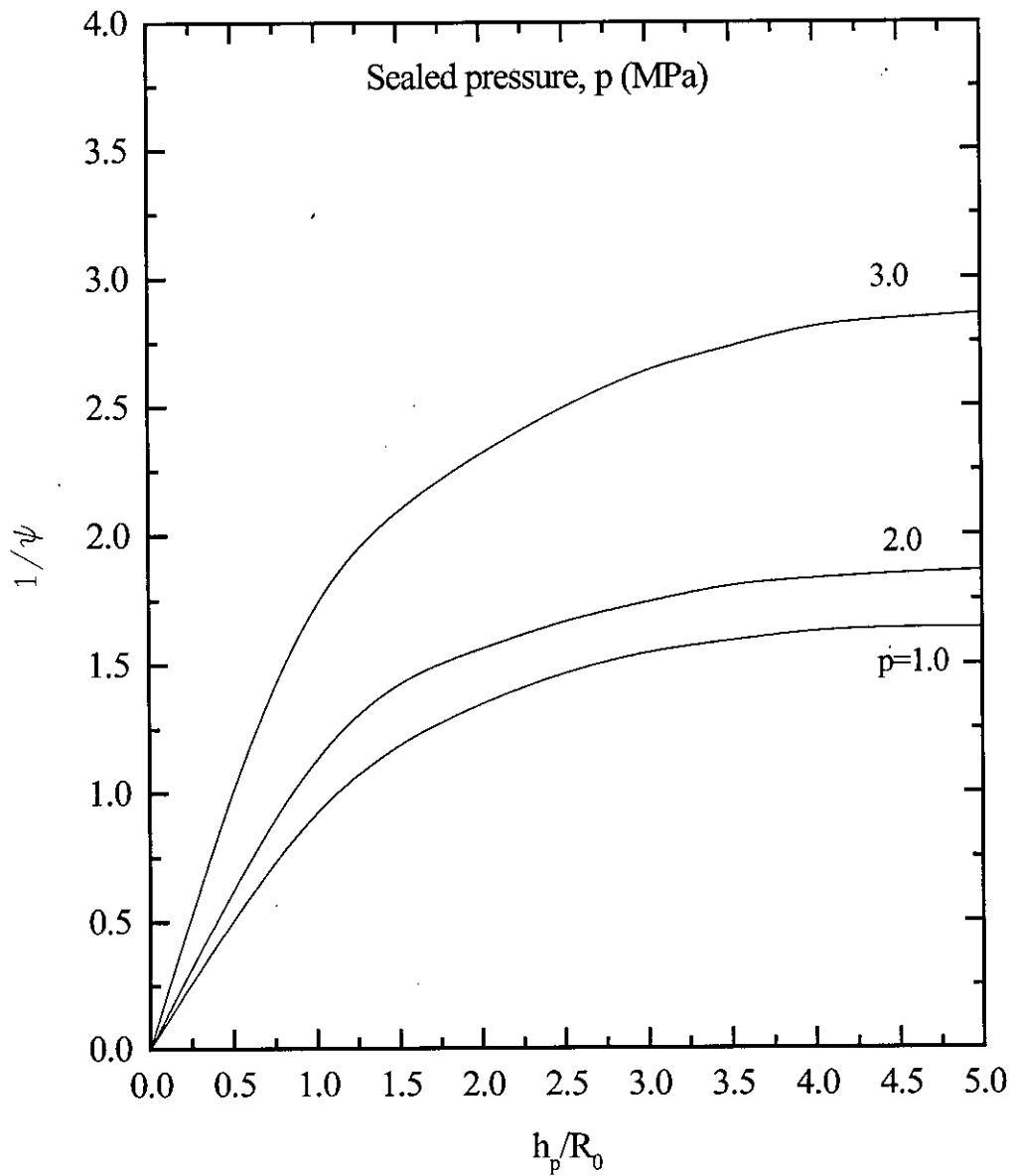
Figure 5.37: Relationship of $1/\psi$ vs. h_p/R_0 at different sealed pressures. Exponential pore, pore ratio 20%

Appendix A

BASIC CONCEPTS

A.1 SURFACE TOPOGRAPHY

Friction is related to the surface topography of interacting surfaces. All real surfaces are composed of texture and structure at both macroscopic and microscopic levels. Texture is related to roughness, waviness and lay of a surface, excluding form error, whereas structure is related to its geometric features. While roughness constitutes shorter wavelength components of a surface profile, form represents longer wavelengths. Waviness lies somewhere in between, on this scale. Lay relates to the directionality in the texture. Surface texture of all manufactured surfaces (also called as engineered surfaces), is determined by the machining operation that it underwent before. Essentially, it is the result of a combined effect of the geometry of the tool and its kinematics during machining. Surface texture can be produced and also measured. Measurements are done by a variety of methods including profilometry, cartography, optical interference and field emission microscopy.

When an apparently smooth machined surface is viewed under a microscope, a number of randomly distributed peaks and valleys of varying heights are observed. Each such element is termed as an asperity. Generally the peaks contribute to the friction whereas the valleys serve as reservoirs for lubricant that is used to reduce friction

A.2 ACTUAL AND MODEL SURFACES

The geometry of an engineered surface is truly random. To represent it deterministically, it is customary to consider the actual random asperities as a selection of different sizes of ideal shapes such as cubes, cones and spheres. A linear profile idealizes saw tooth and sinusoidal asperity models.

Since the idealized shapes bear little resemblance to the actual surface, a few techniques could be used to improve the model. One of them is to represent all the three basic shapes in one model with uniform height. A second method is to consider one basic shape but, with different heights. And a third method is to maintain the same height but use randomness of shape and spacing. Though the actual surface is truly random, the following simplifications are necessary for modeling purposes.

- Instead of an entire length, a representative portion is considered, based on the assumption that there is repeatability in profile.

- This profile is assumed to the isotropic.

- The size, spacing and shape of an asperity are also assumed to be the same all over the sample.

These techniques, though used for random surfaces, are particularly well suited for our patterns of repeated features

A.3 FRICTION

Friction is a dissipation mechanism in which energy gets converted to heat and cannot be utilized. It occurs at the interface of any two contacting bodies when sliding, rolling or separation takes place between them and tends to oppose the very force that causes the relative motion. Friction is usually accompanied by wear, which is a material removal process. Similar to wear, friction is aggravated by contamination, corrosion or environmental degradation. Both friction and wear are minimized by lubrication.

Based on the nature of contact between two surfaces, two broad distinctions of friction can be made when hardness of the two contacting surfaces differs widely or slightly. These are the metal-on-metal and elastomer-on-rigid surface contacts respectively.

A.4 LUBRICATION

Surface to surface contact can be prevented by a lubricant, a viscous fluid that can withstand shear loads. Lubrication is the process of introducing such a fluid film to reduce wear and frictional resistance, and also to carry away the heat produced at the interface. Viscosity, that represents the internal friction of a fluid, relates the local stresses in a moving fluid to its strain rate.

When a fluid is sheared, it begins to move at a strain rate inversely proportional to a property called its coefficient of viscosity, μ, obtained from the well-known equation,

$$\tau = \mu \frac{du}{dy} \tag{A.1}$$

where, τ is applied shear stress, dy is the height of the fluid element cube and du is the relative movement, μ is known as the modulus of viscosity or simply, viscosity. The

term, *dy/du*, indicates the rate of shear (see figure 2.1 for details). From equation (A.1), it follows that the shear stress and strain follow a linear relationship.
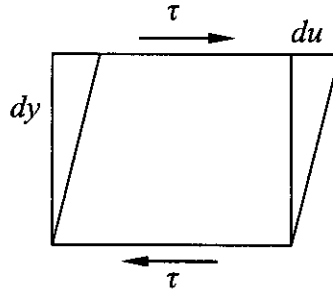
Figure A.1: Shear force on a fluid element

Fluids that obey this linear law are called as Newtonian fluids. The rest, such as grease, are called as Non-Newtonian fluids. Viscosity, also referred here as dynamic viscosity, is given either in terms of poise and the conversion factor is $1 microreyn =$ 5.14 *poise* . It is not always possible to keep the rubbing surfaces apart, especially when speeds are low or the loads are high. This situation is characterized by mixed lubrication in which both the asperities and the lubricant present in the intervening space share the load. A much severe condition of mixed lubrication is known as boundary lubrication. Various types of lubrication regimes can be better understood with the help of a plot of coefficient of friction against generalized Sommerfeld number. This graph is called Striebek curve and is shown in figure A.2.

Higher values on the abscissa are due to higher film thicknesses and this corresponds to thick film or full hydrodynamic lubrication regime. In contrast, very low values indicate solid friction. The transition is represented by boundary and mixed lubrication regimes. The graph *abcde* can be fragmented into different regions *ab* (hydrodynamic), *bcd* (boundary or mixed) and *de* (solid) and the point *c* gives the minimum value of friction. In hydrodynamic regime, *ad*, a fall in the coefficient of friction is attributed due to a reduction in speed and as speed is further reduced, solid friction comes into play due to the contact of asperities. Due to heat generation, fluid viscosity decreases and so does the shear force, resulting in reduction of this

component. Within the boundary regime, the curve requires explanation from all the components of friction as given by the equation,

$$f_{BL} = f_{liq} + f_{solid} + f_{def} \qquad\qquad (A.2)$$
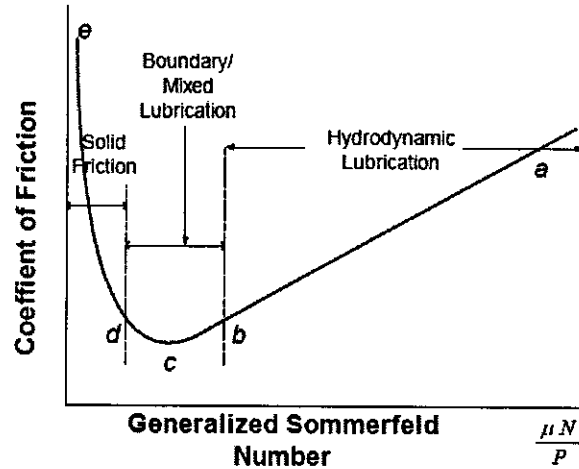
Figure A.2: Striebeck curve [19]

The falling slope of *bc* is explained by a general reduction in f_{liq}, greater than the increase due to f_{solid}. If speed is further reduced, more contact area is created and thus, f_{solid} increases rapidly and overcomes the effect of reduction of f_{liq} due to viscosity. Therefore coefficient of friction rises along *cd*. The segment, *de* corresponds to solid friction where the effect of lubricant is almost negligible. Thus, the minimum point *c* indicates the optimum value. However, a slight disturbance in a system operating at this critical point is likely to destabilize and either a high value of friction coefficient is registered or seizure takes place. Therefore it is recommended to operate the system more into the hydrodynamic regime, along the curve *bca*.

In this present thesis focus is made on hydrodynamic lubrication as the fabrication of micropores on face seal surfaces controls their tribological properties and ensures the provision of lubrication in hydrodynamic region, thus effect the performance of the face seal.

Appendix B

REYNOLDS EQUATION

B 1. REYNOLDS EQUATION

The well known Reynolds equation is one of the fundamental equations used in the field of fluid mechanics. The differential equation governing the pressure distribution in fluid film lubrication was first derived by O. Reynolds in 1886, for incompressible fluid. This was an unnecessary restriction and later the effects of compressibility were included. The Reynolds equation forms the foundation of fluid film theory. This equation establishes a relation between the geometry of the surfaces, relative sliding velocity, the property of the fluid and the magnitude of the normal load the bearing can support.

Before deriving the full equation the assumptions that are to be made must be considered. The assumptions are

1. Body forces are neglected, i.e. there are no extra fields of forces acting on the fluid. This is true except for magnetohydrodynamics.

2. The pressure is constant through the thickness of the film. As the film is only one or two thousandths of a millimeter thick it is always true. With elastic fluids there may be exceptions.

3. Te curvature of surfaces is large compared with film thickness. Surface velocities need not to be considered as varying direction.

4. There is no slip at the boundaries. The velocity of the oil layer adjacent to the boundary is the same as that of the boundary. There has been much work on this and it is universally accepted.

The next assumptions are put in for simplification. They are not necessarily true but without them the equation get more complex. So the assumptions for further simplification along with the above the assumptions are:

5. The lubricant is Newtonian, i.e. stress is proportional to rate of shear.

6. Flow is laminar. In big turbine bearing it is not true and the theory is being slowly developed.

7. Fluid inertia is neglected. Several studies have shown that even if Reynolds number is 1000 the pressure is only modified by about 5 percent.

8. The viscosity is constant through the film thickness. This is certainly not true but leads the great complexity if it is not assumed.

On the basis of the above assumptions the Reynolds equation is developed.

B 2. CONTINUITY OF FLOW OF A COLUMN

Consider a column of fluid of height h and base *dx, dz* (shown in the Figure 2). Fluid flows into the column from the left at a rate q_x per unit width. The volume flow rate is $(q_x dz)$, for the column of *dz* wide. The rate of flow per unit width is

$$q_x + \frac{\partial q_x}{\partial x} dx \qquad\qquad (B.1.1)$$

where, $\partial q_x / \partial x$ is the rate of change of flow in the x direction, and the dx is small enough to $\partial q_x / \partial x$ as linear.. The actual flow out is

$$\left(q_x + \frac{\partial q_x}{\partial x} dx \right) dz \qquad\qquad (\text{B.1.2})$$

$$w_o dxdz$$
$$\left(q_x + \frac{\partial q_z}{\partial z} dz \right) dx$$
$$\left(q_x + \frac{\partial q_x}{\partial x} dx \right) dy$$
$$q_x dz$$
$$q_z dx$$
$$w_o dxdz$$

Lubricant

Moving plate
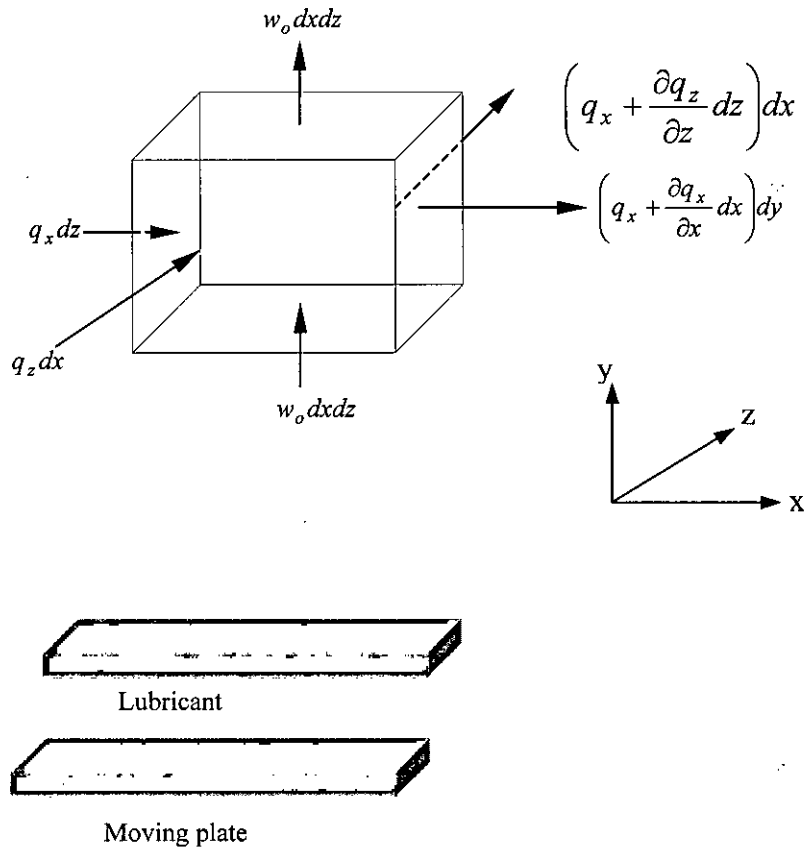
Figure B.1: Continuity of a flow of a fluid element

In the z direction the same argument applies. The flow rate in is $\left(q_x dz \right)$ and out is

$$\left(q_z + \frac{\partial q_z}{\partial z} dz \right) dx \qquad\qquad (\text{B.1.3})$$

The vertical flow is rather different. If the floor of the column moves upwards at a velocity w_0 and if the floor moves upwards as well at a speed w_h the volume of the column changes at a rate $(w_h\text{-}w_0)dxdz$, where $(dx\ dz)$ is the area both of the base and of the roof. Although the base and roof are moving, at the instant considered the height is h, through a fraction of time later it will of course have altered.

For the continuity of the flow, the fluid being of constant density, the rate flowing in must equal the rate flowing out. These can all be added up thus. Flowing into the column

$$q_x\,dz + q_z\,dx + w_o\,dx\,dz \qquad (B.2)$$

Flowing out of the column

$$\left(q_x + \frac{\partial q_x}{\partial x}dx\right)dz + \left(q_z + \frac{\partial q_z}{\partial z}dz\right)dx + w_h dx\,dz \qquad (B.3)$$

The equation 2 and equation 3 are equal. So equating the equations and after cancellations of the same terms we get:

$$\frac{\partial q_x}{\partial x}dxdz + \frac{\partial q_z}{\partial z}dzdx + \left(w_h - w_0\right)dxdz = 0 \qquad (B.4.1)$$

Now $(dxdz)$ is arbitrary and non zero, so canceling the term from the both side yields

$$\frac{\partial q_x}{\partial x} + \frac{\partial q_z}{\partial z} + \left(w_h - w_0\right) = 0 \qquad (B.4.2)$$

In unsteady state conditions the density of the column may change with time, and this must be taken into account. If the density is the same through out the height of the column the analysis leads to:

$$\frac{\partial}{\partial x}\left(\mu q_x\right)+\frac{\partial}{\partial z}\left(\mu q_z\right)+\frac{\partial}{\partial t}\left(\mu h\right)=0 \qquad\qquad\qquad\text{(B.5)}$$

where, μ is the density of the fluid.

B 3. EQUILIBRIUM OF AN ELEMENT
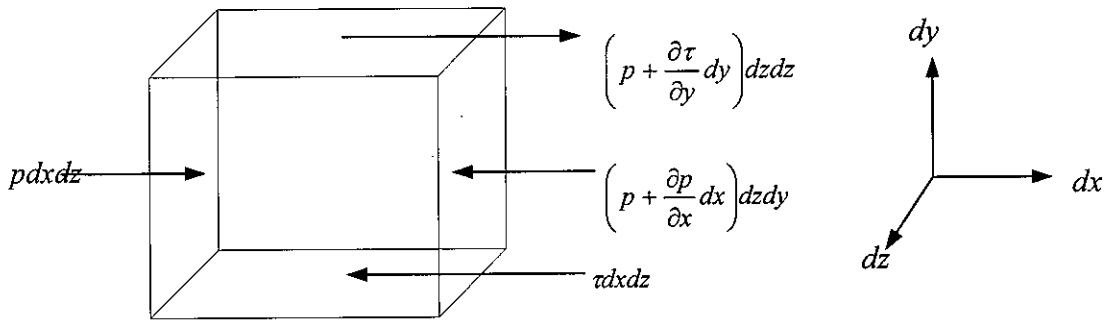
Figure B.2: Equilibrium of an element

Take a small element of fluid of sides *dxdydz*(shown in the figure 2) and consider first the forces in the x direction only. On the left of the element there is a pressure *p* on the face of area *dzdy*, giving a force, acting on the right, of *pdzdy*. On the opposite face the pressure is:

$$p+\frac{\partial p}{\partial x}dx \qquad\qquad\qquad\text{(B.6.1)}$$

The corresponding force is

$$\left(p+\frac{\partial p}{\partial x}dx\right)dz\,dy \qquad\qquad\qquad\text{(B.6.2)}$$

There are shear stress on the top and bottom faces, producing forces. On the bottom face the shear stress τ gives a force ($\tau\ dx\ dz$) acting on the left and on the top face, and acting to the right, is force

$$\left(\tau + \frac{\partial \tau}{\partial y} dy\right) dx dz \tag{B.6.3}$$

The shear stress on the top face being $\left(\tau + (\partial \tau / \partial y) dy\right)$.

These forces acting to the left and right must balance each other so

$$p\,dz\,dy + \left(\tau + \frac{\partial \tau}{\partial y} dy\right) dx\,dz = p + \frac{\partial p}{\partial x} dz\,dy + \tau\,dx\,dz \tag{B.7.1}$$

Expanding and canceling the common terms from the right and left sides of the above equation yield

$$\frac{\partial \tau}{\partial y} dy\,dx\,dz = \frac{\partial p}{\partial x} dx\,dz\,dy \tag{B.7.2}$$

or, $\quad \dfrac{\partial \tau}{\partial y} = \dfrac{\partial p}{\partial x}$ $\hspace{4cm}$ (B.7.3)

According to Newton's Law of Viscosity

$$\tau = \mu \frac{\partial u}{\partial y} \tag{B.7.4}$$

From the equation (7.c) and equation (8) we can write

$$\frac{\partial p}{\partial x} = \frac{\partial}{\partial y}\left(\mu \frac{\partial u}{\partial y}\right) \tag{B.8}$$

In the y direction the shear stresses and pressure can be equated and a similar equation follows

$$\frac{\partial \tau}{\partial y} = \frac{\partial p}{\partial z} \qquad\qquad (B.9.1)$$

$$\tau = \mu \frac{\partial v}{\partial y} \qquad\qquad (B.9.2)$$

From the equation (8.a) and equation (8.b) we get

$$\frac{\partial p}{\partial z} = \frac{\partial}{\partial y}\left(\mu \frac{\partial v}{\partial y} \right) \qquad\qquad (B.9.3)$$

The pressure gradient in the z direction is zero (by definition), so $\partial p / \partial z = 0$.

Considering the equation (8) that can be integrated since p is not the function of z. Integrating the equation (8) we get

$$\mu \frac{\partial u}{\partial y} = \frac{\partial p}{\partial x} y + C_1 \qquad\qquad (B.10)$$

where C_1 is the integration constant.

Now both μ and u are the function of y but it is too difficult to consider both at once so μ is taken as constant with respect to y. It is important to realize that this is a important assumption and the assumption is made only for the simplicity. The inclusion of $(d\mu/dy)$ can modify the equation very considerably in certain circumstances.

However, making the assumption, a further integration is performed to the equation and yield

$$\mu u = \frac{\partial p}{\partial x} \frac{y^2}{2} + C_1 y + C_2 \qquad\qquad (B.10.1)$$

According to assumption 4, the boundary conditions are simple as the speed of the fluid at the surface is the speed of the surface it self,

$$y = h, \quad u = U_1 \tag{B.10.2}$$

$$y = 0, \quad u = U_2 \tag{B.10.3}$$

where U_1 and U_2 are the surface speeds

Substituting the boundary conditions in the equation (10.a), we get accordingly

$$C_2 = \mu U_2 \tag{B.10.4}$$

$$C_1 = \frac{\mu(U_1 - U_2)}{h} - \frac{\partial p}{\partial x}\frac{h}{2} \tag{B.10.5}$$

Finally we get equation (10.a) in the following form after substituting the values of constants into that equation

$$u = \frac{\partial p}{2\mu\partial x}\left(y^2 - yh\right) + \left(U_1 - U_2\right)\frac{y}{h} + U_2 \tag{B.11}$$

where $\partial p/\partial x$ is the pressure gradient, μ is the viscosity, U_1 and U_2 are the surface speeds on $y = h$ and $y = 0$; and of course from the equation (11) the velocity gradient is

$$\frac{\partial u}{\partial y} = \frac{\partial p}{\mu\partial x}\left(y - \frac{h}{2}\right) + \frac{(U_1 - U_2)}{h} \tag{B.12}$$

Now the integrating the above equation from 0 to h will give the flow rate in the x direction per unit width of z (i.e., $q_x = \int_0^h u\,dy$). By integrating the equation (12) will yield

$$q_x = \left[\frac{\partial p}{2\mu\partial x}\left(\frac{y^3}{3} - \frac{y^2 h}{2}\right) + \left(U_1 - U_2\right)\frac{y^2}{2h} + U_2 y\right]_0^h \tag{B.13}$$

Putting the limits and simplifying we get

$$q_x = \frac{-h^3 \partial p}{12 \mu \partial x} + (U_1 + U_2)\frac{h}{2} \tag{B.14}$$

Following the same procedure we get flow rate in y direction

$$q_z = \frac{-h^3 \partial p}{12 \mu \partial z} + (V_1 - V_2)\frac{h}{2} \tag{B.15}$$

where V_1 and V_2 correspond to U_1 and U_2

B 4.   FULL REYNOLDS EQUATION

Now substituting the expression of q_x and q_y in the equation (4.b) (i.e., continuity equation) yield

$$\frac{\partial}{\partial x}\left\{(U_1 + U_2)\frac{h}{2} - \frac{h^3 \partial p}{12 \mu \partial x}\right\} + \frac{\partial}{\partial z}\left\{(V_1 - V_2)\frac{h}{2} - \frac{h^3 \partial p}{12 \mu \partial z}\right\} + (w_h - w_0) = 0 \tag{B.16}$$

This can be further tidied up into following form

$$\frac{\partial}{\partial x}\left(\frac{h^3}{\mu}\frac{\partial p}{\partial x}\right) + \frac{\partial}{\partial z}\left(\frac{h^3}{\mu}\frac{\partial p}{\partial z}\right) = 6\left\{\frac{\partial}{\partial x}(U_1 - U_2)h + \frac{\partial}{\partial z}(V_1 - V_2)h + 2(w_h - w_0)\right\} \tag{B.17}$$

This is Reynolds equation in the three dimensions with everything varying. It is too massive to handle as it is. So further modification is made to simplify it

B 5.   SIMPLIFICATION

To simplify the equation (17), we will put U instead of $(U_1 + U_2)$ and V instead of $(V_1 + V_2)$. These are merely short forms and do not involve any assumptions. Next it is usually possible to rearrange the axes so that either

$\dfrac{\partial}{\partial x}(Uh)$ or $\dfrac{\partial}{\partial z}(Vh)$ is zero.

It is in fact very hard to think of any moving system where there is both a wedge and a velocity in two perpendicular directions. Incorporating the terms to simplify the equation (17) and granting the improbability of having both $(\partial/\partial x)(Uh)$ and $(\partial/\partial z)(Vh)$ non-zero.

$$\frac{\partial}{\partial x}\left(\frac{h^3}{\mu}\frac{\partial p}{\partial x}\right)+\frac{\partial}{\partial z}\left(\frac{h^3}{\mu}\frac{\partial p}{\partial z}\right)=6\left\{\frac{\partial}{\partial x}(Uh)+2(w_h-w_0)\right\} \qquad (B.18.1)$$

A further simplification is to realize that the velocity of a surface does not vary from one point to another point in a bearing. So U is not a function of x and thus

$\dfrac{\partial}{\partial x}(Uh)$ can be written as $U\dfrac{dh}{dz}$

Furthermore, if the surfaces are impermeable so no fluid seeps in or out and they are merely moving relative to each other, and thus

(w_h-w_0) can be written as dh/dt

So the equation (18.a) is further reduced to

$$\frac{\partial}{\partial x}\left(\frac{h^3}{\mu}\frac{\partial p}{\partial x}\right)+\frac{\partial}{\partial z}\left(\frac{h^3}{\mu}\frac{\partial p}{\partial z}\right)=6\left(U\frac{dh}{dx}+2\frac{dh}{dt}\right) \qquad (B.18.2)$$

The first term $(U\,dh/dx)$ of the right hand side of the equation (18.b) describes the normal wedge action and (dh/dt) is called the squeeze film term. In steadily running bearings, of course, dh/dt is zero, but in many practical journal bearings dh/dt is of the same order as $U\,dh/dx$. It is so complex to take into account that it is usually omitted. Now the equation (18.b) after omitting the previously mentioned term becomes

$$\frac{\partial}{\partial x}\left(\frac{h^3}{\mu}\frac{\partial p}{\partial x}\right) + \frac{\partial}{\partial z}\left(\frac{h^3}{\mu}\frac{\partial p}{\partial z}\right) = 6U\frac{dh}{dx} \qquad (B.18.3)$$

The next assumption is to take μ as constant in the z direction. In fact it is considered to be constant everywhere. So it can be taken from inside the differentials and put over to the right-hand side to give

$$\frac{\partial}{\partial x}\left(h^3\frac{\partial p}{\partial x}\right) + \frac{\partial}{\partial z}\left(h^3\frac{\partial p}{\partial z}\right) = 6\mu U\frac{dh}{dx} \qquad (B.19)$$

This is the usually quoted Reynolds equation on which further derivation will be continued.

Appendix C

COMPUTER CODE

C.1 PROGRAM 1

```
/*      Program by Finite Difference Technique to Solve 2-D Reynolds Equation  */

#include<iostream.h>
#include<stdio.h>
#include<conio.h>
#include<stdlib.h>
#include<math.h>

#define m 9
#define n 9
#define M 81
#define N 81

const float mu=25e-03;              // Pa-s
const float vel=9.5;            // m/s
const float err=1e-6;

void xsolve(float[M][N],float[N]);
float int_load(float [M]);
//float hydrostatic(float
float fun1(float x,float z);
float fun2(float x,float z);
float fun3(float x,float z);
```

```
/*  Gloabal variables used in differnt functions of the program  */

float R0=5.;    // Pore radius which will vary
float h0=6.;    // Minimum seal clearance which will vary depending on
                // converging criteria
float psi=R0/h0;// value that depends on h0

void main()
{
FILE *out;
out=fopen("d:\\january7.out","w");
clrscr();
int i,j,k,kk;
float p[M][N],pn[M][N];
float a1,a2,a3;   //having function of H
float sdx,sdz,dx,dz,x1,z1;

/* dx, dz are the step size of the control cell
    sdx, sdz are the mimimum limit of the cell from the center
    x1, z1 are used for determining a2, a3 at the different point of the
    control cell */

float ssdx[M],ssdz[N],rad[m][n],crad[M];
/*  ssdx[M] & ssdz[N] are the 1 dimensional matrix that hold the values
    of the control cell at different point by adding the step size of the
    previous point
    rad[m][n] is the 2 dimensional matrix holding the radius of pore in a
    control cell
    crad[M] is the 1 dimensional matrix holding the radius of the pore from
    2 dimensional matrix rad[m][n] */

float b[M];     // b is the RHS value of the matrix

for(i=0;i<M;i++)
  {
  ssdx[i]=0.0;
  ssdz[i]=0.0;
  b[i]=0.0;
  }               // data initialization

sdx=-2.64;sdz=-2.64; // here -2.64 is the jita value
dx=fabs((2.*sdx)/(m+1));
kk=0;
for(i=0;i<m;i++)
  {
  sdx+=dx;
  sdz=-2.64;
  dz=dx;
```

```
for(j=0;j<n;j++)
    {
    sdz+=dz;
    ssdz[kk]=sdz;
    ssdx[kk]=sdx;
    rad[i][j]=sqrt(pow(sdx,2)+pow(sdz,2));
    crad[kk]=rad[i][j];
    if(rad[i][j]<=1.0)
        {
        a3=(fun3(sdx,sdz))*(dx*dx);
        b[kk]=a3;                    // Reading b matrix
        }
    else b[kk]=1.e-13;       // Reading b matrix
    fprintf(out,"\nrad=%f ssdx=%f, ssdz=%f ",crad[kk],ssdx[kk],ssdz[kk]);
    printf("\ncrad[%d]=%f ssdx=%f, ssdz=%f ",kk,crad[kk],ssdx[kk],ssdz[kk]);
    kk++;
    }//getch();
    }


for(i=0;i<M;i++)
  {
    for(j=0;j<N;j++)
    {
    p[i][j]=0.0;
    }
  }

/* for(kk=1;kk<M+1;kk++){
 printf("b[%d]= %f\n",kk,b[kk]);
 if(kk>9&&(kk%9)==0) getch(); }getch();*/  // no need of this porion

    k=0;
    kk=0;
  for(i=0;i<M;i++)
  {
    if(i==0)
      {
      p[i][i]=-4.;
        for(j=i+1;j<i+4;j++)
          {
          if(j!=i+2)p[i][j]=1.;
          if(j==i+3)p[i][j]=1.;
          }
      }

    if(i!=0&&i<=2)
      {
        for(j=i-1;j<N;j++)
```

```
                {
                    if(j==i-1)p[i][j]=1.;
                    if(j==i) p[i][j]=-4.;
                    if(j==i+1&&i==1)p[i][j]=1.;
                    if(j==i+3) p[i][j]=1.;
                }
            }

        if(i>2)
        {
            if(crad[i]<1.0)
                {
                x1=ssdx[i];
                z1=ssdz[i];
                a1=(fun1(x1,z1))*(dx/2.0);
                a2=(fun2(x1,z1))*(dx/2.0);
//              printf("\ncrad[%d]=%f, a1[%d]=%f,
a2[%d]=%f",kk,crad[kk],kk,a1,kk,a2);
//              printf("\ncrad[%d]=%f, a1[%d]=%f,
a2[%d]=%f",(i+1),crad[i+1],(i+1),a1,(i+1),a2);
//              getch();

                p[i][k]=1.-a2;
                for(j=i-1;j<N;j++)
                    {
                    if(j==i-1&&(i%3)!=0)p[i][j]=1.-a1;
                    if(j==i) p[i][j]=-4.;
                    if(j==i+1&&(j%3)!=0)p[i][j]=1.+a1;
                    if(j==i+3) p[i][j]=1.+a2;
                    }
                }
            else
                {
                p[i][k]=1.;
                    for(j=i-1;j<N;j++)
                    {
                        if(j==i-1&&(i%3)!=0)p[i][j]=1.;
                        if(j==i) p[i][j]=-4.;
                        if(j==i+1&&(j%3)!=0)p[i][j]=1.;
                        if(j==i+3) p[i][j]=1.;
                    }
                }
            k++;
        }
    kk++;
    }
cout<<"\n";
fprintf(out,"\n");
```

```
for(i=0;i<81;i++)
{
   for(j=0;j<81;j++)
   {
//    cout<<p[i][j]<< "  ";
     fprintf(out,"%.1f ",p[i][j]);
   }
//cout<<endl;
//cout<<b[i]<<endl;
 fprintf(out,"%.4f \n\n",b[i]);
/*
if(i==2)
cout<<"-----------------------------------------------------------"<<endl;
if(i==5)
cout<<"-----------------------------------------------------------"<<endl;
if(i==8)
cout<<"-----------------------------------------------------------"<<endl;
}            getch(); */ // no need of this portion
}
 xsolve(p,b); //function to solve by iteration technique
 getch();
}


// Function for solving matrix by iteration technique

void xsolve(float p[M][M],float b[N])
{
FILE *out;
FILE *ot;
out=fopen("d:\\january7.out","a");
//ot=fopen("graph.out2","w");
int i,j;
float x[M],xn[M],er[M];
float save,beta;
float sum;      // to gte the integrated load
   for(i=0;i<M;i++)
   { xn[i]=0.0;
     x[i]=0.0;
     er[i]=0.0;}
     int iter=1;
loop:
   iter++;
   for(i=0;i<M;i++)
   { save=p[i][i];
     xn[i]=b[i]/save;
     for(j=0;j<M;j++)
     { if(j!=i)
```

```
            xn[i]=xn[i]-(p[i][j]*xn[j])/save;  // Gauss-Seidel Method
//          xn[i]=xn[i]-(p[i][j]*x[j])/save;  // Jacobi Method
      }
    printf("x%d",i+1);
    fprintf(out,"x%d",i+1);
    printf(" = %.6f \n",xn[i]);
    fprintf(out," = %.6f \n",xn[i]);
   }
        for(i=0;i<M;i++){
          er[i]=fabs((xn[i]-x[i])/xn[i]);
```

/*************   The Relaxation Method   ****************/

```
        beta=1.53;
        xn[i]=beta*xn[i]+(1-beta)*x[i];
          x[i]=xn[i];
        }
        for(i=0;i<M;i++){
        if(iter>200){
        cout<<"The system is not converging";
        getch();
        abort();}
        if(er[i]>err) goto loop;
         }
 printf("No of Iteration=%d",iter);
// getch();
 sum=int_load(xn);
 printf("The integrated load on the cell is W0 = %f", sum);
 }

float int_load(float xn[M])
{
 int i,j,k;
 float sdxl,sdxh,sdzl,sdzh;
 float x[m+2][n+2];
 float dx,dz;   // step size for the integration
 float sum,sum1,sumj;

 sdxl=-2.64;sdxh=2.64;sdzl=-2.64;sdzh=2.64; // l:lower and h: upper limits

 // step size calculation
 dx=(sdxh-sdxl)/(m+1);
 dz=(sdzh-sdzl)/(n+1);

 sum=0.0;sum1=0.0;sumj=0.0;

  for(i=0;i<M;i++)
    {
```

```
   while(xn[i]<0)xn[i]=0.0;
   printf("%f\n", xn[i]);
   }
 for(i=0;i<=m+1;i++)
   {
   for(j=0;j<=n+1;j++)
      {
       x[i][j]=0.0;
      }
   }
     k=1;
     for(i=1;i<=m;i++)
      {
       for(j=1;j<=n;j++)
        {
         x[i][j]=xn[k];
         k++;
        }
      }
     for(j=1;j<=m+2;j++)
      {
       sum1=0.0;
       for(k=1;k<=n+2;k++)
        {
         if(k==1)
             sum1+=x[j-1][k-1];
         if(k!=1 && (k%2==0))
             sum1+=4.*x[j-1][k-1];
         else if(k>1 && k<(n+2))
             sum1+=2.*x[j-1][k-1];
         if(k==n+2)
             sum1+=x[j-1][k-1];
        }
       if(j==1)
         sumj+=sum1;
       if(j!=1 && j%2==0)
         sumj+=4.*sum1;
       else if(j>1 && j<(m+2))
         sumj+=2.*sum1;
       if(j==m+2)
         sumj+=sum1;
      }
 sum=(dx*dz/9.)*sumj;
 return sum;
}

float fun1(float x,float z)
{
```

```
  float f1;
 f1=(-3 ln(1+psi)*x)/(pow((x*x +z*z) ,.5));
  return f1;
  }

float fun2(float x, float z)
{
  float f2;
 f2=(-3 ln(1+psi)*z)/(pow((x*x +z*z) ,.5));
  return f2;
  }

float fun3(float x, float z)
{
  float f3;
 f3= (-ln(1+psi)*x)/(pow((x*x +z*z) ,.5))*(1/((1+psi)*exp(-ln(1+psi)*pow((x*x
+z*z),0.5))));

  return f3;
  }
```

C.2 PROGRAM 2

```
/*   Program to find out the integrated hydrodynamic pressure on a control cell     */


#include<stdio.h>
#include<conio.h>
#include<math.h>
#include<iostream.h>

#define M 81
#define mm 9
#define nn 9

/* Program Main */

void main()
{
  FILE *in, *out;
   in=fopen("d:\\TC\\Input\\data3.txt","r");
  //in=fopen("d:\\TC\\Input\\data2.txt","r");
  //out=fopen("result.out","w");

  clrscr();
  int i,j,p;
  int m,k;
```

```
float a,b,c,d;
float x[mm+2][nn+2], xn[M];
float h1,h2;
float sum,sum1,sumj;

m=10;p=10;                          // no. of intervals
a=-2.64;b=2.64;c=-2.64;d=2.64; // lower and upper limits
// step size calculation
h1=(b-a)/m;
h2=(d-c)/p;

sum=0.0;sum1=0.0;sumj=0.0;

 for(i=0;i<M;i++){
   fscanf(in,"%f\n",&xn[i]);
   while(xn[i]<0)xn[i]=0.0;
   }

/*  for(i=0;i<M;i++){
   printf("%f\n",xn[i]);
   //fprintf(out,"%f\n",xn[i]);
   }*/
//  getch();
   for(i=0;i<=mm+1;i++)
   {
     for(j=0;j<=nn+1;j++)
     {
        x[i][j]=0.0;
     }
   }
    k=1;
   for(i=1;i<=mm;i++)
   {
     for(j=1;j<=nn;j++)
     {
        x[i][j]=xn[k];
        k++;
     }
   }

/*  for(i=1;i<=mm;i++){
    for(j=1;j<=nn;j++){
    printf("%f\n",x[i][j]);}}getch();*/

/*  for(i=0;i<=mm+1;i++){
    for(j=0;j<=nn+1;j++){
    printf("%.6f ",x[i][j]);}
    printf("\n");getch();}   */
```

```c
for(j=1;j<=m+1;j++)
{
  sum1=0.0;
      for(k=1;k<=p+1;k++)
      {
        if(k==1)
        sum1+=x[j-1][k-1];
        if(k!=1 && (k%2==0))
        sum1+=4.*x[j-1][k-1];
        else if(k>1 && k<(p+1))
        sum1+=2.*x[j-1][k-1];
        if(k==p+1)
        sum1+=x[j-1][k-1];
      }
  if(j==1)
  sumj+=sum1;
  if(j!=1 && j%2==0)
  sumj+=4.*sum1;
  else if(j>1 && j<(m+1))
  sumj+=2.*sum1;
  if(j==m+1)
  sumj+=sum1;
}

sum=(h1*h2/9.)*sumj;
printf("\nThe integrated value = %f",sum);
getch();
}
```

BIBLIOGRAPHY

1. Bharat Bhushan, Principles and Applications of Tribology, 1st ed., Newyork, John Wiley & Sons (1999)
2. Salama, M. E., " The effect of macroroughness on the performance of parallel thrust bearings.", in Proc. I. Mech. Engg., London, 163, pp 149-158, (1952).
3. Pape, J. G., " Fundamental Research on Radial Face Seals." ASLE Trans., 11, 4, pp 302-309 (1968).
4. Etsion, I, " The effect of combined coning and waviness on the separating force in mechanical face seals.", Jour. of Mech. Engg. Sci., 22, 2, pp 59-64, (1980).
5. Hamilton, D. B., Walowit, J. A. and Allen, C. M., " A theory of lubrication by microirregularities.", ASME Journal of Basic Engineering,88, 1, pp 177-185,(1966).
6. Anno, J. N., Walowit, J. A. and Allen, C. M., " Microasperity lubrication.", ASME Jour. of Lubr. Tech., 91, 2, pp 351-355, (1968).
7. Anno, J. N., Walowit, J. A. and Allen, C. M., "Load Support and Leakage from Microasperty – Lubrication Face Seals," ASME Jour. of Lubr. Tech., 9, 4, pp 726-731, (1969).
8. Sneak, H. J., "The effects of geometry and inertia on face seal performance-Laminar flow," ASME Journal of Lubrication Technology, pp 333-340, (1968)
9. Sneak, H. J., "The effects of geometry and inertia on face seal performance-Turbulent flow," ASME Journal of Lubrication Technology, pp 342-350J, (1968)
10. Findlay, J.A., " Cavitation in mechanical face seals", ASME Jour. of Lubr. Tech., pp 356-364, (1968)
11. Cheng, H. S., Chow, C. Y. and Wilcock, D. F., " Behavior of hydrostatic and hydrodynamic noncontacting face seals", ASME Jour. of Lubr. Tech., pp 510-518, (1968)
12. Snegovsky, F. P., Buljuk, N.G., "Study of Lubrication of Sliding Bearings with Microcavities on Journals." *Friction and Wear*, 4, 2, pp 321-328, (1983)
13. Lai, T. W., " Development of non-contacting, non-leaking spiral groove liquid face seals", Lubrication Engineering., 50, 8, pp 625-640, (1980)
14. Etsion, I .and Burstein, L., "Model of Mechanical seals with regular micro surface structure.", STLE Tribology Transactions, Vol. 39, 3, page-677-683, (1996).
15. Etsion, I., Halperin, G. and Greenberg, Y., " Increasing mechanical seals life with laser-textured mechanical seal faces", Proc., 15th Int'l Conference on Fluid Sealing, BHR, pp 3-11, (1997).
16. Etsion, I., Kligerman, Y., and Halperin, G., Analytical and Experimental Investigation of Laser-Textured Mechanical Seal Faces", *Tribology Transactions*, 42(3), pp 511516, (1999)
17. Ronen, A., Etsion, I. and Kligerman, " Friction reducing surface texturing in reciprocating automotive components", *Tribology Transactions*, 44(3), pp 359366, (2001)

18. Dudley D. Fuller, Theory and Practice of Lubrication for Engineers, 2nd ed., Newyork, John Wiley & Sons, (1984)
19. Moore, D.F., Principles and Applications of Tribology, *Pergamon Press Inc.*, New York, 1975.
20. Cameron, A., Basic Lubrication Theory, *Oxford University Press*, 1969.
21. Cameron, A., Principles of Lubrication, 1st ed., Newyork, John Wiley & Sons, (1966)
22. Miller, Brad A and Green, Itzhak, " Numerical techniques for computing rotodynamic properties of mechanical gas face seal", ASME Journal of Tribology, Vol. 124, pp 755-761, (2002)
23. Elsharkawy, Abdullah A., " On the hydrodynamic liquid lubrication analysis of slider/disk interface", Int. Jour. of Mechanical Sciences, 43, pp. 177-192, (2001).
24. Chapra. S. C. and Canale, R. P., Numerical Methods for Engineers: With Programming and Software Applications, 3rd ed., New York, McGraw Hill Company Limited, (2000)
25. Gerald, C. F. and Wheatley, P. O, Applied Numerical Analysis, 6th ed., Singapore, Pearson Education Inc, (2002)
26. Lebeck, A. O., Principles and Design of Mechanical Seals, John Wiley and Sons.